Technische Universität München

Fakultät für Medizin

Klinik & Poliklinik für Innere Medizin I

Klinikum rechts der Isar

Sphingolipids improve vascular barrier function and systemic blood pressure by reducing pericyte loss during LPS-mediated inflammation

Farah Abdel Rahman

Table of contents

Abstract

Thesis title: Sphingolipids improve vascular barrier function and systemic blood pressure by reducing pericyte loss during LPS-mediated inflammation

by: Farah Abdel Rahman   Supervisor: Prof.Dr.Christian Kupatt

key words: Sepsis, Sphingosine-1-phosphate, Pericytes, Endothelial cells, VE-Cadherin

Septic shock is a systemic host response to an infection characterized by a systemic hypotension due to dramatic increase in vascular permeability resulting from capillary disintegration. Endothelial cells and pericytes are key regulators of the endothelial barrier and it has been reported by us and others that during sepsis a significant reduction in capillary density is observed. This leads to compromised barrier function and increased capillary leakage. Septic patients exhibit low Sphingosine-1-phosphate (S1P) levels that correlate with low survival rates. So, S1P emerged as bioactive lipid mediator that signals through endothelial S1P receptors to retain capillary density and LPS induced hyperpermeability. In this work, we investigate the potential of S1P during LPS induced sepsis on hemodynamic function, capillary density, endothelial barrier and survival. We show that treating septic mice with S1P results in improved permeability due to pericyte retention in the perivascular niche and promote adhesion protein trafficking such as VE-Cadherin and N-Cadherin. As a result, S1P treatment improves systemic blood pressure and survival. Furthermore, we investigated S1P treatment in cell culture model of sepsis to elucidate the signaling cascade involved. There we show that S1P preserves adhesion proteins such as VE-Cadherin and N-Cadherin that is mediated by a reduction in Src and VE-Cadherin phosphorylation. Besides, exogenous administration of S1P leads to a reduction in the cytosolic pool of G-actin promoting the nuclear translocation of MRTF-A that regulates genes implicated in pericyte retention. Finally, our findings indicate that S1P retains pericyte in the microcirculation and preserves the microvascular unit during LPS induced systemic inflammation, results indicative of the potential therapeutic role of S1P to override microvascular disintegration during sepsis.

1. Introduction

1.1. Sepsis, Severe sepsis and Septic shock

Sepsis is a systemic inflammatory reaction caused by a dysregulated immune response to an infection. Sepsis results in a range of hemodynamic, immune and vascular aberrations leading to organ dysfunction and death. In order to be diagnosed with sepsis the following criteria must be present according to the society of critical care medicine and the European society of intensive care medicine [1]:

- Suspected or proven infection with at least 2 criteria of the systemic inflammatory response syndrome (SIRS):
  - Tachycardia (heart rate >90 beats/min)
  - Tachypnea (respiratory rate >20 breath/min)
  - Fever or hypothermia (temperature >38 or <36 °C)
  - Leukocytosis, leukopenia (white blood cells >1,200/mm^3, <4,000/mm^3 or bandemiac 10%).

The term severe sepsis is proposed to describe sepsis with the presence of signs of organ dysfunction. The clinical features of organ dysfunction are as follow:

- Atrial hypoxemia (Partial Pressure PO_2 <75mmHg in room air or PPO_2/ Inspired PO_2 <300)
- Increased serum creatinine (>0.5mg/dl or >44 umol/L)
- Thrombocytopenia (Platelet count< 100.000/mm^3)
- Hyperbilirubinemia (Increased plasma bilirubin >4 mg/dl)
- Acute oligouria (Urine output <0.5ml /kg/hr or around 45 ml/hr for with 2 hours)
- Paralytic ileus (Paralysis of intestinal muscles and abscess of bowel sound)
- Altered mental status

One could transition from sepsis to septic shock if the criteria of sepsis are met in addition to the presence of systemic hypotension (blood pressure ≤90 mmHg or arterial pressure ≤65) or if a septic patient requires vasopressors to maintain a blood pressure ≥ 65mmHg after the administration of the intravenous fluid bolus [2].

1.2. Epidemiology

Sepsis is the leading cause of death worldwide affecting 30 million patients annually [3]. Despite sepsis being of global relevance, its incidence varies vastly between countries. Data analysis of more than 2.4 million septic patients in the U.S. between January 2010 and September 2016 reveals a 9 % annual increase in the incidence of sepsis with an overall 12.5% percent morality rate. The average treatment cost for a septic patients is approximately 51,022$ making it the most expensive fatal disease in the U.S. with total hospital expenses exceeding 22.2 billion USD annually [4]. Figures from the European intensive care units are comparable to a large extent. In Germany, there is a shortage of epidemiological data on the incidence of sepsis and the latest updates are based on a 2016 report conducted by Fleischmann et al. to assess prevalence of the disease on a national level. An array of analysis performed on registered septic patients between 2007 and 2013 reveals an unexpectedly high incidence of sepsis accounting for 134-314 cases per 100.000 people. Although the incidence of sepsis is decreasing by 0.8 % per year, it is still considered the third most prevalent cause of death in Germany. There, the cost of treatment has reached 8.2 billion euros in 2013 representing 3% of the total German healthcare budget [5].

1.3. Pathological Process

Sepsis results from a systemic infection that triggers an aggressive immune response. While gram negative bacteria are the most frequent cause of sepsis, gram positive bacteria, fungi, viruses and parasites can also cause sepsis [6]. Bacterial lipopolysaccharides (LPS) and endotoxins found on the outer surface of gram negative bacteria serve as a class of pathogen associated molecular pattern (PAMP). PAMPs activate pattern recognition receptors (PRRs) to elicit an innate immune response. The PRR comprise a family of cell surface receptors mainly Toll like receptors (TLRs), nucleotide-binding oligomerization domain-like receptors (NLRs), retinoic acid like receptors (RLRs), and C-type lectin receptors (CLRs) that crucially facilitate the innate immune response. LPS acts as a ligand to TLR4 which initiates a proinflammatory signaling cascade mediated by myeloid differentiation primary response 88 (MYD88) or TIR-domain-containing adapter-inducing interferon-β (TRIF). These activate nuclear factor kappa-light-chain-enhancer (NF-κB), c-JUN and N-terminal Kinase leading to an aggressive immune response [7]. Upon activation, NFκB family of transcription factors translocate to the nucleus and regulate chromatin state of target

genes through the DNA binding domain called Rel homology domain (RHD) to induce transcription of inflammatory genes [8]. The ultimate consequence of NFκB activation is excessive production of Interleukin 6 (Il-6), a potent pro inflammatory cytokine [9]. This explains why septic patients show a dramatic surge in the Il-6 plasma levels exceeding 1mg/mL with a normal range between 1-5pg/ml [10]. Il-6 mediates several biological functions such initiating local immune response by promoting the infiltration of mononuclear leukocytes. Besides regulating the immune system, Il-6 signaling enhances osteoclast formation [11], glucose metabolism [12], and regulates the activity of sympathetic neurons [13]. Therefore Il-6 is referred to as a pleiotropic cytokine. In endothelial cells, Il-6 mediates its pro inflammatory effect via a soluble receptor known as Il-6 soluble receptor (Il-6S). Upon binding, Il-6/Il6-S complex dimerizes with a ubiquitously expressed cell surface receptor known as glycoprotein 130 (gp130) triggering downstream activation of Janus kinases (JAKs) and mitogen-activated protein kinase (MAPK) pathways. As a result, transducer and activator of transcription factors (STAT3) gets activated and retained from the cytoplasm to the nucleus. There, dimerized STAT3 binds to DNA elements and initiates transcription of target genes such as VEGF [14]. The distinct downstream effects of VEGF are increased endothelial permeability and vascular leakage because VEGF contributes to phosphorylation and internalization of VE-Cadherin, an essential structural protein to preserve the endothelial barrier [15]. This model provides a possible explanation that correlates IL-6 plasma levels with endothelial dysfunction, a casual factor for microvascular injury [16], Figure 1.
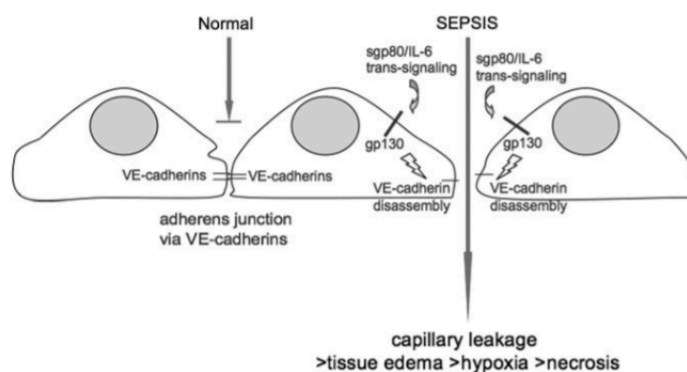
Figure 1: Under normal physiological conditions, VE-Cadherin mediates the adhesion between endothelial cells forming a semi permeable endothelial membrane. During inflammation, the circulating Il-6 couples to the soluble Il-6 soluble receptor initiating trans-signaling cascade via the membrane bound gp130 to induce VE-Cadherin disassembly. Adopted from Kruttgen et al [9].

Left uncorrected, severe defects in the microcirculation lead to poor intra organ blood perfusion leading to hypoxic zones and organ dysfunction. Since non-surviving septic patients exhibit pronounced alterations in the microcirculation than surviving ones, manipulating the microcirculation in sepsis represents a promising approach in tackling this severe disease [17].

1.4. The microcirculation

The microcirculation refers to a branching network of capillaries that are terminally connected to arteriols and venules. Unlike arteries and veins, the components of the microcirculation lack the classical membranous linings of: tunica intima, tunica media and tunica adventitia. Arterioles are surrounded by vascular smooth muscle cells (VSMCs) more frequently than venules, while capillaries are sporadically covered with pericytes, Figure 2. These are mural cells located within the basement membrane of the capillary[18]. The microcirculation is the prominent exchange site of fluid and gas between blood and the surrounding tissues as it fundamentally regulates blood flow and basal vascular tone in response to external stimuli. Since the functionality of the surrounding tissue depends on the integrity of the capillary unit, several conditions such as sepsis manifests multi-organ failure and hemodynamic aberrations resulting from microvascular dysfunction.
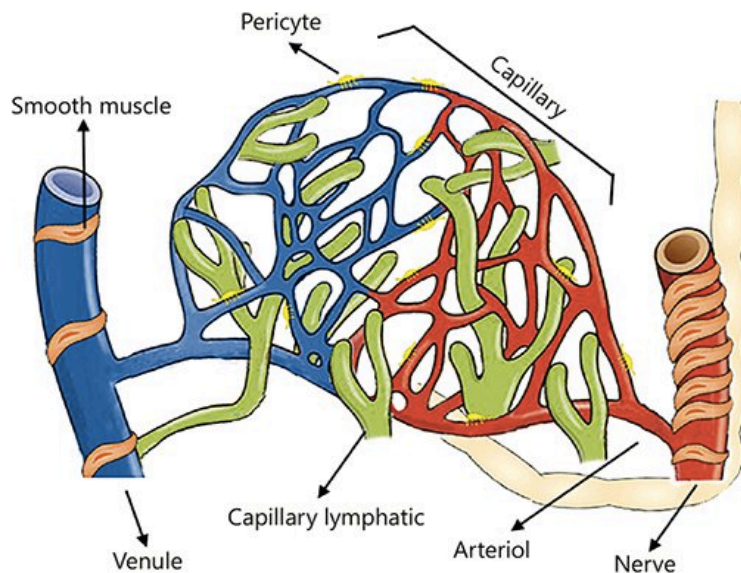
Figure 2: Schematic representation of the microcirculation. Anatomically, the capillary is the smallest vascular unit surrounded by lymphatic network to drain extravascular fluid in the venous system. Endothelial cells (EC) and pericytes are the main constituent of the capillary network while vascular smooth muscle cells (VSMC) are additionally present in the arteriols and aenuels. Adapted from Guven et al[19]

1.4.1. Pericytes

Pericytes were initially described by Charles Rouget at the end of the 19th century and their biologic function remained unclear for long. On their surface, they display markers overlapping with the fibroblasts and VSMC compartments. Anatomically, pericytes are identified based on their peri-endothelial location on the abluminal surface of blood vessel. Their prominent shape and cytoplasmic secondary extensions distinguish them from endothelial cells. The endothelial-pericyte interface is often separated by a basement membrane except at the peg and socket contacts and through adhesion plaques, Figure 3. Pericytes communicate directly with endothelial cells either through gap junctions and peg socket contacts or indirectly through adhesion plaques. The peg-socket junction requires a pericyte finger shape peg inserted into an endothelial socket. However, the adhesion plaque maintains the endothelial-pericyte connection through mainly fibronectin and the cell adhesion molecule N-cadherin [20].
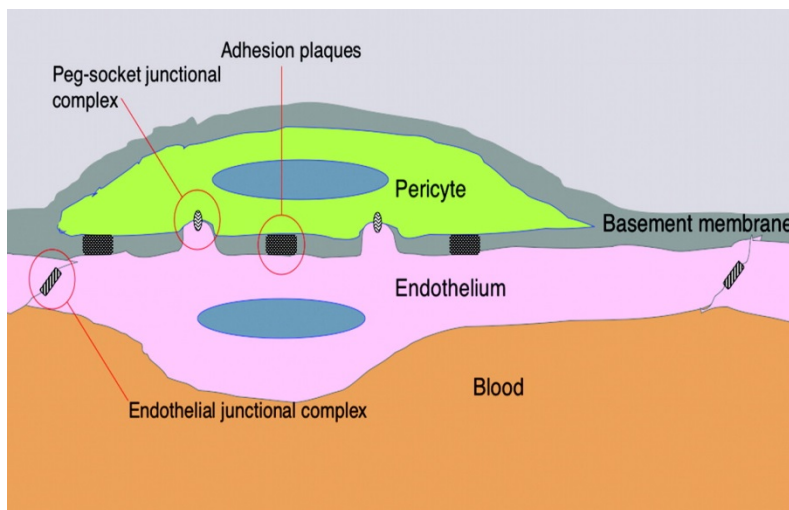
Figure 3: Representation of the spatial localization of the ECs and pericyte within the microvessel. Pericytes and ECs are separated by a BM and they communicate via Peg-socket junctions and adhesion plaques. Adapted from Armulik et al [21]

1.4.2. Biologic function of pericytes

Understanding the biologic function of pericytes has garnered a lot of interest and an emerging body of evidence points to an essential role of pericytes in regulating vascular permeability. This observation is based on the significant variations in pericyte density in different organs. To illustrate, the central nervous system has the highest pericyte coverage that is pronounced in the blood brain barrier (BBB), while other organs such as kidney and liver are regarded as regions with low pericyte abundance. Since pericyte coverage is inversely associated with vascular permeability in those regions, it is suggested that these cells regulate vascular permeability and contribute to the barrier function [20]. Therefore, the biologic role of pericytes has been intensively studied in the neurovascular unit where mural cells are an essential component of the BBB.

Joyce et al and others described pericytes as contractile cells of the microvascular wall since they abundantly express actin and myosin filaments that are essential for contraction [22, 23]. Owing to their contractile capacity, pericytes regulate vascular permeability via their primary processes that surround endothelial cells. In response to vasoconstrictors, pericytes generate an actomyosin mediated contraction that is enough to alter endothelial/pericyte adhesion leading to pericyte detachment and thus vessel destabilization [24]. Co-culture experiments indicate that pericytes inhibit the growth of endothelial cells in vitro via TGFβ signal, indicating the importance of the spatial proximity of both cell types [25]. On the other hand, pericytes contribute to endothelial migration and proliferation through paracrine secretion of basic fibroblast growth factor bFGF [26]. In response to bFGF, the endothelium produces urokinase-type plasminogen activator which is implicated in angiogenesis, cell migration and proliferation [27]. Additionally, pericytes release Sphingosine-1-phosphate (S1P), a sphingolipid metabolite that binds to the endothelial differentiation gene receptor (EDG) on endothelial cells. S1P signaling promotes the expression of adhesion molecules mainly VE-cadherin and N-cadherin located on the endothelial cells surface that enhances vessel tightness and barrier function [28]. At the same time, loss and gain of function studies suggest that pericyte-derived Ang1 signals to the endothelium via the endothelial Tie2 receptor to initiate vessel maturation and stabilization. Ang1- or Tie2-deficient mice die during gestation due to poor cardiovascular development. These animals develop drastic phenotypes such as functionally defective basement

membrane (BM), impaired angiogenesis, pericyte drop-out and poor pericyte coverage [29, 30]. Finally, pericytes contribute to the BM production through secreting ECM proteins such as laminin, fibronectin, collagen type IV and vitronectin [31, 32]. The BM acts as mechanical barrier to prevent the infiltration of large molecules and malignant cells in cases of tumor [33]. Also, it influences endothelial cell differentiation and migration during angiogenesis [34]. Beyond their contribution to endothelial cell quiescence and microvessel stability, pericytes are implicated in other biological processes such as tissue regeneration and angiogenesis. In a recent study, Bribrair et al. show that the myogenic property of pericytes makes them competent to induce muscle regeneration after skeletal muscle injury [35]. Additionally, they demonstrate that pericytes accumulate in organs such as brain, spinal cord, lungs and kidneys at the sites of lesion suggesting their contribution to tissue repair [36]. Regarding angiogenesis, computational models reveal that pericytes stay in close proximity to sprouting endothelial cells due endothelial VEGF signaling. There, pericytes regulate Notch-DLL4 signal between endothelial 'tip' and 'stalk' cells to direct endothelial sprouting and ensure an adequate endothelial tip/stalk ratio, Figure 4 [37].
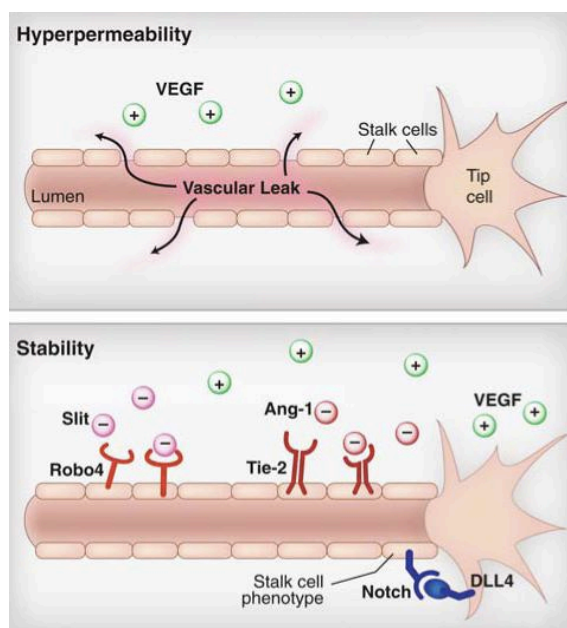
Figure 4: Signaling mechanisms implicated in vascular permeability. The binding of VEGF on the surface of endothelial cells results in hyper-permeability. This effect is counteracted through the coupling of Ang-1 to the endothelial Tie2 receptor. Adapted from London et al [38].

1.4.3. The Endothelium

1.4.3.1. Endothelial regulation of vascular tone

The endothelium is a continuous monolayer that lines the entire vascular system and assists in maintaining efficient blood flow around the body. In response to hemodynamic changes, the endothelium reacts by releasing vasoactive substances that regulate the vascular tone. For example, increased blood flow leads to the secretion of endothelial Nitric oxide (NO) which is a potent dilator of the arteries and also reduces the risk of plaque formation [39]. NO regulates the activity of VSMC where it is taken up via soluble enzyme guanylyl cyclase (sGC) [40]. NO/sGC complex catalyzes the production of GTP from cGMP which in turn induces VSMC relaxation [41]. However, when the blood flow decreases, endothelial cells secret Endothelin (ET), another potent regulator of the vascular tone. ET exists in 3 different isoforms Endothelin (ET-1) ET-2 and ET-3. Endothelial cells exclusively produce ET-1, which exerts its action via the G proteins couple receptors ET_A and ET_B. ET-1 binds to ET_A that is selectively expressed by VSMCs leading to a powerful vasoconstriction that compromises vascular permeability and contributes to local regulation of the vascular tone [42].

1.4.3.2. Endothelium and neovascularization

Besides regulating the vascular tone, the endothelium contributes to vascular development mainly through the angiopoietin-Tie ligand system. Endothelial cells express the Tie 2 receptor tyrosine kinases that have a binding affinity to Angiopoietin Ang 1 [43]. When abundantly expressed, Ang1 couples to Tie 2 receptor facilitating vessel stabilization and counteracting VEGF induced hyper-permeability. Besides, Ziegler and colleagues show that Ang2 competes with Ang1 and acts as its anagonist. Therefore, blocking Ang2 blunts pericyte drop of in peripheral muscles and heart during sepsis phenotype and reduces permeability [44]. VEGF is a potent regulator of vascular permeability. It is produced in hypoxic tissues and promotes endothelial sprouting along a VEGF gradient [45]. However, baseline VEGF secretion is crucial for endothelial cell proliferation and new vessel formation [46]. VEGF signals through the endothelial transmembrane receptor tyrosine kinase receptors denoted as VEGFR1-3. However, it initiates a proangiogenic signal mainly through VEGF receptor 2 (VEGFR2), as has been shown in VEGFR2 KO mice [47].

1.4.3.3. *Endothelial activation during systemic inflammation*

The endothelium is the first line of defense against pathogens and tissue damage. In response to a pathogen associated molecule like LPS, endothelial cells are stimulated via the PRR family of receptors and most notably TL receptors. TLR2 and TLR4 mediate innate immune defense mechanisms via the NF-kB pathway [48]. Notably, NF-kB leads to the transcription of pro-inflammatory cytokines such as IL-6 and adhesion molecules such as, vascular adhesion molecule-1 (VCAM-1), intracellular adhesion molecule (ICAM-1) and E-selectin that attract immune cells to the site of infectious insults [49, 50] a process termed endothelial activation. While E-selectin mediates leukocyte tethering and rolling [51], ICAM and VCAM form adhesion and ICAM-1 directs transmigrating leukocytes between endothelial cells [52]. Moreover, LPS exposure activates TLR4 which ultimately leads to an increased Ca^{2+} influx [53]. Intracellular Ca^{2+} binds to calmodulin and activates myosin light chain kinase (MLK) leading phosphorylation of myosin. This event triggers a cross bridge cycle that results in cytoskeletal contraction and retraction of endothelial cells increasing the trans-endothelial gap [54]. Additionally, Ca^{2+} influx activates protein kinase C (PKC) which is implicated in the VE-Cadherin disassembly and therefore barrier dysfunction [55].

1.5. Loss of barrier function

The endothelium forms a continuous semi-selective barrier for the exchange of fluids and molecules between the blood and tissue. This monolayer is held together by tight junctions, gap junctions and adherent junctions. VE-cadherin is a principle component of the adherens junctions deposited at the sites of contact between endothelial cells and contributes vastly to maintaining barrier integrity. The homophilic adhesion of VE-cadherin between endothelial cells is supported by cytoplasmic adaptor proteins consisting of p120, α and β-catenin. p120 and β-catenin bind directly to the cytoplasmic tail of VE-Cadherin forming an adhesion complex, while α-catenin anchors VE-Cadherin/catenin complex to the actin cytoskeleton. In quiescent endothelium, thick cortical actin bundles cluster at the apical surface of the endothelial membrane producing a mechanical force to maintain the linearity VE-Cadherin deposition, Figure 5 [56].
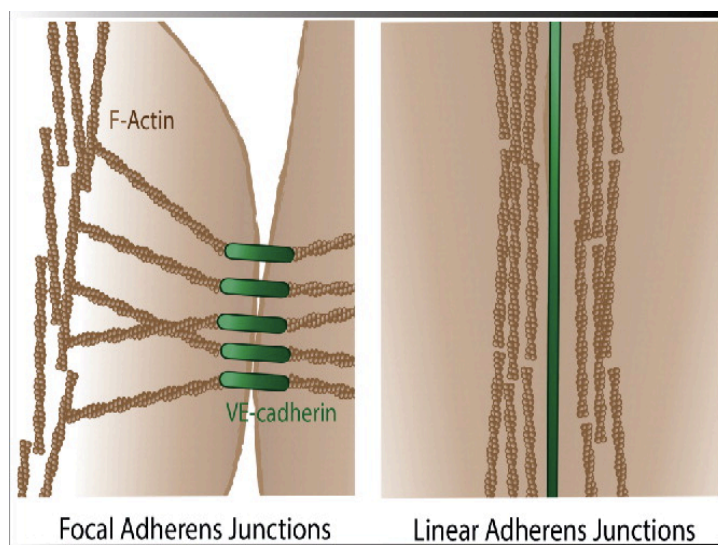
Figure 5: Left: F-actin filaments rearrange in a perpendicular orientation to the radial actin and exert an inward pulling force on the VE-Cadherin to increase cellular gaps and permeability. Right: Cortical actin clusters in close proximity exerting mechanical support the adhesion junctions- Adapted from Van Buul et al.[57]

Under the influence of an inflammatory stimulus, TLR4 activation promotes Src kinase phosphorylation which phosphorylates tyrosine residues of VE-Cadherin and zona occludens which are structural protiens implicated in the stabilization of the endothelial barrier [58]. Once phosphorylated, VE-Cadherin is targeted to ubiquitination and degradation which compromises the structural integrity of the endothelial barrier. Besides, phosphorylation of VE-Cadherin at Tyr [685] blocks the docking site of p120 and β-catenin to its cytoplasmic domain therefore impairing the VE-Cadherin/catenin complex[59]. Of note, the cytoplasmic domain of VE-Cadherin consists of 8 conserved tyrosine residues among which Tyr^{645}, Tyr [731], and Tyr [685] are the phospho-accepting sites[60]. In the light of this observation, Wallez et al. strongly suggest that Tyr^{685} is a unique substrate for Src kinase activity given that point mutation at Tyr [685] prevents VE-Cadherin ubiquitination and internalization in response to bradykinin [59].

The loss of barrier function in sepsis is secondary to pronounced alterations in the actin cytoskeleton orchestrated by Rho family of GTPase. Inflammatory stimuli are transferred mainly through guanosine nucleotide exchange factors (GEF) mediated activation of GDP-bound RhoA to GTP bound RhoA [61]. Activated RhoA mediates the reorganization of cortical actin to contractile stress fibers [62, 63]. RhoA couples with actin binding proteins that affect the rate of actin assembly and disassembly. Given

that Rho kinase (ROCK 1 and 2) are the main substrates for Rho A activity, Rho-ROCK activation promotes the phosphorylation of myosin light chain (MLC) which accounts for the contractility feature of F-actin bundles[64]. The newly formed F-actin bundles influence endothelial cell shape and para-cellular gaps as cells retract from their border during contraction. As observed by Cao et al., stress fibers are peripherally attached to junctional molecules such as VE-Cadherin, therefore upon contraction they exert an inward pulling force driving the disassembly of the adhesion[65]. There are several suggested mechanisms mediating the LPS induced VE-Cadherin downregulation in addition to tyrosine phosphorylation and Rho/ROCK/MLC activation. Wan et al. suggest that LPS induces the production of Urocortin (ucn1), a pro-inflammatory cytokine which triggers the phosphorylation of β-catenin mediated by protein kinase D leading to the dissociation of VE-Cadherin/catenin complex [66].

1.6. Rescuing the microcirculation in sepsis

Pericytes influence endothelial cell migration, proliferation and quiescence via a number of soluble mediators and extracellular matrix proteins [67]. Therefore, pericyte retention in the microcirculation is key to sustain endothelial integrity and function, since pericyte drop out has been frequently observed during sepsis [44, 68]. For this purpose, the following series of studies highlights the involvement of several molecular mediators in enhancing pericyte recruitment during sepsis.

In a pre-clinical study, Kupatt et al. report that a combination of VEGF-A / PDGF-β therapy induces pericyte retention and collateral growth resulting in better perfusion in hibernating pig myocardium and rabbit hind-limbs. Intrestingly, r.AAV transduction of VEGF-A is unable to increase pericytes coverage although it induces irregular capillary network. However, the combination of VEGF-A/PDGF-β transduction results in enhancing neovascularization and better global myocardial function and perfusion (Figure 6) [69]. This indicates that VEGF-A treatment tailors short term neovascularization and angiogenesis, however it is the crucial role of PDGF-β to retain pericytes, stabilize newly formed vessels and inhibit their regression[70].
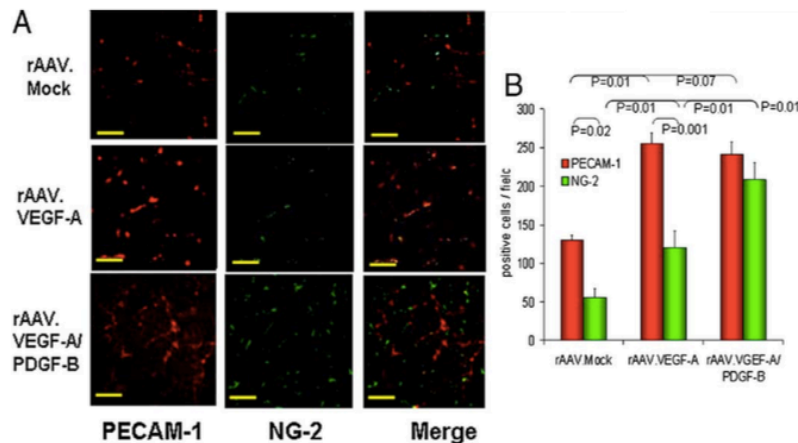
Figure 6:(A) Combination therapy rAAV.VEGF-A/PDGF-β significantly enhances pericyte coverage in the microvascular unit. (B) rAAV.VEGF-A/ PDGF-β transduction is effective in restoring capillary density. Adapted from Kupatt et al [69]

Second, Thymosin beta 4 (Tβ4), an actin binding protein, is shown to be reduced in sepsis and its application reduces inflammation and mortality [71]. Indeed, Tβ4-diffcient mice lack pericyte coverage and display aberrant vascular development [72]. In the light of this observation, Bongiovanni et al. demonstrate that overexpression of Tβ4 promotes pericyte recruitment and prevents hyper-permeability observed in LPS induced sepsis, Figure 7 [68]. Moreover, r.AAV.Tβ4 application ameliorates endothelial cell activation and leukocyte infiltration. One possible explanation is that Tβ4 peptide treatment retains G-actin in the cytosol thus freeing Myocardin Related Transcription Factor-A (MRTF-A) from its G-actin bound state. Unbound MRTF-A translocate from the cytosol to the nucleus and activates serum response factor (SRF) target genes , which are potent angiogenic factors [73]. Indeed, coactivtion of SRF with MRTF-A induces the activation of proangiogenic genes such as CCN1 and CCN2. While of CCN1 promotes capillary growth, CCN2 enhances pericyte retention and vessel maturation [74]. These studies elucidate a significant pathway tailored to enrich for pericyte retention, which proves to be efficient in restoring capillary function during systemic inflammation.
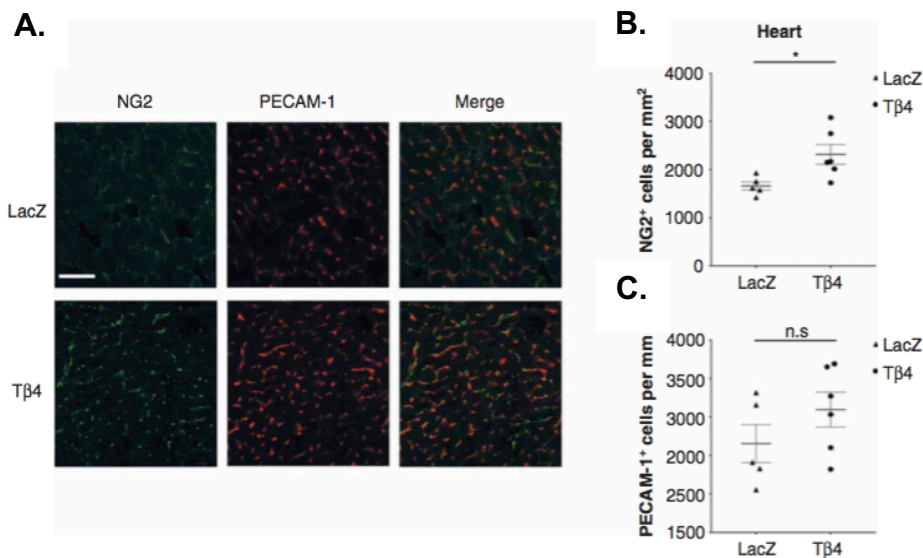
Figure 7: (A) rAAV.Tβ4 transduction ameliorates pericytes loss during LPS induced sepsis as compared to LacZ controls. **(B+C)** Quantification analysis reveals a significant increase in the NG2 and PECAM-1 positive cells correlating to endothelial cells and pericytes. Adapted from Bongiovanni et al.[68]

Equally important is the Ang1/Tie 2 signaling cascade that is shown to preserve the microcirculation in sepsis and attenuates pericyte loss [44]. As described previously, pericytes secrete Ang1, a ligand for endothelial Tie2 receptor to maintain endothelial quiescence [30]. On the other hand, endothelial expression of Ang2 antagonizes Tie2 and induces hemodynamic alterations. Ziegler et al observed that overexpression of Ang1 or PDGF-β is effective in restoring vessel stability and reducing capillary leakage observed in the Ang2 overexpressed mice, Figure 8 [44]. A growing body of evidence suggests that PDGF-β rescues the microcirculation by promoting the binding of pericytes to the ECM. Indeed, transgenic mice strain lacking PDGF-β display an impaired investment of pericytes and severe microvascular defects [75]. Taken together, these series of studies suggest that pericyte investment in the vascular wall could be a potential therapeutic approach to circumvent capillary rarefaction and hemodynamic dysfunction observed in systemic inflammation.
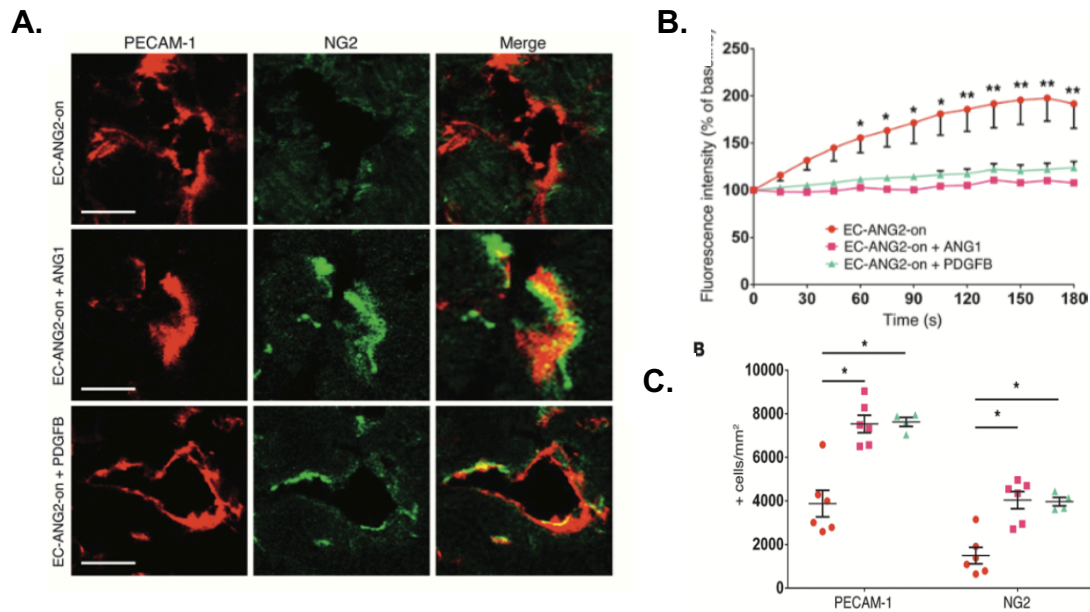
Figure 8:(A+B) Ang2 overexpression (ANG2-on) reduces pericyte coverage (NG2 positive cells) of capillaries (PECAM-1). Treatment with Ang1 or PDGF-β ameliorates pericyte reduction. **(C)**Transduction with rAAV.ANG1 or rAAV.PDGF-β results in decrease vascular leakage in the ear vasculature of EC-ANG2-on animals. Adapted from Ziegler et al. [44]

1.7. Current therapeutic approaches and challenges

Despite advances in its treatment the mortality of sepsis is still high due to hypotension, refractory multi-organ failure and poor perfusion. In the management of sepsis, early administration of treatment is paramount. Early administration of antimicrobial therapy (within the first 6 hours) has been shown to ameliorate severe complications and decrease mortality. Therefore, the concept of early detection and resuscitation has been described as the 'Golden hour 'and 'The silver day' [76]. A recent retrospective analysis study reveals that during the early stages of sepsis a one hour delay in administering therapy is sufficient to increase the risk of mortality in patients by 7.6% [77]. Additionally, early selection of a specific antimicrobial treatment is crucial in enhancing survival. This requires sensitive and selective detection of the micro-organism. However, the current microbiologic techniques to screen micro-organisms lack specificity leading to unsuccessful antimicrobial therapy and poor prognosis [78].

The classical clinical interventions during sepsis include intravenous administration of 20mL/Kg of saline or crystalloid since septic patients experience drop in systemic blood pressure [79]. When diagnosed with severe sepsis, patients may receive transfusion of blood products if the hemoglobin levels drop below 7g/dl to main an

adequate oxygen supply to the organs. After fluid loading, the introduction vasopressors such as epinephrine or norepinephrine may be administered as a second line treatment in cases of a severe drop in the mean arterial pressure [80]. Although pharmacological intervention using dopamine and adrenaline infusion increases cardiac output and oxygen delivery, some studies call for the re-evaluation of vasopressor infusions due their adverse metabolic side effects [81]. Despite decades of research and significant clinical endeavors, there are still no major breakthroughs to improve the patient outcome in sepsis.

1.8. Modulating the immune system

Up to date, the search for an adequate immune modulatory therapy remains a clinical necessity. Although more than 100 randomized clinical trails have investigated the immunomodulation rationale, none of them resulted in a new treatment. Due to discouraging history of anti-inflammatory treatments, these clinical trails are referred to as the 'graveyard' for pharmaceutical companies [82]. However, all the clinical attempts share a common ground that might explain their inefficacy. To start with, the inadequate timing of intervention can predict poor outcome of the disease. For example, anti-cytokine treatments have failed because patients enlisted in these studies have already established sepsis. Cytokines exhibit short half live and their levels peak within 24 hour post infection resulting in a 'cytokine storm', a hallmark feature of sepsis. Therefore, cytokine therapy such as Il-1 and Il-6 antagonists failed in treating septic patients[83]. Amid complex immune response and activation of overlapping layers of pro-inflammatory pathways, targeting a single modulator may be ineffective. Also, the heterogeneity of the patient population represents another crucial problem for immune therapy in sepsis. Septic patients are of diverse age ranges, underlying health conditions and different stages of the disease. Additionally, the immune response gets modified within in the same patients in different disease stages. Therefore, small pilot studies that showed to be effective within a narrow pool of patients often fail to be recapitulated in large scale phase III clinical trails [84]. Finally, the lack of accurate animal models to study the immune response adds another layer of complexity to establishing an immune therapy in sepsis in patients. Immune modulation therapy to combat sepsis is still an essential clinical demand. However, there should be an increasing emphasize on restoring the physiologic capillary

function since the cytokine storm results in severe damage in capillary damage and a disintegration of the microcirculation.

1.9. Sphingosine- 1- phosphate as a potential treatment

It has been shown that plasma S1P levels decrease in septic patients which makes it potential therapeutic target to restore vessel homeostasis and retain endothelial function. In a recent clinical study, Winkler et al. identified S1P as a surrogate marker of sepsis and suggested that its reduction results in capillary leakage and endothelial dysfunction [85]. Coldewey et al. recapitulated this observation and additionally showed that reduction of plasma S1P levels in septic patients and murine models of sepsis is associated with impaired cardiac systolic function. This study provides a proof of concept that administering S1P reduces cardiac dysfunction and results in a better outcome [86]. Therefore, S1P emerged as a therapeutic approach to overcome vascular and cardiac aberrations in sepsis.

1.9.1. Sphingosine-1-phosphate (S1P)

Sphingosine-1-phosphate (S1P), a lipid metabolite, is the end product of the sphingomyelin metabolism. Sphingomyelin is catalyzed by sphingomyelinase to generate ceramide that is further broken down via ceramidase into Sphingosine and a free fatty acid. Sphingosine kinases (S1Pk1 and S1Pk2) phosphorylate sphingosine to catalyze the production of S1P. In contrast, S1P is broken down to sphingosine by S1P phosphatase or by S1P Lyase to produce hexadecenal and phosphoethanolamine [87]. Once produced, S1P is transported by spinster 2 which is involved in the extra cellular release of S1P [88]. S1P levels are highest in the plasma (1uM) and lowest in the interstitial fluid (100nM) [89]. In the circulation, S1P is bound either to HDL(50%) or albumin (40%) [90]. A growing body of evidence suggests that in addition to platelets and erythrocytes, endothelial cells are also geared toward S1P secretion.

Endothelial cells are identified as the non-hematopoietic source of the plasma S1P levels. Studies reveal that irradiated S1Pk triple allele knockout mice denoted as S1Pk (3N) exhibit normal levels of S1P after receiving a wild type bone marrow transplant, the source of hematopoietic cells. However, bone marrow transplant from the S1Pk (3N) mice into WT mice maintained normal plasma level of S1P indicating a non-hematopoietic origin of S1P. Further on, gene analysis assay validates the

involvement of endothelial cells in the production of S1P via S1Pk dependent manner [91]. Additionally, the metabolism of sphingolipids by erythrocytes reveals that S1P is constantly secreted by RBC to the extracellular milieu in a stimuli independent manner. Interestingly, these cells lack the enzymatic machinery to break down S1P such as S1P lyase and S1P phosphohydrolase suggesting their role in constant plasma supply of S1P [92].

1.9.2. S1P receptor signaling

Once produced, S1P exerts its physiological function upon coupling to cell surface G proteins coupled receptors known as endothelial cell differentiation gene (EDG) receptors or sphingosine-1-phosphate receptors (S1PR). S1PR1-3 are distributed widely in all tissues, whereas S1PR4 and S1PR5 are predominantly expresses in lymphoid vessels and nervous system [93]. S1P couples with a G-protein subunit (Gαi, Gαq/11,or Gα12/13), inducing various intracellular signaling events leading to platelet activation, cytoskeletal rearrangements and enhanced barrier function [94]. Here, the focus is on S1PR1-3 since these are abundantly expressed in endothelial cells.

S1PR1 is expressed in endothelial cells and it was first described in 1998 as a potent regulator of vascular tone [95] and cortical actin assembly [96]. Besides, S1PR1 signaling is implicated in angiogenesis and embryonic development. Indeed, double null/mutant mice for S1PR1 display impaired vasculogenesis due to a malfunction receptor signaling which halts embryonic development. S1PR1 KO mice display the highest frequency of hemorrhage and death compared to other S1PR KO animals [97]. Unlike S1PR1, S1PR2 couples to several G proteins such as Gi/o, Gs, Gq, and most potently to the G12/13 thereby activating of the RhoGTPase signalling cascade [98]. S1PR2 is the second cloned S1P receptors from rat aorta in 1993 and was initially referred to as EDG-5 [99]. Endothelial cells overexpressing S1PR2 show a disturbed VE-Cadherin localization. This phenotype is coupled with the activation of Rho-ROCK pathway and actin cytoskeletal rearrangements tailored to increase permeability. Additionally, S1PR2 is implicated in the phosphorylation of VE -Cadherin resulting in a disruption in the endothelial barrier [100]. While S1PR2 induces vasoconstriction, ex vivo studies show that S1P3 mediates HDL bound S1P vasodilation. The vasodilation effect is entirely dependent on the endogenous NO production [101]. Consistently, Forrest et al. show that S1P elicits a transient reduction in mean aterial pressure in WT mice but not in S1PR3 KO animals indicating the involvement of S1PR3 in involvement of in

blood pressure regulation [102]. Of note, S1PR1,2 and 3 orchestrate their functions during early embryogenesis since double null (S1PR2 and 3) and triple null (S1PR1,2 and 3) embryos result in impaired vasculogenesis [97]. This indicates that the impact of S1PR signaling in the vasculature remains poorly understood, Figure 9.
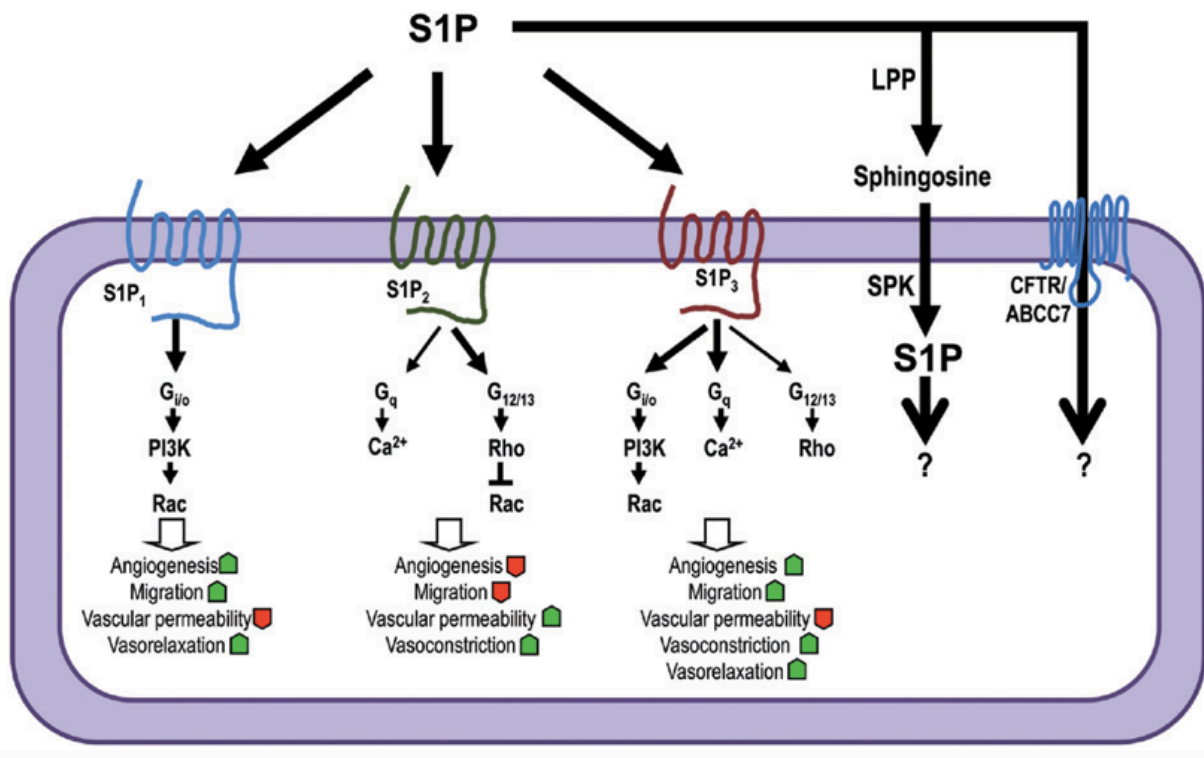
Figure 9: Three out of the five subtype S1P receptors are expressed by endothelial cells(S1PR1-3) mediating the pleiotropic effects of sphingosine-1-phosphate on the vascular wall. Upon binding to S1P, S1PR1,2 and 3 couple with a G protein to initiate downstream signal transduction regulating angiogenesis, migration, permeability and vascular tone. Adapted from Weaber et al.[103].

1.9.3. Physiologic functions of S1P

Functionally, S1P has been shown to regulate the vascular tone upon inducing eNOS activation[104]. Indeed, the intra-arterial administration of the S1P reduced the mean arterial blood pressure and induces NO production via S1PR3 in an Akt dependent signaling mechanism [101]. S1P has been used as a therapeutic approach in several disease model to address vascular leakage. Peng et al. show that administration of the S1P analogue, FTY720, ameliorates LPS induced leakage in acute lung injury at 6 and 24 hour post LPS injection [105]. Furthermore, the S1P signaling axis is implicated in regulating immune function and ameliorate immune cell trafficking during the course

of anaphylactic shock. In fact, increased endogenous S1P production in anaphylactic mice resulted in enhanced histamine clearance from the blood and lowered cytokine production [106]. Besides, *in vitro* experiments confirm that treatment of endothelial cells with S1P increases the trans-endothelial electric resistance through promoting junctional formation which correlates to the barrier integrity. That is because it induces the localization of adhesion proteins such as VE-Cadherin, PECAM, JAM and Claudin5 to the sites of endothelial junctional regions. The notion by which S1P enhances the barrier functions is mediated by the redistribution of ZO-1 to the sites of tight junction formation, a mechanism that is mediated by the G_i/Akt/Rac pathway [107]. In light of this observation, Mehta et al. showed that S1P induces Ca2+ release from the ER which is prerequisite for Rac activation and junction assembly [108]. Additionally, S1P modulates permeability in microvessels upon inhibiting the rearrangement of VE-Cadherin and occluding and enhancing the formation of cortical actin to stabilize the junctional complex in vivo[109]. Unfortunately, the intravenous administration of S1P is challenging due to its short half-life [110]. So, the FDA approved a functional agonist of sphingosine known as Fingolimod (FTY720) which is show to be effective in the treatment for relapsing and remitting multiple sclerosis [111]. In fact, FTY720 is phosphorylated by sphingosine kinase in endothelial cells which induces adherent junction arrangement along the endothelial border. It has been shown that FTY720 counteracts the effects of VEGF induced vascular permeability as it is implicated in the regulation of angiogenesis and controlling barrier function in sepsis[112]. Together, these studies highlight the fundamental role of S1P as a potent regulator of endothelial cell junction in the microvascular unit.

2. Objectives

In the light of these findings, we hypothesize that Sphingosine-1-phosphate exerts a critical role in antagonizing microcirculatory disassembly and subsequent circulatory aberrations in vivo.

Therefore, the objective of this work is to:

1. Determine the effect of S1P on adhesion protein trafficking (VE-Cadherin and N-Cadherin) in the mouse model of sepsis and *in vitro*
2. Elucidate the signaling mechanism underlying LPS induced downregulation of VE-Cadherin
3. Determine whether S1P is capable of antagonizing LPS- mediated cytoskeletal rearrangements
4. Investigate the involvement of RhoA in cytoskeletal remodeling
5. Determine the influence of actin remodeling on MTRF-A cellular localization and highlight the role of S1P on MTRF-A activity

3. Materials and Methods

3.1. Animal model of LPS induced sepsis

Systemic inflammation was induced in C57BL/6J mice from Charles River using 20 mg/kg of LPS from *E. coli* (L2880, Sigma-Aldrich). To investigate the therapeutic effects of S1P on LPS induced sepsis, animals were injected intraperitoneal with (20mg/kg) S1P or PBS 12 hours before the systemic induction of sepsis to prime endothelial cells and induce maximum responsiveness. Animals continued receiving S1P every 12 hours after LPS injection.

Hemodynamic and vascular readouts were performed at different times points. First, permeability was assessed at 6 hours and non-invasive blood pressure measurement was performed at 12 and 24 hours. Blood plasma samples were taken at 12 hours for Il-6 measurement. Severity of sepsis was assessed using a score assay system at 12 hours post induction of sepsis and continued every 12 hours, Figure 10.
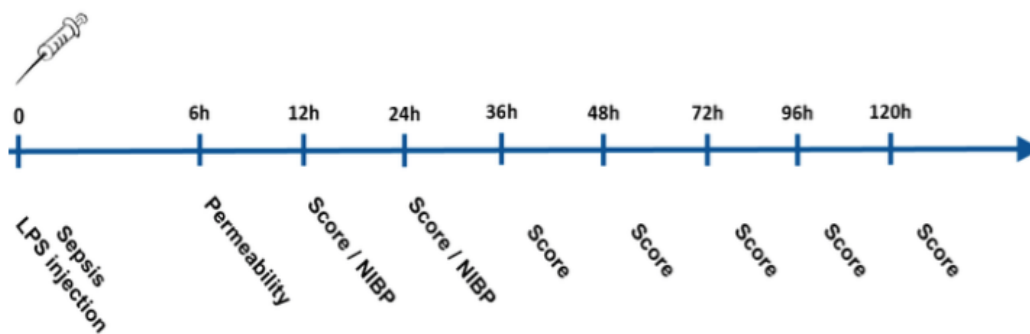
Figure 10: Time line chart represents the experiments performed at different time points post LPS injections in C57BL/6J mice. Animals were pretreated with PBS or S1P before induction of sepsis. 6 hours post LPS injection permeability was assessed. Blood pressure were performed at 6 and 12 hour and score was assessed every 12 hours.

3.2. Score Assay

After the onset of sepsis, endotoxemia severity was assessed in a blinded fashion as represented in the timeline above. This assessment is based on the following parameters behavior, weight loss, ascites, dysponea and pain. A score of 20 or higher was equated with the death of the animal.

points	0	5	10	20
behaviour	normal movement of the mouse in the cage, regular escape reflex	movement slowed down, mouse still moving on it's own	no movement on it's own, tipping on mouse results on movement	mouse comatose / apathetic
weight loss	0 - 5 %	5 - 10%	10 - 15%	> 15%
ascites	none	mild	moderate	severe
dyspnoea	none	mild	moderate	severe
pain	no signs of pain	mouse with bent back, impaired cleaning behaviour	mild change in walking pattern, shivering	severe change in walking pattern, shivering

Figure 11: A point system is used to assess the severity of sepsis in which points between 0 and 20 are classified in 5 categories. Experiments on animals scoring 20 or more are immediately terminated.

3.3. Anesthesia and antagonism

Mice were anesthetized using a mixture of midazolam, medetomidine and Fentanyl (MMF). This procedure was performed intraperitoneal prior to permeability assessment and blood pressure measurement. The animals were weight and the corresponding dose of anesthesia was determined as represented below:

(MMF)mixture	Medetomidin	Midozolam	Fentanyl
mg/ml	1	1	0.05
ml	0.5	5	1
mg/kg KG	0.5	0.005	0.005

At the end of the experiments, the effect of MMF mixture was counteracted by an antagonist mixture. Since the anesthetic exhibit a longer half-life than the antagonist, it was injected 2/3 intraperitoneal and 1/3 subcutaneously depending of the animal's weight as represented:

Antagonist	Atipamezol	Flumazenil	Naloxone
mg/ml	5	0.1	0.4
ml	0.5	5	3
mg/kg KG	2.5	0.05	1.2

3.4.   Permeability measurement

Permeability was measured in mouse ears using a 2-photon laser scanning microscope (LaVision biotech) with a single point scanning mode. Prior to imaging, the mice were sedated as describe in chapter 2.3. and the mouse ear was placed on the microscopic stage orthogonal to the optical axis. A defined area of the mouse ear was determined using a second harmonic generation signal of collagen (447/60 –nm filter). The initial data points were recorded with a 200× 200 × 36 μm 10 planes stacks in a 15 second increments for 5 minutes. Then, a PBS dilution of 750ug TRITC-dextran (T1037, Sigma-Aldrich) was injected in the tail vein and measured at 580/560 nm. Data analyses was performed by recording the mean gray values (MGV) of 3 areas adjacent to the vessel of size 100 $μm^2$. The intravascular fluorescence was measured at 3 times in the range of 15-45 seconds after in the TRITC-dextran injection. T_0 was defined as the time of 100% intravascular fluorescence. The rest of MGVs were calculated as a percentage of the starting point. Images were quantified using ImageJ software (W.S. Rasband, US National Institutes of Health, http://imagej.nih.gov/ij/).

3.5.   Non-Invasive Blood pressure measurement

Non-invasive blood pressure measurement was performed at 12 and 24 hours post LPS injection using a measuring system for rodent. Mice were anesthetized and the volume pressure was recorded by a recording cuff called the VPR cuff which is connected to an occlusion cuff at the root of the mouse tail. While measurement, the occlusion cuff tightened and contributed to building up the pressure to stop the blood flow in the tail. Then the pressure was released to allow the blood to flow back which

was recorded by the VPR. Using this system and its software, the systolic, diastolic and mean arterial pressure were determined. The noninvasive blood pressure measurement was performed using the CODA-2 system.

3.6. Organ removal and specimen analysis

After terminating the experiments, murine hearts were immediately removed and cut into smaller pieces on dry ice. The tissues were embedded using embedding media for frozen tissue and sectioned into a 7μM thickness slides using Leica Cryostat, CM1850. Frozen blocks were stored at -80°C.

3.7. Il-6 serum measurement

The Il-6 ELISA kit purchased from abcam was used to measure the serum Il-6 levels in mice. First blood was withdrawn from animals and centrifuged at 4°C for 15 minutes. The plasma was collected and the samples were prepared and diluted as instructed. The standard curve and the samples were added in duplicates (100 ul) to the Il-6 plate and incubated at room temperature for 2.5 hours on a shaker. The solution was later discarded and the wells were washed with the supplied washing buffer. Later, 100 ul of the biotinylated Il-6 detection antibody was added to each well and incubated for 1 hour at room temperature. The solution was discarded and the washing steps were repeated. Finally, 100ul of the one step substrate reagent was added into each well and incubated for 30 minutes at room temperature in the dark. The reaction was stopped using 50ul of stop solution and the absorbance was measured at 450 nm. The absorbance for the standard curve and the controls was calculated and a standard curve was plotted. Finally, the sample concentration was determined and multiplied by the dilution factor.

3.8. Histology

Heart samples from control, septic and treated mice were analyzed for capillary density using PECAM-1 and NG2 antibodies to detect endothelial cells and pericytes respectively. Additionally, the expression of VE-Cadherin and N-Cadherin in heart sections was assed histologically. Frozen section were thawed at room temperature for 10 minutes and fixed for 15 minutes with 4% paraformaldyhyde solution. Then, section were rinsed twice with PBS and permeabilized with permeabilization buffer for 10 minutes. Later blocking buffer was added for 1 hour at room temperature (refer to buffers section). Then sections were incubated with primary antibody in blocking

solution overnight at 4°C . Prior to incubation with secondary antibody, slides were washed 3 times with PBS and secondary antibodies diluted in blocking solution were added at room temperature for 1 hour. Finally, the slides were washed 3 times with PBS and mounted with DAPI.

3.9.   Primary cell culture of Mouse Lung endothelial cells (MLECs)

3.9.1. Lung endothelial cells isolation

Mouse lung endothelial cells were used as a second line of endothelial cells in addition to the commercially available bEnd3 cells. Cells were extracted from 8 week old C57/BL6 wild type (WT) mice and cultured till the fifth passage. The lungs extraction procedure was performed in a sterile environment. First mice were sacrificed using cervical dislocation and each lung was removed and kept in 5 ml biotech solution on ice until the end of the sacrifice procedure. Then, lungs were put in 10 cm plate inside the laminar flow hood and minced into small pieces using disposable scalpel blades. The minced tissue was then incubated in pre-warmed dispase solution to allow digestion and left at for 1 hour in a shaking water bath. Of note, each lung was digested in 5 ml dispase solution. After 1 hour, the digested organs were homogenized mechanically using 2.5 ml pipet and passed through a 70uM cell strainer in a 50 ml falcon tube. The strainer was washed with 5ml media and the solution in the 50 ml falcon tube was transferred into 10 ml falcon tubes and centrifuged for 5 minutes at 1200 g. This allowed for better collection of the pellet. Then, the supernatant was removed and the cells from each lung were incubated with the 4ul beads diluted in 500 ul 0.5% Hanks buffer for 1 hour on a shaker (refer to beads coating section). After 1 hour, the cells/bead mixture were re-suspended to prevent cells from clustering. After incubating of cells with VE-Cadherin coated magnetic beads, coated cells were purified using a magnetic bar. Then captured cells were washed 3 times with 0.5% hanks solution using magnetic bar. This bar hold 0.5 ml tubes and the cell/bead mixture got trapped on the wall of the tubes once inserted into the bar. After each wash the tubes were left 2 minutes in the magnetic bar to allow the capturing of all the coated cells and then the supernatant was discarded. After the final wash the cells from each lung were re-suspended in 250 ul 20% DMEM(1X)/F12 media mixture (refer to Media section for details) and plated on 24 well-plates coated with 1% gelatin. During the first 2 passages, cells were cultured in 20% DMEM(1X)/F12 media mixture. At the third passage, the media was switched to 10% DMEM/F-12 (1X). The media was changed

24 hours later and the cells were split in a 1:1.5 ratio until the third passage. Prior the first passage, cells were purified again in a 'clean up' procedure as described below to obtain a relatively pure endothelial population. Then MLECs were propagated in a 1:2 ratio until the fifth passage. After the third passage, cells were either propagated or frozen.

3.9.2. Beads coating

Magnetic coated beads were purchased from Invitrogen and used to coat primary endothelial cell in the MLEC isolation protocol. For every lung, 4 ul of beads were diluted in 500 ul 0.5% Hanks buffer and washed 3 times with 0.5% Hanks buffer. After every wash, the tubes were inserted into the magnetic bar and the beads were collected on the wall of tubes. Meanwhile the washing buffer was aspirated and the beads were washed again . This step was repeated 3 times to wash out the Sodium Azide that is present in the originally supplied beads buffer. Then the beads were re-suspended with of Hanks buffer without Mg^{2+} and Ca^{2+}. The volume hanks buffer added was 4ul/lung and the beads solution was later incubated with the anti VE-Cadherin antibody purchased from BD Pharmingen™. After the final wash, the beads were re-suspended in an equal volume of hanks solution without Mg^{2+} and Ca^{2+} and incubated with anti-VE-Cadherin antibody. The antibody was diluted in a 1/6 ratio of the beads volume and incubated for 1 hour at the shaker in the dark .

Finally, the beads/ antibody solution was washed 3 times with 0.5% hanks buffer and the beads were collect using the magnetic bar as described in the washing steps above. Finally, beads were diluted (4:500 ul in 0.5% hanks solution) and this mixture was incubated with a cell pellet collect from one lung.

3.9.3. Plate coating and cell plating

Cells extracted from every lung were plated in one well of a coated 24 well plate. Prior to plating, the 24 well plate was coated with 1% autoclaved bovine gelatin and incubated at 37ºC for 1 hour. Then the wells were washed 3 times with PBS and 250 ul of the cell suspension was added in addition to 250ul media.

3.9.4. MLEC Clean up

Prior to passaging the cells, MLECs were purified again using VE-Cadherin coated magnetic beads to ensure high yield of pure endothelial cell population. To start with, 4 ul of beads/ lung or 4 ul beads/ 1 well of a 24 well plate dilutions were prepared. Beads were washed 3 times in 0.5% Hanks buffer to remove the sodium azide present and the beads were later collected via the magnetic bar as described in the section above. After the final wash the beads were re-suspended in an equal volume of Hanks buffer without $Ca2^+$ and $Mg2^+$ and incubated with anti VE-Cadherin antibody purchased from BD Pharmingen™. The volume of VE-Cadherin antibody that was added was fifth the volume of Hanks solution. The beads and antibody were incubated at room temperature for 1 hour on the shaker. After the incubation period the beads were washed 3 times and collected with the magnetic bar as described above. Then the beads were re-suspended in 300 ul of 0.5% Hanks buffer/well. Meanwhile, cells were washed with PBS and each well was incubated with 300 ul of 0.5% Hanks buffer coated beads solution for 30-40 minutes at room temperature in the dark. Finally, the beads were washed off and the cells were washed with PBS prior to passaging.

Trypsin was added (500 ul/well) and incubated for 5 min at 37 °C. The de-attached cells were collected with 10% DMEM/F-12 (1X) media. The cell suspension solution was centrifuged at 1000 g for 4 minutes and MLECs were split at 1:1.5 ratio and plated on a 1% gelatin coated plates.

3.10. Cell culture method

Commercially available endothelial cell lines (bEnd3, ATCC, USA) were purchased as used as a second line of cells . bEnd3 were seeded on 10 cm plates and grown in complete Dulbecco's Modified Eagle's Medium (DMEM supplemented in with 10% fetal calf serum FCS and 1% penicillin). Cells were left to reach 80% confluency before seeding for an experiment. Before splitting the plate was washed twice with PBS incubated with 2 ml trypsin was for 5 minutes at 37 °C. Later, 8 ml of the complete DMEM to collect the cells and centrifuged at 1000g for 5 minutes. The media was aspirated and the pellet was re-suspended in complete DMEM and split at a ratio of 1:10 to propagate the culture.

Likewise, pericytes (CCL-226/C3H/10T1/2 Clone8, ATCC, USA) were purchased and used according to the manifacturer's instructions. Cells were grown in complete Eagle Basal medium (MEM) supplemented in with 10% FCS and 1% penicillin. Cells were grown in T75 flasks and split in similar manner as described above using complete Eagle Basal medium instead. Cultures were maintained in complete medium and incubated at 37°C in a humidified atmosphere of 5% CO_2.

3.11. Cell culture model of LPS induced sepsis

Endothelial cells and pericytes were grown in complete media at a confluency of 200.000 per 6-well plates for Rho ELISA and SDS-PAGE experiments. Prior to the experiment cells were starved overnight with starving media (cell line specific media with 0.2% FCS and 1% penicillin). Treatments of either LPS, S1P or its agonist were diluted in starving media and incubated for a desired a time point (5,10,15 or 30 minutes.) The experimental groups were divided as follow: A control group receiving only starved media, a treated group with LPS, and a treated group with LPS+ 1μM S1P receptor agonist.
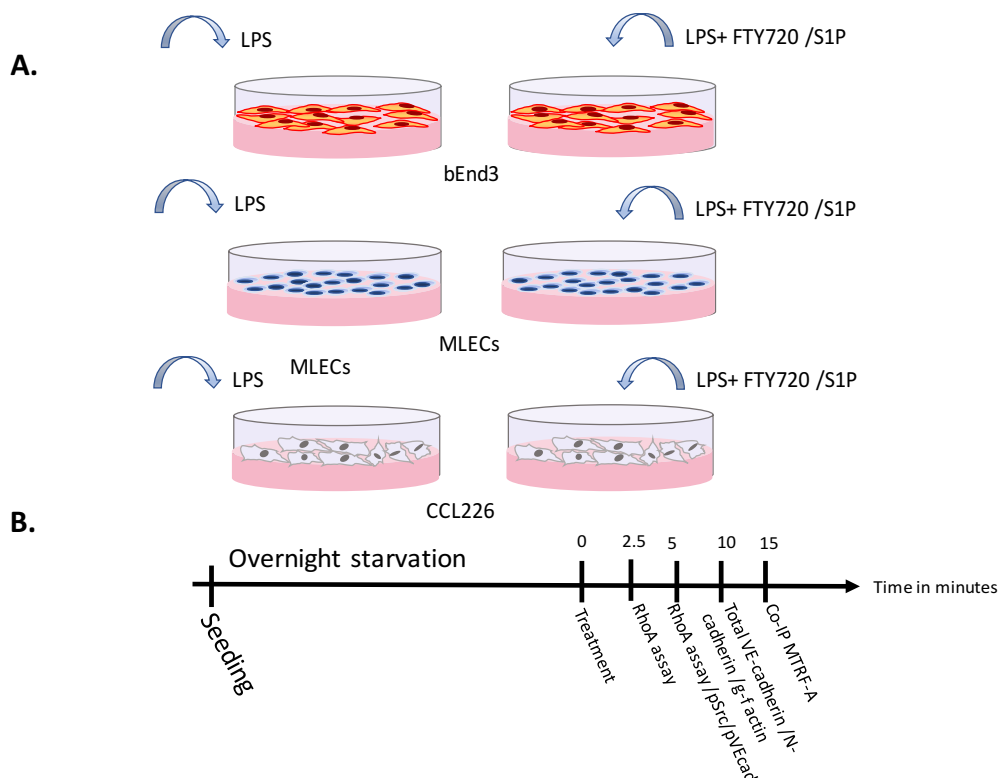

Figure 12: (**A**) The Cell culture model of sepsis consists of endothelial cells (MLECs or bEnd3) and pericytes (CCL-226) treated with LPS and FTY720 or S1P. (**B**) Performed Cell culture assays are RhoA ELISA, Western blot, Co-immunoprecipitation(IP) at different times of treatment.

3.12. Protein extraction and quantification

Prior to the experiment cells were starved in a 0.2% DMEM medium overnight. Cells were treated according to a desired time point. After treatment cells were lysed in 200 ul RIPA buffer purchased from sigma. Then, lysates were homogenized and centrifuged at 4000 g for 5 minute and the supernatant was collected. The protein concentration was determined according the Bio-Rad Assay kit. 8 ug of the lysates was mixed with 1X DTT and boiled at 95°C for 10 minutes. The samples were either stored at -80 °C or processed for SDS-PAGE.

3.13. Immunoprecipitation of MRTFA

For MRTF-A immunoprecipitation, $1x10^6$ cells were seeded in 10 cm plates and treated for 15 min. The crosslinking of amino groups to form stable amide bonds was performed using disuccinimidyl substrate (DSS) purchased from Thermofisher. DSS was dissolved in DMSO to a final concentration of 10mM and diluted to 1mM in PBS prior to the experiment. After treatment, cells were cross linked with a the DSS solution and the reaction mixture was incubated for 30 minutes at room temperature. Then 20 mM of Tris solution was added to quench the reaction. The quenching reaction was incubated for 15 minutes at room temperature. Then, cells were washed 3 times and lysed in 1 ml lysis buffer with protease and phosphatase inhibitors. Lysates were homogenized using U-40 insulin needles and centrifuged for 10 min at 13.000 rpm. After determining the protein concentration as described above, 500 ug of the sample was incubated with 5ul of the anti-Actin antibody for 1 hour at 4°C. Meanwhile, the protein agarose beads were washed 3 times with the lysis buffer and centrifuged for 2 min at 4.000 rpm. After 1 hour, samples were incubated with the beads at 4°C and left overnight. Next the mixture of beads and sample was washed 3 times with lysis buffer and centrifuged at 4.00 rpm for 2 minutes. The final wash was done with PBS and the supernatant was replaced with RIPA buffer. Finally, samples were boiled at 95°C for 10 minutes and loaded on 10% SDS- polyacrylamide electrophoresis gels or stored at -80°C.

3.14. G/F Actin

To assess the G/F actin ratio, $2x10^5$ cells were seeded in 6-well plates. Prior to the experiment cells were starved in a 0.2% DMEM medium overnight. The cells were treated for 10 min as described above. After treatment, endothelial cells were incubated with 1mM DSS solution (1ml/ well) for 15 minutes at room temperature. Then Tris solution was added to quench the reaction for another 15 minutes. Then the wells were washed twice and 200 ul of lysis buffer was added to each well. The samples were then processed for western blot as described below.

3.15. SDS-PAGE

The lysates were resolved on 10% SDS- polyacrylamide electrophoresis gels (SDS-PAGE). Then, the proteins were electro-transferred to a methanol pre-activated PVDF membrane for 90 minutes at 250mA. The membranes were then blocked and incubated against primary antibody overnight at 4°C in TBST buffer . All the primary antibodies were diluted 1:1000 in 5%TBST solution. Likewise, secondary antibodies were diluted and incubated for 1 hour at room temperature. Finally, chemiluminescence was added on the PVDF membrane according to the manufacturer's protocol.

3.16. RhoA activity

3.16.1. RhoA G-LISA

Rho A activity was measured using a luminescence based G-LISA Rho A activation assay kit (BK#121, cytoskeleton, Inc., Denver, CO) according to the manufacturer's instructions. Briefly, bEnd 3 cells were seeded in 6 well plate and starved overnight in starving media prior to stimulation. Then cells were challenged with 10ug/mL LPS for the following time points 0, 2.5 and 5 minutes in the presence and absence of S1P agonist, FTY720. Briefly, this assay employs a 96 well plates coated with Rho GTP binding protein. Cell lysates containing GTP-bound Rho A will bind to the plate while the inactive GDP-bound Rho A will be washed out during the washing steps. The active GTP bound Rho A will be detected with a specific Rho A antibody followed by secondary HRP. Prior to the end of the secondary antibody incubation, HRP detection reagent was added after which the absorbance was measured at 490 nm using a microplate spectrophotometer. The samples were prepared as follows. Cells were washed with ice cold PBS and lysed with the supplied lysis buffer and protease

inhibitors (1:100). The lysates were homogenized by centrifugation at 10,000 X g, 4°C for 1 minute.

The protein concentration was determined according to the protocol and the lysates were Snap-frozen in 100ul aliquots until they were processed according to the manufacturer's manual. The samples concentration was equalized to 1 mg/ml using ice cold lysis buffer. Then, the samples were plated on the supplied 96 well plate and placed at 4°C at 400 rpm. After 30 min, the primary antibody was removed and the plate was washed 3 times before adding the secondary antibody for 45 min followed by the HRP detection reagent for 10-15 min at 37°C. The absorbance was measured using a spectrophotometer at 490 nm using a microplate spectrophotometer. The absorbance was corrected for the background absorbance by subtracting the reading from a blank well at 490 nm.

3.16.2. Total RhoA

Cell extracts prepared for the RhoA G-LISA (Cat# BK124) were used to determine the total RhoA ELISA assay (Cytoskeleton, BK150). Accordingly, cell lysates were thawed at room temperature and 24 μL of each sample was plated on the 96 well RhoA binding plate at room temperature for 2 hours. After 3 washes, the primary RhoA antibody was added in a 1:2000 dilution and incubated for 1hour at room followed by 3 washes. The RhoA levels were determined using a horseradish peroxidase(HRP) conjugate secondary antibody system that was provided similar to the one described above and absorbance was measured at 490mn. The ratio of active Rho A to the total RhoA determined the percentage of the active RhoA.

3.17. Immunofluorescence

Cells were harvested and seeded at a low density onto cover slips pre-coated with 1% gelatin solution for 1 hour. Cells were starved and treated for 10 min as described. Then, cells were fixed with 4% PFA for 15 minutes are room temperature. After that, cells were washed twice with PBS and permeabilized with 0.5% permeabilization buffer for 15 minutes. The glass slides were blocked for 1 hour at room temperature with PBST solution followed by and overnight incubation of the primary antibody at 4°C (refer to table 1). The glass cover slips were then rinsed 3 times with PBS and incubated with species specific secondary antibody in 5% PBST. Phalliodin was co-stained with the secondary antibody at a 1:500 dilution. Finally, the cover slips were

rinsed 3 times in PBS and mounted with DAPI. The slides were viewed with a confocal microscope.

3.18. Confocal Microscopy

Immunohistochemical images were captured using Leica TCS SP8. The images were acquired at 60X magnification . Z stack was generated to acquire the images at different focal planes creating a 3D projection of the image. The images were processed using the Leica LASX software.

3.19. Statistical analysis

The results are represented as mean values s.e.m. The variance analysis between 2 groups was performed using student's T-test. However, comparison between multiple groups was performed using one way anova analysis of variance. When, a significant result is obtained, further statistical analysis was performed between the groups that is the student –Newman-Keul's test (IBM SPSS 19.0, IBM Chicago, IL, USA). The difference between the group was considered to a sign of significance.

3.20. Used materials

3.20.1. Chemicals

Bovine Serum Albumin, Fraction V (BSA)	Roche Holding AG, Basel, Switzerland
Dimethyl Sulfoxide	Roche Holding AG, Basel, Switzerland
L-ascorbic acid	Sigma-Aldrich, St. Louis, USA
L-glutathione	Sigma-Aldrich, St. Louis, USA
Methanol	Sigma-Aldrich, St. Louis, USA
Praraformaldyhe	Sigma-Aldrich, St. Louis, USA
Sulfuric Acid	Carl Roth GmbH& Co. Kg, Karlsruhe, Germany
Trisma base	Sigma-Aldrich, St. Louis, USA
Triton x- 100	Sigma-Aldrich, St. Louis, USA

3.20.2.   Histology

Antifade Mounting Medium with DAPI	Vector Laboratories, California, USA
Circle Cover Slips,12mm Glass slides	Thermo Fisher Scientific Inc., Waltham, USA
Thermo Scientific™ Polysine Adhesion Slides	Thermo Fisher Scientific Inc., Waltham, USA

3.20.3.   Western Blot

1,4-Dithiothreitol	Roche Holding AG, Basel, Switzerland
Invitrogen™PVDF/Filter Paper Sandwiches, 0.45 µm, 8.3 x 7.3 cm (for mini gels)	Invitrogen, Carlsbad, USA
Mini-PROTEAN TGX	Bio-Rad Laboratories, California, USA
ROTI®Free Stripping Buffer	Carl Roth Gmbh & Co. Kg, Karlsruhe, Germany
Tris Buffered Saline	Sigma-Aldrich, St. Louis, USA
TruPAGE Running Buffers	Sigma-Aldrich, St. Louis, USA
TruPAGE™ Transfer Buffer	Sigma-Aldrich, St. Louis, USA

3.20.4.   Surgical Accessories and animals handling

4kDA TRITC-Dextrane	Sigma-Aldrich, St. Louis, USA
0.9% NaCl	B. Braun Melsungen AG, Melsungen, Germany
Annexate	Roche Holding AG, Basel, Switzerland
Arterenol®	Sanofi, Paris, France
Dorbene Vet®	Pfizer, New York, USA
Fine Bore LDPE Tubing	Smiths Medicals, Minnesota, USA
Hamilton Microsyringe	Hamilton, Reno, USA

Midozolam-ratiopharm®	Ratiopharm, Ulm, Germany
Micro-tip catheter pressure transducer	Millar Instruments, Huston, USA
MPVS Ultra® Pressure-Volume Loop Systems	Millar Instruments, Huston, USA
Naxolone	Inresa, Freiburg, Germany

3.20.5. Equipments

BioChemVacuuCenter	Vacubrand, Wertheim am Main, Germany
Centrifuge 5804/ 5804 R	Eppendorf, Hamburg, Germany
Heating Thermoshaker HTM Shaker	Biotech, Bavaria, Germany
Heratherm Microbiological Incubator	Thermofisher, Waltham, USA
IKA Laboratory shaker Rocke	IKA, Staufen, Germany
ImageQuant LAS 500	Tecan Trading AG, Männedorf, Switzerland
Infinite® 200 PRO	GE Healthcare Bio-Sciences, Chicago, USA
Leica cryostat CM 1850	Leica Microsystems, Wetzelar, Germany
Leica TCS SP8 MP	Leica Camera, Wetzelar, Germany
MBL3200 Inverted Microscope	Krüss, Hamburg, Germany
Micro centrifuge Micro Star 17R	VWR, Randor, USA
Mini Trans-Blot® Cell	Bio Rad, Hercules, USA
RS-VA 10 vortex mixer	Phoenix Instruments, Naperville, USA
Safe 2020 Class II Biological Safety Cabinets	Thermo Fisher Scientific Inc., Waltham, USA
Shaking Water Bath	GFL, Burgwedel, Germany

3.20.6.   Software

i-control™	Tecan Trading AG, Männedorf, Switzerland
Image J	USA. National Institutes of Health, Bethesda, USA
Leica	Leica Camera, Wetzelar, Germany

3.20.7.   Cell culture

BS3 Crosslinker	21555	Thermo Fisher Scientific Inc., Waltham, USA
cOmplete™ Protease Inhibitor Cocktail	11697498001	Roche Holding AG, Basel, Switzerland
Dispase II (neutral protease, grade II)	28405300	Roche Holding AG, Basel, Switzerland
DNase I	11284932001	Roche Holding AG, Basel, Switzerland
Dulbecco's Modified Eagle Medium	41965-039	Thermo Fisher Scientific Inc., Waltham, USA
Dulbecco's Modified Eagle Medium	11880-028	Thermo Fisher Scientific Inc., Waltham, USA
Dulbecco's Modified Eagle Medium F12 Nutient Mixture (Ham)	21041-025	Thermo Fisher Scientific Inc., Waltham, USA
Dynabeads™ Sheep Anti-Rat IgG	11035	Invitrogen, Carlsbad, USA
DSP cross linker	322133	Merck Group , Darmstadt, Germany
Fetal calf serum (FCS)	F0804	Sigma-Aldrich Biochemistry GmbH,
F-12 Nut Mix (ham)	21765-029	Thermo Fisher Scientific Inc., Waltham, USA

FTY720	SML0700	Sigma-Aldrich Biochemistry GmbH, Hamburg, Germany
Gibco™ Penicillin-Streptomycin	151-40-122	Sigma-Aldrich Biochemistry GmbH, Hamburg, Germany
Hanks' Balanced Salt Solution	H6648	Sigma-Aldrich Biochemistry GmbH, Hamburg, Germany
Hanks' Balanced Salt solution (without $Ca2^{+,}Mg2^+$)	H9394	Sigma-Aldrich Biochemistry GmbH, Hamburg, Germany
LPS	L2630	Sigma-Aldrich Biochemistry GmbH, Hamburg, Germany
Minimum Essential Medium	21757	Thermo Fisher Scientific Inc., Waltham, USA
MEM alpha (Minimum Essential Medium)	32561	Thermo Fisher Scientific Inc., Waltham, USA
Phosphate-Buffered Saline	10010023	Thermo Fisher Scientific Inc., Waltham, USA
PhosSTOP™	4906845001	Roche Holding AG, Basel Switzerland
Protein A/G PLUS-Agarose	Sc-2002	Santa Cruz, Dallas, USA
RIPA Buffer	R0278	Sigma-Aldrich Biochemistry GmbH, Hamburg, Germany
Sphingosine 1 phosphate	S9666-1MG	Sigma-Aldrich Biochemistry GmbH, Hamburg, Germany
Trypsin-EDTA (0.25%), phenol red	25200-056	Thermo Fisher Scientific Inc., Waltham, USA

3.20.8. Kits

Amersham ECL Prime Western Blotting Detection Reagent	RPN2232	GE Healthcare Europe, Freiburg, Germany

G-LISA RhoA Activation Assay	BK124	Cytoskeleton, Denver, USA
Mouse IL-6 Elisa Kit	Ab 100712	Abcam, Cambridge, UK
Pierce BCA Protein Assay	23225	Bio Rad Laboratories GmbH, Munich, Germany
Total RhoA ELISA Biochem kit	BK-150	Cytoskeleton, Denver, USA

3.20.9. Consumables

Cell culture 6-well plate	TPP, Trasadingen, Switzerland
Cell culture10 cm plate TPP, Trasadingen, Switzerland	TPP, Trasadingen, Switzerland
Cell culture 24-well plate	TPP, Trasadingen, Switzerland
Cryovials	Sigma-Aldrich Biochemistry GmbH, Hamburg, Germany
Corning cell scrapers	Corning, New York, USA
Counting chamber	Sigma-Aldrich Biochemistry GmbH, Hamburg, Germany
DynaMag™-2 Magnet	Thermo Fisher Scientific Inc., Waltham, USA
Falcon™ centrifuge tubes	Corning, New York, USA
Falcon™ Disposable Polystyrene Serological Pipets	Corning, New York, USA
Sterican® 30 G x 1⁄2	B. Braun Melsungen AG, Melsungen, Germany
Microtome blades	Thermo Fisher Scientific Inc., Waltham, USA
70uM cell strainer	Corning, New York, USA
Mr. Frosty™ Freezing Container	Thermo Fisher Scientific Inc., Waltham, USA
1.5 ml tubes	Eppendorf, Hamburg, Germany
1-ml U40 insulin needles	Omnican, Karlshuhe, Germany

3.20.10. Primary Antibodies

Anti-beta Actin antibody	mAbcam 8226	Abcam, Cambridge, UK
Anti-Mkl1/MRTFA antibody	ab49311	Abcam, Cambridge, UK
Anti-GAPDH (14C10)	2118	Cell Signaling, Danvers, USA
β-Actin (13E5) Rabbit	4970	Cell Signaling, Danvers, USA
MouseVE-Cadherin Antibody	Af1002	R&D systems, Minneapolis, USA
N-Cadherin antibody [5D5]	GTX82992	GenTex, Zeeland, USA
NG2 Antibody	orb 157978	Biorbyt, Cambridge ,UK
PECAM-1 mouse monoclonal IgG	Sc-376764	Santa Cruz, Dallas, USA
Phospho-Src Family (Tyr416)	2101	Cell Signaling, Danvers, USA
Purified Rat Anti-Mouse CD144	555289	
Src Antibody	2108	Cell Signaling, Danvers, USA
VE-Cadherin (Tyr-685), phospho-specific	CP1981	ECM biosciences, Versailles, USA

3.20.11. Secondary Antibodies

Alexa Fluor™ 594 Phalloidin	A12381	Thermo Fisher Scientific Inc., Waltham, USA
Anti-Goat IgG, HRP conjugated	HAF	R&D systems, Minneapolis, USA
Anti-Mouse HRP conjugated	HAF018	&D systems, Minneapolis, USA
Anti-Mouse HRP conjugated	HAF018	R&D systems, Minneapolis, USA
Anti-Rabbit HRP conjugated	HAF008	R&D systems, Minneapolis, USA

Donkey anti-Goat Alexa Fluor 488	A32814	Thermo Fisher Scientific Inc., Waltham, USA
Goat anti-Mouse IgG, Alexa Fluor 488	A-10680	Thermo Fisher Scientific Inc., Waltham, USA
Goat anti-Rabbit Alexa Fluor 488	A-11008	Thermo Fisher Scientific Inc., Waltham, USA

3.20.12. Buffers and Media

Biotech solution	L-Glutathion (500 mg/ml)+ L-ascorbic acid (500mg/ml) in 200ml MEM (21757) in F21 Nut mix ham
Complete DMEM	DMEM (41965-039) +10% FCS+1% penicillin
Complete MEM	MEM (32561) +10% FCS+1% penicillin
Dispase solution	DNAS!(2000u/mg)+ 5mg/Lung Dispase II in
10% DMEM/F-12 (1X)	DMEM/F12 +10% FCS+1% penicillin
10% DMEM/F-12 (1X)	DMEM/F12 +10% FCS+1% penicillin
20% DMEM/F12 (1:1)	F-12 Nut Mix (ham)+ DMEM (11880-028) + 20%FCS+1% penicillin
Fixation buffer 4% PFA	4 g PFA in PBS solution
0.5% Hanks buffer	Hanks' Balanced Salt Solution+ 0.5% BSA
Histology blocking buffer: PBST	5%BSA, 0.1% triton in PBST
Permeabilization Buffer	0.1% triton X in PBS solution
Starving DMEM	DMEM (41965-039) + 0.2% FCS+1% penicillin
Starving MEM	MEM (32561) +0.2% FCS+1% penicillin
TRIS solution	20mM Tris in water, ph7
Western blot blocking buffer: TBST	0.1%tween, 5%BSA in water

4. Results

4.1. Correlation of plasma Interleukin-6 levels and sepsis

To asses the proper modulation of inflammation, plasma interleukin-6 level was first examined in sham, PBS and S1P treated mice since elevated Il-6 levels correlate with sepsis [113]. In sham controls plasma Il-6 values were low compared to LPS and S1P treated septic animals which revealed the highest Il-6 levels indicating the prevalence of systemic inflammation (sham 35± 19 vs. PBS 16680 ± 51 pg/ml, Figure 13). We noticed that S1P treatment had no effect on plasma Il-6 levels (S1P: 17800 ± 4253 pg/ml). This finding provides a proof of concept that LPS induces severe inflammatory reaction mimicking that of sepsis given the Il-6 figures in the LPS treated group while S1P treatment has no effect in that regard.
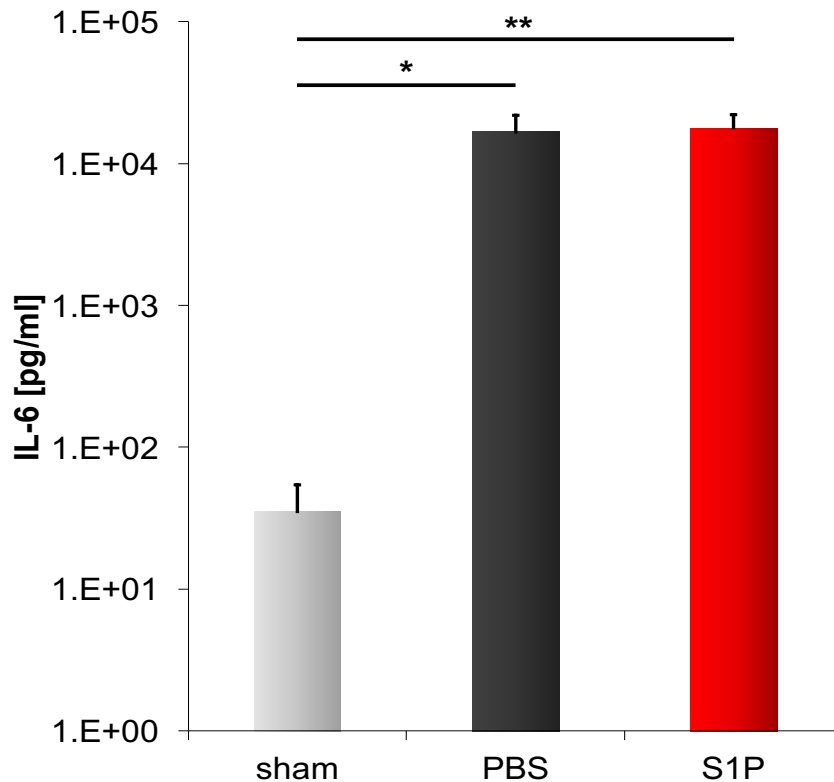

Figure 13: Quantification of Il-6 levels in sham, PBS and S1P treated animal groups are represented above. LPS induces a stark increase in the plasma Il-6 that is not diminished by the administration of S1P. (* p<0,05 for sham vs. PBS/ * p<0,05 for sham vs S1P, n=8 for sham, n=8 for PBS, n=12 for S1P). Adapted from Abdel Rahman et al. [114]

4.2. Influence of S1P on capillary density

Sepsis is associated with a reduction in endothelial cells and pericytes [115] while S1P has been regarded as a potent pericyte attractant to the microcirculation [116]. Therefore, we examined morphological changes in the microvascular unit in response to LPS and S1P using histological analysis for PECAM-1 and NG2 that mark endothelial cells and pericytes respectively. LPS treatment led to a dramatic decrease in endothelial cells and pericytes, results indicative of microvascular disintegration. However, S1P treatment enhanced pericyte coverage and endothelial cell density as observed in histological stains from small capillaries in heart sections (PBS 3491 ± 244 vs. S1P 4565 ± 243 cells/mm2). Similarly, pericyte coverage was significantly enhanced in the presence of S1P (PBS 2219 ± 158 vs. S1P 3504 ± 181 cells/mm2, Figure 14).
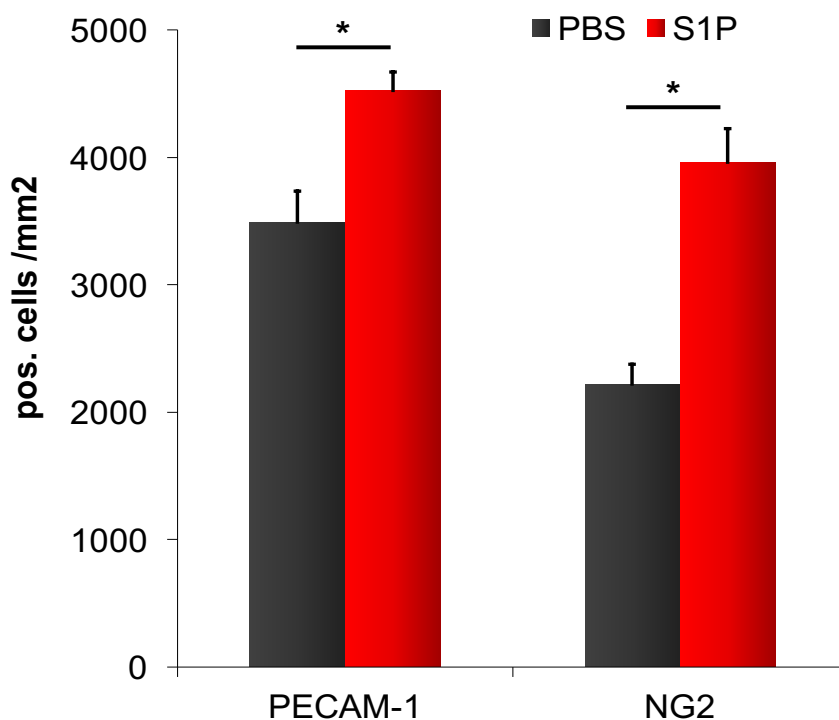

Figure 14: Quantification of endothelial cells (PECAM-1) and pericytes (NG2) reveals a significant increase in cell density in the S1P treated group compared to septic animals. (* $p < 0,05$ for PBS vs. S1P/, n=5 for PBS, n=5 for S1P). Adapted from Abdel Rahman et al.[114]

4.3. S1P and vascular leakage

Endotoxins and circulating inflammatory mediators such as Il-6 elicit injuries in the microcirculation leading microvascular disintegration and capillary leakage [9].To determine whether alterations in the capillary density and pericyte investment correlate to changes in vascular leakage and stability, a fluorescent dye, TRITC-dextran was injected and the extravascular fluorescent intensity was recorded. At the onset of the experiment, fluorescent extravasation was only recorded in the LPS treated group that increased dramatically with time indicating unstable leaky vessels. However, extravasation was kept low in the S1P treated group correlating to an amelioration of barrier dysfunction. The quantification of the respective images revealed increased leakage in the septic group within 20 seconds while S1P administration counteracted this phenotype (240 seconds: PBS 199 ± 22 vs S1P 119 ± 10 % of baseline, Figure 15). These results collectively indicate that S1P stabilizes the microcirculatory structure leading to an improved barrier function.
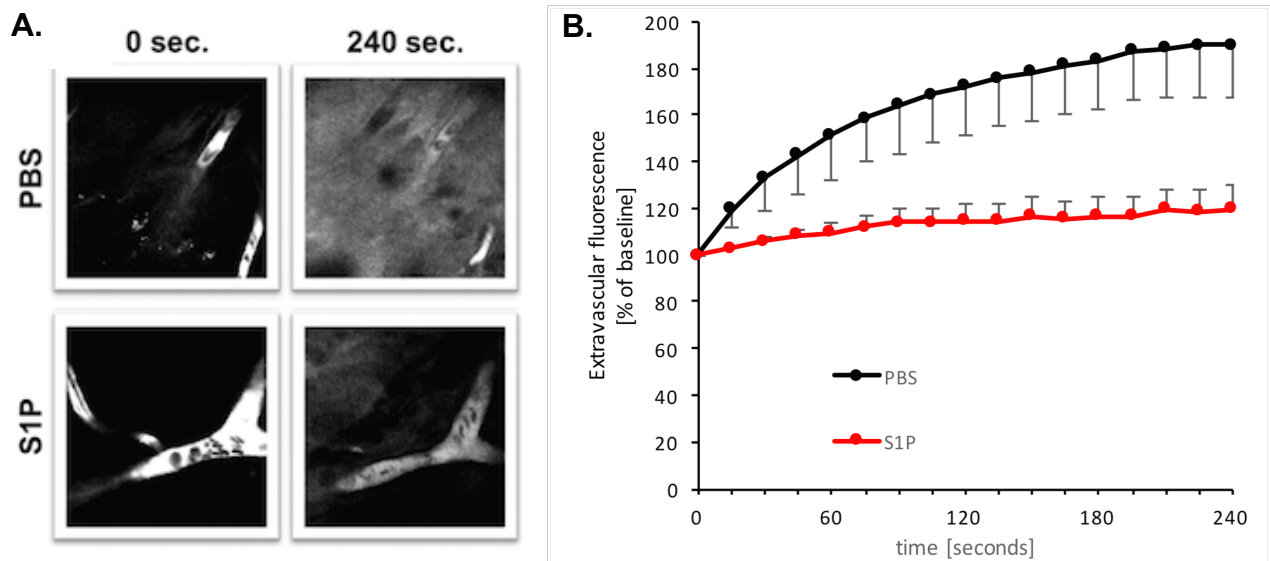

Figure 15: (A) Images of the fluorescence in the mouse ears reveal an increase in the extravascular signal at 240 sec post LPS injection. **(B)** Quantification of the respective images indicates a reduction in extravasation in the S1P treated group (* p<0.05 for PBS vs. S1P, n=4 for PBS, n=4 for S1P) Adapted from Abdel Rahman et al.[114]

4.4. Hemodynamic alterations

Alterations in the capillary surface area and vascular permeability are two variables that influence blood flow and ultimately mean arterial pressure. Therefore, the blood pressure was measured in mice in response to LPS and S1P. Due to vascular destabilization and leakage, septic mice developed systemic hypotension at 12 and 24 hours (PBS controls: 116 ±5 compared to septic mice at 12 hours 44 ± 3 and at 24 hours 44 ± 4 mmHg, Figure 16). However, treatment with S1P led to a hemodynamic improvement manifested by a significant increase in the mean arterial pressure (PBS: 124 ± 4 at t_0 compared to septic mice treated with S1P at 12 hours 81 ± 8 and at 24 hours 70 ± 6 mmHg).
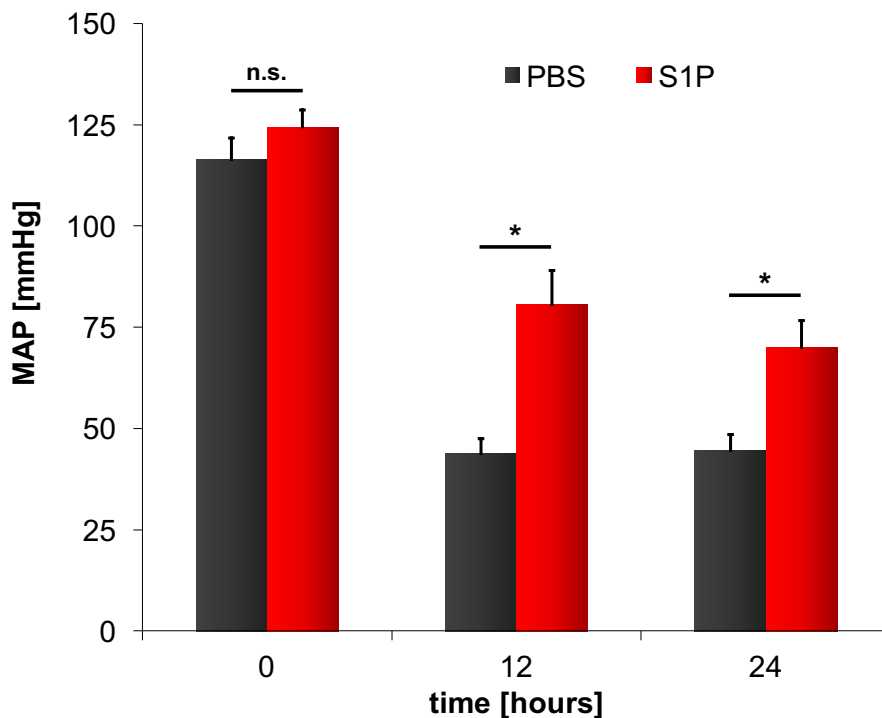

Figure 16: Mice challenged with LPS develop systemic hypotension at 12 and 24 hours while S1P treatment significantly ameliorates the drop of mean arterial pressure. (*p<0.05 for PBS vs. S1P at 12 hours, * p<0.05 for PBS vs. S1P at 24 hours, n =7 for PBS at 0h, n=7 for PBS at 12h, n=5 at PBS at 24h, n=8 S1P at 0h, n=15 at S1P at 12h, n=13 at S1P at 24h). Adapted from Abdel Rahman et al.[114]

4.5.   Survival of septic animals

Due to the pronounced effects of S1P on capillary density, microvascular integrity, and mean arterial pressure, we interrogated survival. In the early phase of sepsis, within 12 hours, both animal groups exhibit a similar survival rate (PBS: 80% vs. S1P: 80% after 12 hours, Figure 17). However, after 36 hours, all of the septic control mice die while 45% of S1P treated animals survive beyond this time point (PBS: 0% vs. S1P: 43 % after 36 hours).
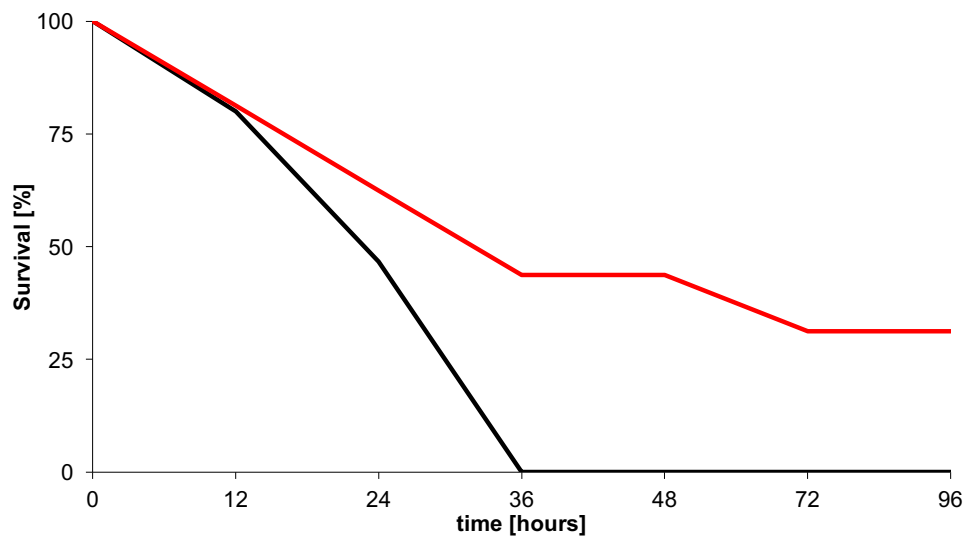

Figure 17: At 36 hours latest, septic control animals (black line) die whereas S1P treated animals (red line) exhibit a higher survival rate. (*p<0,05; Log Rank: p=0,032, n=15 for PBS, n=16 for S1P). Adapted from Abdel Rahman et al.[114]

4.6. Alterations in adhesion proteins during inflammation

Though pericyte detachment and endothelial regression are clearly associated with the degree of systemic inflammation, the mechanism of microvascular disassembly is opaque. One possible reason to the observed leaky vessels is due to the breakdown of the endothelial barrier due to shedding of adhesion proteins such as VE-Cadherin and N-Cadherin [117]. Therefore, we examined the changes in the adhesive structures that are the main composite the endothelial barrier.

4.6.1. S1P induced N-Cadherin trafficking

Histological stains from heart section were made to visualize the expression of N-Cadherin when septic animals were treated with S1P. As can been seen in Figure 18, the deposition of N-cadherin (*white*) between the endothelial cells (*red*) and pericytes (*green*) was abolished in septic controls (PBS). However, administration of S1P restored N-cadherin expression along the endothelial barrier indicating strong structural interaction between both cell types. This observation provides evidence that S1P strengthens the endothelial barrier by promoting the trafficking of N-Cadherin to the sites of cell contact.
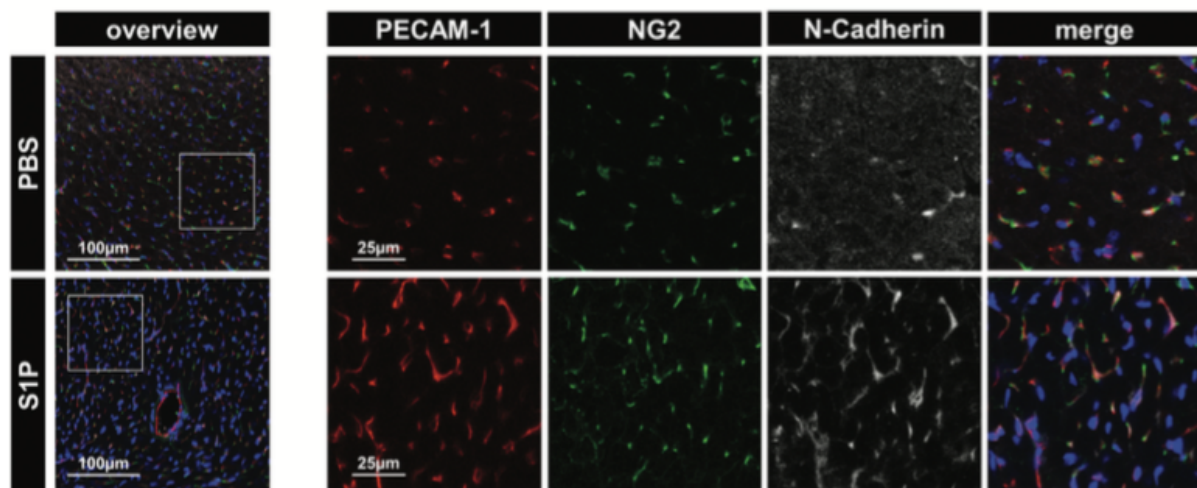

Figure 18: Heart section stained for total N-Cadherin (*Tight junction, white*), PECAM-1 (*Endothelial cells, red*), NG2 (*pericyte, green*) and DAPI (*nucleus, blue*). Septic animals display a stark decrease in N-Cadherin staining 12 hours after sepsis induction, which is ameliorated in mice treated with S1P. (n=3 for all groups). Adapted from Abdel Rahman et al.[114]

4.6.2. S1P mediated VE-cadherin localization

Similarly, confocal images revealed a dramatic reduction of VE-Cadherin (*white*) along the endothelial border (red) in septic animals (PBS) which correlated to aberrant vessel function. The expression pattern of VE-Cadherin was strongly restored with the administration of S1P, Figure 19. This indicates that S1P positively regulates the endothelial barrier by enhancing the deposition of adhesion proteins to counteract LPS induced microvascular disintegration.
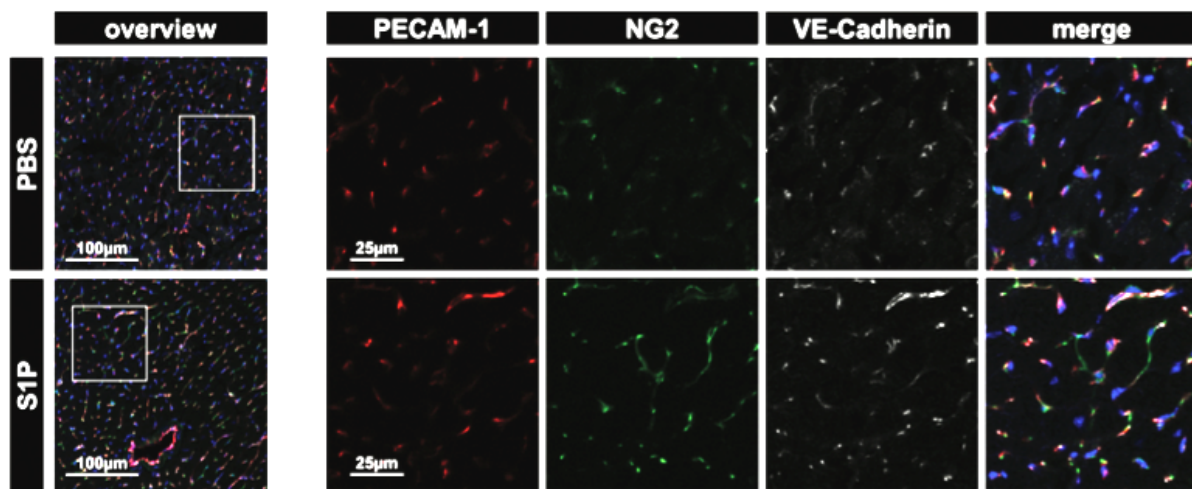

Figure 19: Heart section stained are for total VE-Cadherin (*tight junction, white*), PECAM-1 (*endothelial cells, red*), NG2 (*pericytes, green*) and DAPI (*nucleus, blue*). LPS treated animals reveal a decrease in the VE-Cadherin deposition along the endothelial border which is restored with the administration of S1P. (n=3 for all groups). Adapted from Abdel Rahman et al.[114]

4.7. Cell culture model of sepsis

To investigate underlying signaling mechanisms we utilized a cell culture system to mimic sepsis.

4.7.1. Involvement of STAT3 in LPS- induced inflammation

4.7.1.1. pSTAT3 activation in endothelial cells

To determine whether LPS elicits an inflammatory response in cultured endothelial cells, phosphorylation of STAT3 at tyrosine 705 was examined next. It was observed that pSTAT3 (Tyr^{705}) in primary endothelial cells increased in a time dependent manner. As observed in Figure 20, untreated endothelial cells lack pSTAT3 (Tyr^{705}) indicating a quiescent state. However, challenging the cells with LPS induced rapid and sharp activation of pSTAT3 (Tyr^{705}) within 5 minutes, a signal that remained strong until 30 minutes. This experiment is a proof of concept that LPS induced a pro-inflammatory response in endothelial cells marked by the involvement of STAT3 signaling pathway.
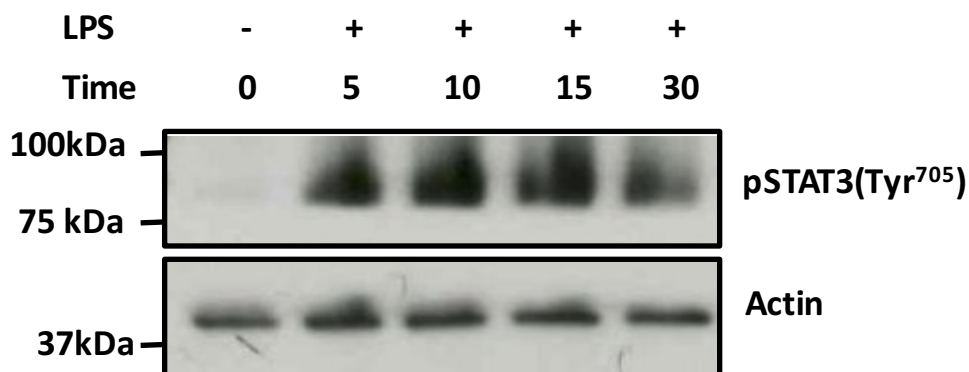

Figure 20: Treating endothelial cells (MLECs) with LPS results in activation of STAT3 in a time dependent manner. Western blot densitometric images are normalized to beta actin and represented as fold change of the untreated control. (n=3)

4.7.1.2. pSTAT3 activation in pericytes

In parallel, pericytes (CCL-226) were also treated with (10 mg/mL) LPS over a 30 minutes time course and phosphorylation of STAT3 (Tyr^{705}) was examined. Under normal culture condition, pSTAT3 (Tyr^{705}) was not detected in pericytes (CCL-226). However, when challenged with LPS, pSTAT3 (Tyr^{705}) levels peak within 5 to 15 minutes indicating a rapid transient response until 30 minutes when the phosphorylation was completely diminished. This indicates that STAT3 signaling axis is involved in the early inflammatory response in pericytes as well. Therefore, this model can be used to mimic endothelial and pericyte activation in response to LPS.
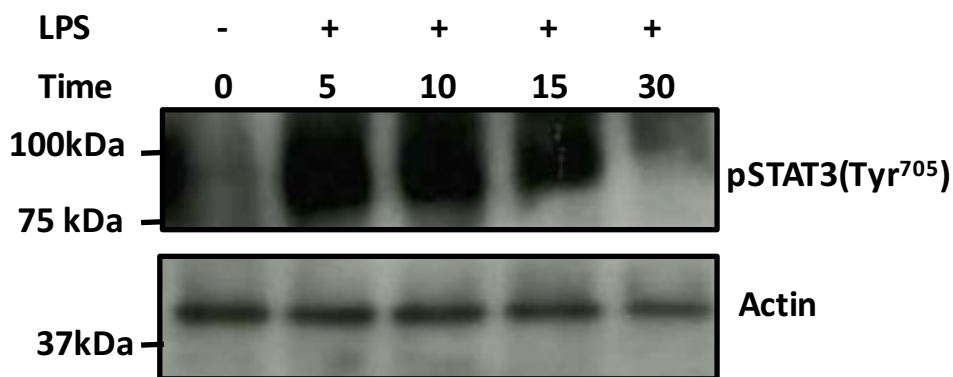

Figure 21: Treating pericytes (CCL-226) with LPS results in the activation STAT3 in a time dependent manner. Western blot densitometric images are normalized to beta actin and represented as fold change of the untreated control. (n=3)

4.8. LPS and adhesion proteins expression

4.8.1. Temporal downregulation of VE-Cadherin in response to LPS

Since our cell culture model can mimic endothelial activation during inflammation we analyzed VE-cadherin expression in a time dependent manner. So, endothelial cells (MLECs) were challenged with 10mg/mL LPS for timespan of 30 minutes to determine the time needed for LPS to exhibit its maximum effect. Western blot analysis revealed 60% reduction in VE-Cadherin within 5 minutes of LPS exposure, Figure 22. These results validate the notion that LPS meditates the rearrangement of VE-Cadherin observed in vivo upon attenuating its expression in a time dependent manner.
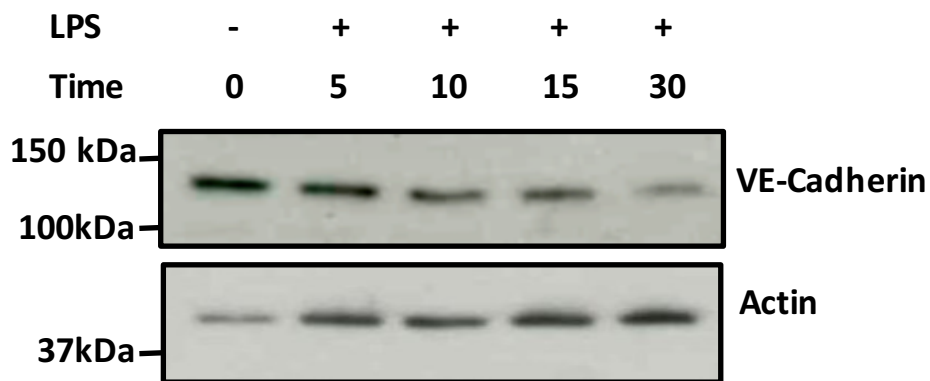

Figure 22: Treating endothelial cells (MLECs) with LPS induces VE-Cadherin downregulation in a time dependent manner. Western blot densitometric images are normalized to beta actin. (n=3)

4.8.2. Modulation of VE-Cadherin by S1P agonist

Given that a reproducible cell culture model of sepsis has been established, it was set out to elucidate further signaling mechanisms implicated in the barrier dysfunction and the influence of FTY270 on adhesion protein trafficking.

The previous experiments revealed that downregulation of VE-Cadherin is an early event that occurs within 10 minutes post LPS stimulation. So, endothelial cells (bEnd3) were challenged with LPS and S1P agonist (FTY720) and VE-Cadherin was imaged. As observed in Figure 23, under normal conditions, endothelial cells express VE-Cadherin abundantly along the border forming a continues lining between adjacent cells. However, challenging the cells with LPS resulted in a compromised VE-Cadherin deposition marked by increased gaps between cells. Administration of S1P agonist compensated for the loss of VE-Cadherin and proved to be effective in restoring linear VE-Cadherin expression along the endothelium overcoming the disheveled organization observed during inflammation.
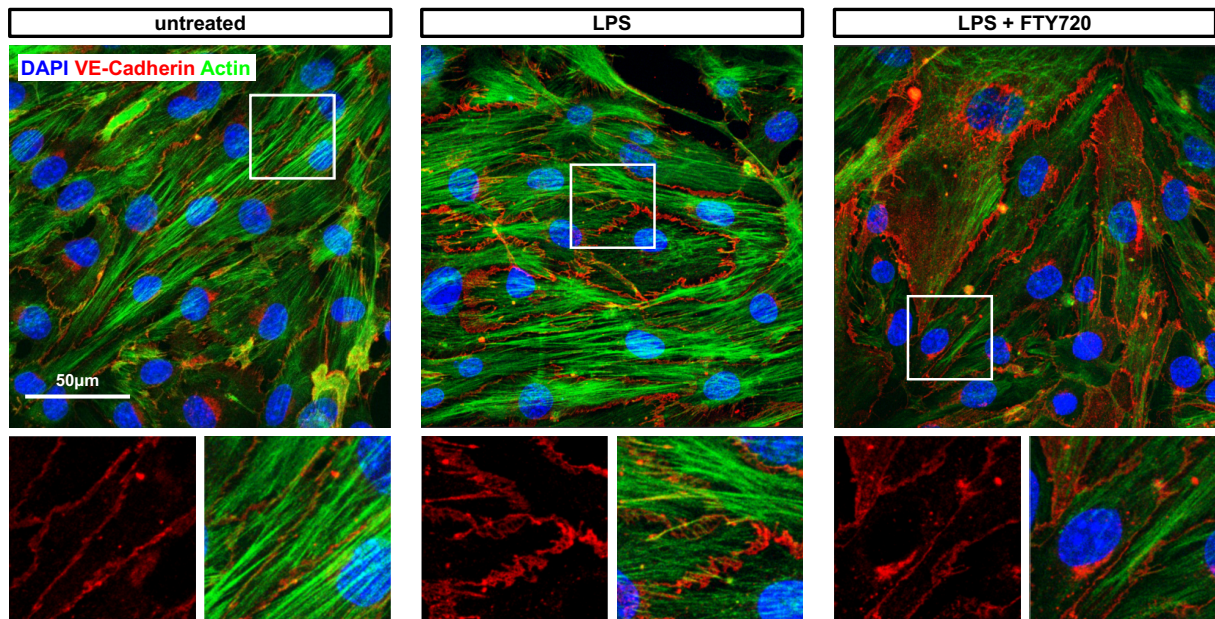
Figure 23: Endothelial cells (bEnd3) are stained with anti VE-Cadherin antibody (*red*), actin (*green*) and DAPI (*blue*) to image VE-Cadherin deposition. Confocal images reveal a disheveled deposition in the LPS treated groups with an increased stress fiber formation. Administration of S1P agonist restores the continues VE-Cadherin deposition similar to the untreated group. (n=3 for all groups). Adapted from Abdel Rahman et al.[114]

4.8.3. Localization of N-Cadherin in pericytes

Confocal imaging was performed on cultured pericytes (CCL-226) stained with N-Cadherin to reproduce the previously obtained results obtained results. Immunofluorescence images reveal that LPS impaired the trafficking of N-Cadherin at the sites of contact between pericytes and the administration of S1P was effective in reversing this phenotype, Figure 24. This observation indicates that in response to inflammation, both endothelial cells and pericytes are activated and reduce adhesion protein trafficking at sites of cell-cell contact. The drastic reduction in N-Cadherin correlates to weak endothelial-pericyte interaction that is prior to pericyte drop off during systemic inflammation.
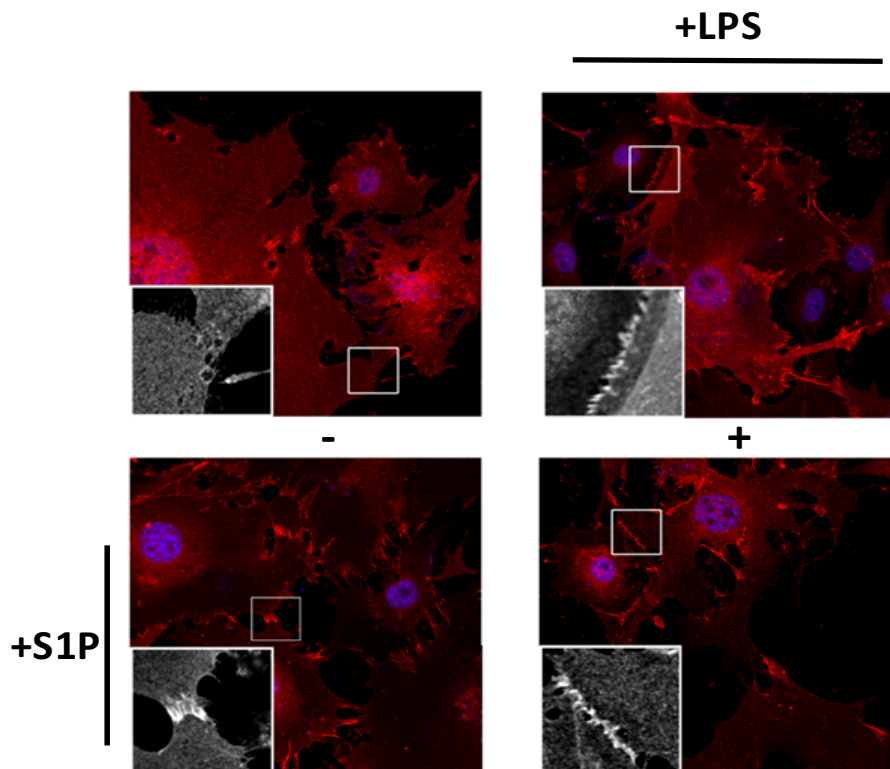

Figure 24: Pericytes (CCL226) stained with anti N-Cadherin antibody (*red*), and DAPI (*blue*). Confocal images reveal reduction in N-cadherin deposition the cytoplasmic extension between pericytes in the LPS treated groups which is restored with the administration of S1P (n=3 for all groups).

4.9. Src dependent VE-Cadherin phosphorylation

Systemic inflammation is characterized by dramatic loss of adhesion proteins such N-Cadherin and VE-Cadherin and the downregulation of VE-Cadherin is potentially secondary to its phosphorylation by Src at the tyrosine residue 685 which promotes its internalization and further degradation. Therefore, we investigated the phosphorylation of VE-Cadherin and Src in response to LPS and S1P agonist, FTY720. As can be observed in Figure 25A, LPS increased the phosphorylation of VE-Cadherin after 5 minutes of which was attenuated with the administration of S1P agonist. This correlated with a stark increase in Src phosphorylation in response to LPS that was also reduced with the administration of FTY720, S1P agonist, Figure 25B.

This indicates that the mechanism of VE-Cadherin downregulation in response to LPS is mediated by the phosphorylation at tyrosine 685 by Src kinase and S1P acts upstream to attenuate pSrc levels.

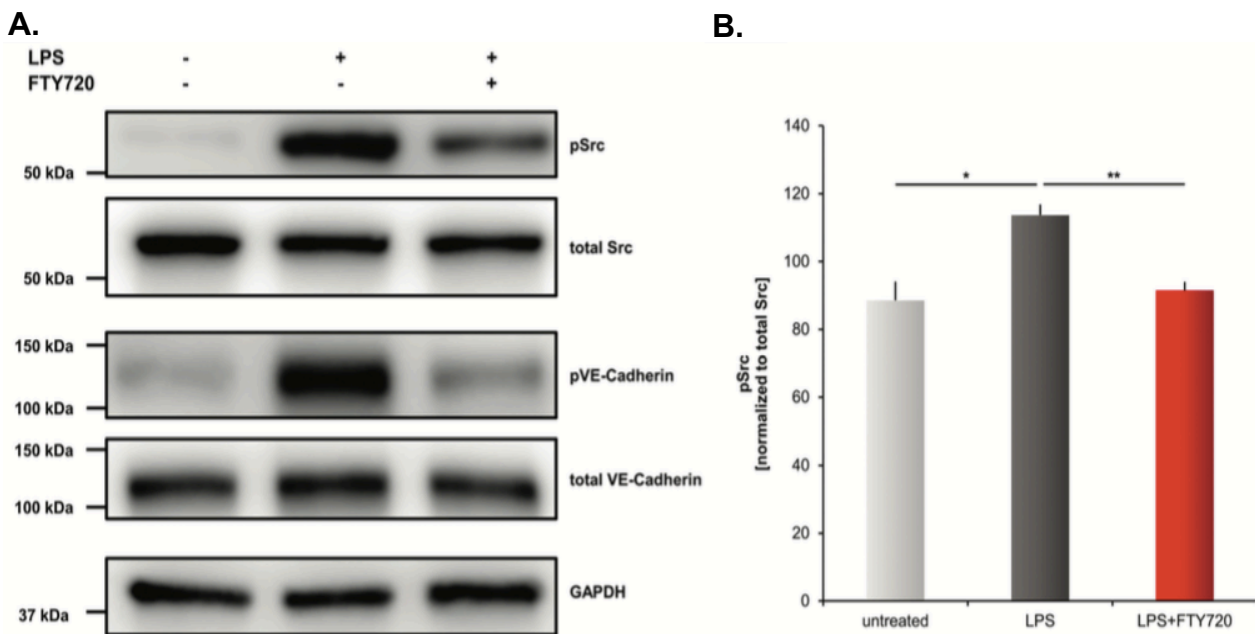**Figure25:(A)** Challenging endothelial cells (bEnd3) with LPS induces phosphorylation of Src at Tyrosine 416 and VE-Cadherin at Tyrosine 685 within 5 minutes which is ameliorated with the S1P agonist. **(B)** Western blot densitometric images for pSrc are normalized to total Src and represented as fold change of the untreated control (* p<0,05; ** p<0,001, n=4). Adapted from Abdel Rahman et al. [114]

4.10. Rho A activation

Internalization of VE-Cadherin is an active process that requires mechanical regulation of the actin cytoskeleton. Since RhoA is a crucial regulator of the actin cytoskeleton and it has been shown to promote F-actin assembly, RhoA activity was next to be determined in endothelial cells under resting condition and when stimulated with LPS and S1P agonist.

Briefly, RhoA alternates between 2 conformational states, GDP-bound inactive state and GTP-bound active state and therefore RhoA activity is marked by the hydrolysis of GDP to GTP [118]. The quantitative levels of GTP-bound RhoA were determined in endothelial cells at 150 / 300 seconds post LPS and S1P agonist treatments. Data from the ELISA assay revealed that RhoA activity increased in the both LPS and LPS+FTY720 treated cells with a stark increase in the S1P agonist treated group (LPS 164 $\pm$ 24 vs. LPS+FTY720 423 $\pm$ 23 % at 300 sec, Figure 26).

This observation provides a solid proof that the protective effects of S1P on endothelial cells requires pronounced activation of RhoA tailored to restore actin cytoskeleton re-arrangements.
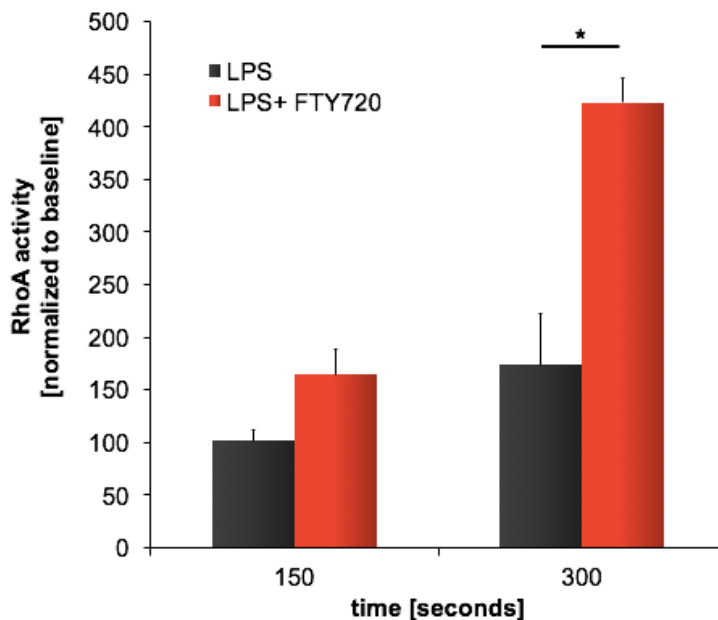

Figure 26: RhoA activation assay measured by G-Elisa kit reveals an increase in the RhoA activity when endothelial cells (bEnd3) cells were challenged with LPS at 150 and 300sec. RhoA activation is pronounced when FTY720, an S1P agonist, is administered (n=3 for all groups, * p<0,05). Adapted from Abdel Rahman et al.[114]

4.11. RhoA and actin cytoskeleton rearrangement

The effect of RhoA activation on actin cytoskeleton rearrangement was next to be determined by quantifying the ratio of globular to filamentous actin post crosslinking the cells with DSS. Here, endothelial cells were treated with LPS and S1P agonist for 10 minutes since downregulation of VE-Cadherin was observed within that timespan indicating potential cytoskeletal rearrangement.

Figure 27A illustrates the G/F actin blot where the smear correlates to F-actin and the 37kDa band represents G-actin. The quantification of the represented images in Figure 27B indicates 5-fold increase in the G/F actin ratio in the LPS treated group due to a stark increase in the cytosolic pool of G actin. Administration of FTY720 restored the G/F actin ratio upon enhancing the formation of F-actin bundles. This observation indicates that LPS induces cytoskeletal rearrangement leading to the loss of barrier function while S1P agonist attenuates cytoskeletal alterations by restoring the G/F actin ratio, a mechanism orchestrated by RhoA activation.

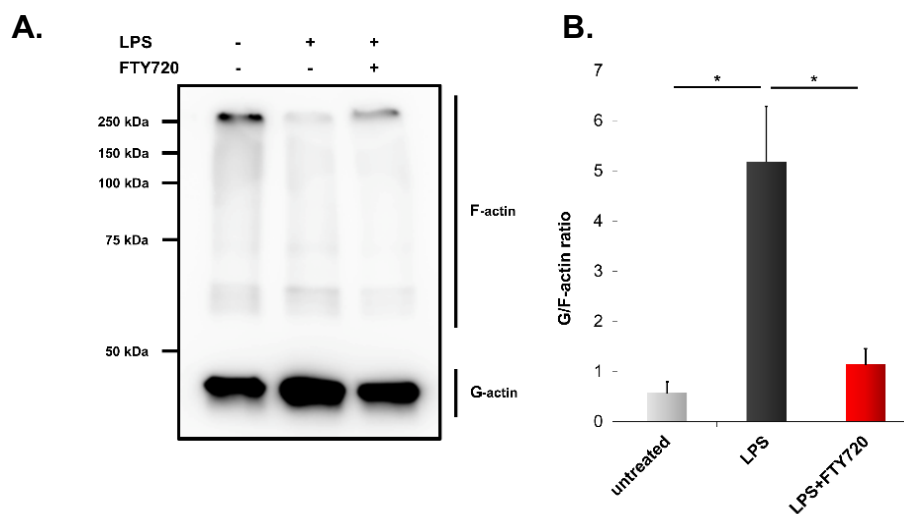**Figure 27(A+B): (A)** Crosslinking endothelial cells (bEnd3) with DSS, a non-cleavable cross linker, reveals that LPS increases the G/F actin ratio which is restored with the administration of S1P agonist. **(B)** Western blot densitometric images for G-F actin are normalized represented as fold change of the untreated control (* $p<0.05$; * $p<0.05$, n=3). Adapted from Abdel Rahman et al.[114]

4.12. G-actin dependent MRTF-A regulation

Under resting conditions, MRTF-A localizes to the nucleus regulating the transcription of SRF target genes involved in vessel maturation and pericyte retention [74]. However, MRTF-A exhibits high binding affinity to G-actin that retains it in the cytosol. Since we observed an increase in the cytosolic G-actin with LPS treatment, we further investigated the effect of LPS on binding on the of G-actin to MRTF-A. Therefore, immunoprecipitation of G-actin was performed at 15 minutes post LPS treatment and prior to lysis, cells were cross linked with DSP. Western blot analysis of the lysates revealed an increase in the binding of MTRF-A to G-actin in the LPS treated cells indicating a reduction in the nuclear localization. However, stimulation with S1P agonist decreased the G-actin bound MRTF-A thereby enhancing its nuclear entry, Figure 28.

This indicates that the cytoskeletal sequeale of events in repsonse to LPS are tailored to capture MRTF-A in the cytosol that is couteracted with the administration of S1P agonist.
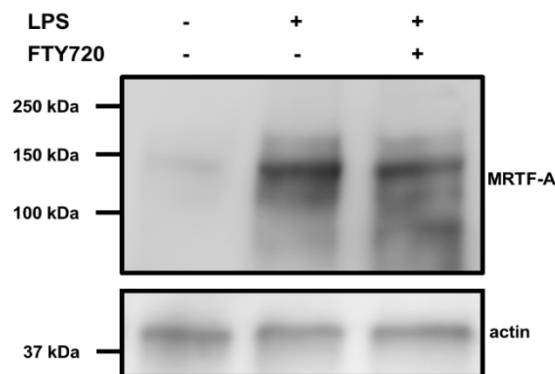

Figure 28: Endothelial cells (bEnd3) are cross-linked with a DSP prior to lysis. Western blot densitometric images for MRTF-A show an increase in G-actin bound MRTF-A during inflammation which is ameliorated with administration of the S1P agonist (n=3). Adapted from Abdel Rahman et al.[114]

4.13. Cellular localization of MRTF-A

In the light of the aforementioned results we further investigated the localization of MRTF-A using immunofluorescence staining. Therefore, endothelial cells were treated with LPS and S1P FTY720 for 15 minutes to examine the MRTF-A cellular localization. Confocal images revealed that under resting conditions MRTF-A clustered in the nucleus while LPS led to an in increased cytosolic retention of MRTF-A. However, the administration of S1P agonist enhanced its nuclear localization similar to the control group (Untreated: 172 ± 16 compared to LPS 60.8 ± 2 and LPS+FTY720 107 ± 10, Figure 29B). This indicates that S1P exhibits a novel effect by decreasing the binding of G-actin to MRTF-A promoting its nuclear localization and regulation of target genes involved in vessel maturation and pericyte retention
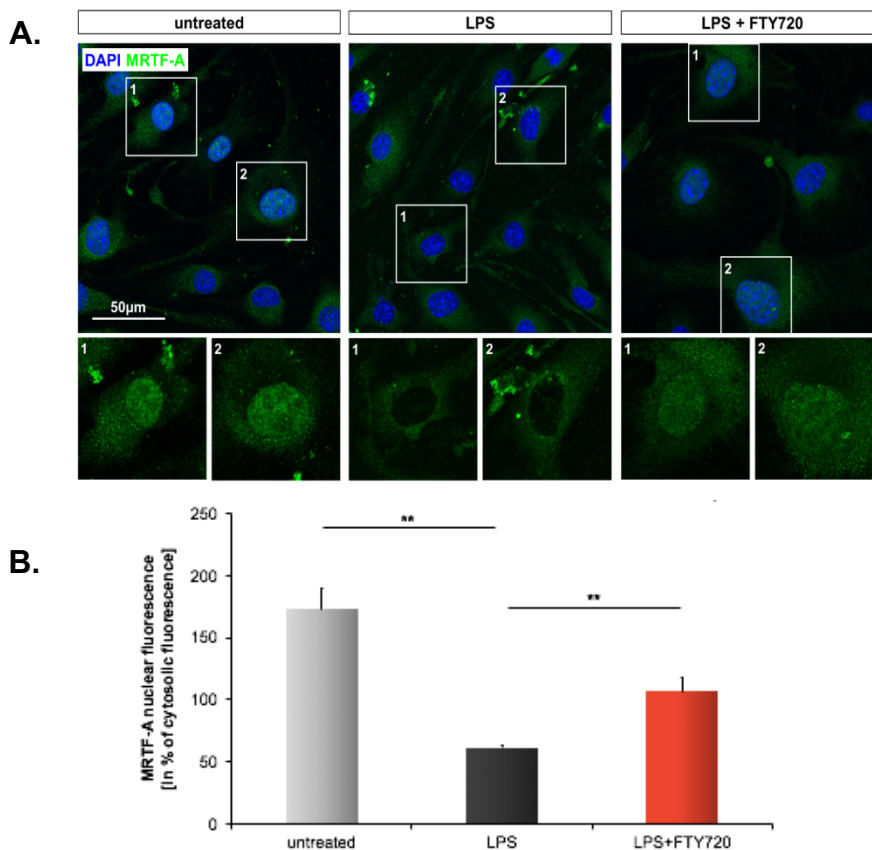
Figure 29 (A+B): (A) Endothelial cells (bEnd3) stained with anti MRTF-A antibody (*green*) and DAPI (*blue*). Confocal images reveal a reduction translocation of MRTF-A in the LPS treated groups that is restored with FTY720. **(B)** Quantification of the confocal images shows a significant reduction in the cytosolic MRTF-A only in the LPS treated cells compared to the untreated and the S1P agonist treated cells (* $p<0,05$, n=24). Adapted from Abdel Rahman et al.[114]

5. Discussion

5.1. Overview

Sepsis is an inflammatory response to an infection characterised by systemic hypotension due to severe microvascular aberrations such as disintegration of the endothelial barrier and pericyte drop off. In this study, we investigated the influence of sphingosine-1-phosphate (S1P) on the endothelial barrier and pericyte retention during sepsis since S1P has been described as a positive regulator of the microvascular wall.

We found that S1P enhances trafficking of VE-Cadherin and N-Cadherin to seal the gap between endothelial cells and promote pericyte investment across the vascular wall. Increased tightness of the vascular wall was the driving force to reduce extravascular leakage and improved hemodynamic function which led to higher survival rates in S1P treated septic animals. Additionally, we reproduced LPS induced inflammation in vitro to elucidate the molecular events implicated in the loss of adhesive structures. There, we showed that S1P enhances the endothelial barrier by reducing phosphorylation of Src that phosphorylates VE-Cadherin at a tyrosine residue which is implicated in VE-Cadherin internalization. Since trafficking and redistribution of adhesive proteins are mechanical events associated with dynamic rearrangement of actin cytoskeleton we investigated the influence of S1P on actin cytoskeleton rearrangement. There, we found that LPS induces an increase in the pool of G-actin which retains MTRF-A in the cytosol preventing its nuclear entry. However, exogenous administration of S1P overrides this effect and elicits pronounced activation of RhoA favouring the formation of F-actin bundles thereby reducing the pool of cytosolic G-actin (Figure30). This correlated to enhanced nuclear localization of MRTF-A which regulates the transcription of genes involved vessel maturation and pericyte retention, results indicative of the mechanism by which S1P mediates vessel stability, promotes pericyte retention and maintains endothelial cell quiescence.

5.2. LPS induced sepsis

LPS induced inflammation is a practical single variable model that contributes to sepsis and manifest an aggressive immune phenotype. Although there are significant variations in the cytokine response between the endotoxima model and the true incidence of sepsis, a surge in the Il-6 production remains the common denominator to the incident of the disease [119] as it is observed in mice injected with LPS (Figure 13). Il-6 elicits a cytokine storm corresponding to the early pro-inflammatory phase of the disease [120]. Although increased Il-6 plasma levels inversely correlate with diminished serum S1P levels in septic patient [85], exogenous administration of S1P shows no reduction in Il-6 plasma levels (Figure 13) suggesting the role of S1P in vessel stabilization and pericyte retention rather than modulation of the immune response [109].

5.3. S1P regulation of capillary density

Perciyte loss and microvascular dysfunction are the hallmark signs of sepsis. Vascular disintegration during systemic inflammation is initially caused by the degradation of the endothelial glycocalyx, a membrane bound layer of proteoglycans and glycoproteins [121, 122] while pericytes drop off is attributed to the increased expression of endothelial angiopoietin 2 [44]. Here, we reveal that administration of S1P is effective in overcoming capillary rarefaction by enhancing pericyte coverage and increase endothelial density (Figure 14) which is associated with reduced para-cellular permeability (Figure15 A +B). Modulation of basal permeability by S1P has been implicated in several lines of studies [100, 109, 112]. In an elegant study, Peng et al. demonstrate that in the model of acute lung injury 1uM of S1P is sufficient to attenuate LPS induced edema which correlates to a decrease in neutrophil infiltration to the perivascular space [105]. When injected locally, S1P results in a 60% increase in endothelial cell density compared a vehicle control in limb ischemia reperfusion model [123]. While the mechanism by which S1P facilitates mural cell recruitment is not well understood, it has been shown that S1P signalling induces the secretion of ECM soluble components that attract migrating cells [124].

Retaining pericyte in the capillary is of valuable importance as they signal through several ligand systems to maintain endothelial cell maturation. The constitutive secretion of pericytes derived Ang1 binds to the endothelial Tie2 receptor to promote endothelial quiescence and enhance the expression of VE-Cadherin contributing to

endothelial stability [125]. Indeed, mice overexpressing Ang1 are resistant to leaks upon exposure to VEGF [126]. In alignment with previous studies, challenging cultured MLECs with LPS increases Ang2 expression that counteracts Ang1/Tie2 signaling resulting in leaky vessels. In a novel study, Zeng et al. demonstrate that LPS induced pericyte loss is due to a reduction in Sirtuin3 levels, a protein known to be implicated in regulating post translational modification in aging and ischemia [115]. Although it is unclear whether the loss of pericytes in sepsis is due to apoptosis [127] or de-attachment [128], pericytes coverage is essential to maintain regular blood flow, vascular tone and endothelial cell quiescence.

5.4. S1P and hemodynamic variables

We sought to determine the hemodynamic effects of S1P treatment in septic animals since accumulating evidence suggest that reduced capillary density in sepsis correlates to systemic hypotension [44, 68, 69]. S1P treatment reveals enhanced vessel functionality depicted by an increase in the mean arterial blood pressure (Figure 16) leading to improved survival (Figure 17).

Of note, to elicit maximal response, animals were pretreated with S1P prior to the induction of sepsis. In a similar attempt, Lee et al. show that pre-treatment with S1P in the hepatic ischemia/reperfusion model is prerequisite to attenuate systemic inflammation and endothelial injury [129]. Additionally, pre-treatment with S1P or its agonist is shown to improve vascular reactivity to contractile stimuli post cardiopulmonary bypass mediated by S1PR1 [130].

The literature is replete with studies to determine receptor signaling underlying the influence of S1P on the vascular tone. For example, Salmone et al. demonstrate that in vascular smooth muscle cells, S1P induces vasoconstriction in cerebral arteries mediated by S1PR3 suggesting the S1P/S1PR3 axis as a potential therapeutic target for cardiovascular disease [131] excluding the role of S1PR2 in the vasoconstriction of basilar artery [132]. The question whether S1PR2 mediate vasoconstriction is still controversial because studies on S1PR2 KO mice yielded uncertain results. However, Lorenz et al. show that S1PR2 KO mice reveal ameliorated vascular response to epinephrine and potassium chloride indicating the tonic role of S1PR2 in regulating the myogenic response [133]. Additional studies suggest that the coupling of S1PR2 with the Gq induced vasoconstriction mediated by receptor activates Ca^{2+}/IP_3 and the

G_{13} /Rho A pathways [134]. Indeed, RhoA/Rho kinase mutants exhibit a diminished regulation of the vascular tone in Spk overexpressed mice [135].

5.5. Regulation of VE-Cadherin

The loss of barrier function is a hallmark sign of sepsis as it has been observed in numerous animal models of systemic inflammation. Here, we observed significant reduction in N-Cadherin and VE-Cadherin and in vivo (Figure 18+19) and in vitro (Figure 23+24) in response to LPS. On the other hand, treatment with S1P or its agonist restores the barrier function and enhances adhesion protein trafficking. We observe that the downregulation of VE-Cadherin coincides with increased Src and VE-Cadherin phosphorylation at tyrosine 685 (Figure 25A+B) that aligns with a growing body of evidence suggests that tyrosine 685 is a unique site for Src kinase [59]. The phosphorylation of VE-Cadherin is perquisite for its internalization and lysosomal degradation [136]. In a series of studies, Chichger et al. elucidate the mechanism by which Src mediate VE-cadherin downregulation in the LPS induced acute lung injury model. There, Src kinase regulates the endocytic trafficking of VE-Cadherin by tethering to early endosome and increasing the phosphorylation of endocytic protein p18 that determines the fate of VE-Cadherin. Upon phosphorylation, p18 mediates the interaction between the early endosome containing VE-Cadherin and Rab7 leading to its degradation. Otherwise, the early endosome binds to Rab4 which mediates it recycling [137, 138].

Phosphorylation of VE-cadherin is a prominent mechanism to reduce the VE-Cadherin/ β-catenin complex, thereby increasing endothelial permeability [139]. β-catenin and plakoglobin dock on the juxta membrane domain of VE-Cadherin known as the catenin binding domain and they mediate junction assembly and anchoring of VE-Cadherin to the actin cytoskeleton. Indeed, it is shown that in migrating endothelial cells co-immunoprecipitated plakoglobin with VE-Cadherin decrease significantly indicating the dissociation of the VE-Cadherin/catenin complex [140]. The tight control of VE-Cadherin by p120 has been investigated using fluorescence recovery after photo bleaching experiments (FRAP). Indeed, mutant VE-Cadherin for the p120 binding site showed higher mobile fraction compared to WT animals indicating the crucial role of p120 stabilizing VE-Cadherin and decreasing its motility along the endothelial surface [141]. Moreover, Joshua P. Garrett et al. show that the binding of

catenin to VE-Cadherin is prerequisite for its trafficking to the cell junction [142]. In parallel, Chen and colleagues highlight role of catenin in the trafficking of N-Cadherin to cell membrane and contributing to the junctional stability. This process is mediated by binding of p120 to the juxta-membrane domain of N-Cadherin and with kinesin, a motor protein moving along the MT, facilitating its trafficking sites of cell-cell junction [143].

5.6.   JAK/STAT3 signaling pathway and permeability

Beside downregulating VE-Cadherin at endothelial cell-cell contact, LPS induces an increase in the endogenous production of Il-6 due to the activation of NF-κB pathways by PAR [8, 144]. Upon secretion, Il-6 induces pro-inflammatory activation of endothelial cells through the JAK/STAT3 second messenger system which has been shown to play a central role in cell fate decision, tumor progression and migration [8, 145]. Consequently, the JAKs gets trans-auto-phosphorylated leading to an overactive STAT3 response [146]. In agreement, we demonstrate that LPS induce transient phosphorylation of STAT3 in endothelial cells and pericytes (Figure 20+21).

The phosphorylation of STAT3 at Tyrosine 705 serves as a sentinel for its dimerization followed nuclear entry and subsequently DNA binding. A growing body of evident suggests that phosphorylated STAT3 enhances ICAM-1 expression [147]. ICAM-1 is implicated in cellular migration, and leukocyte endothelial interaction which is primary to loss of barrier function and increase vascular permeability [147]. phosphorylation of STAT3 in endothelial cells makes its distinct from a quiescent endothelium since it is associated with a decrease in the mRNA levels of ZO-1, VE-Cadherin, PECAM-1, nectin-2 and claudin-5. These proteins are important for stabilizing the cell-cell junction and contribute to the stability of the endothelial wall [148]. In agreement with these studies, we observed an increase in STAT3 phosphorylation in endothelial cells and pericytes in a time dependent manner coinciding with VE-Cadherin and N-Cadherin downregulation. Overlapping studies suggest that knockdown of STAT3 ameliorates Il-6 mediated loss of barrier function and reduces vascular permeability as it coincides with strengthened VE-Cadherin complex [149, 150]. However, overexpression of STAT3 by itself isn't sufficient to induce barrier dysfunction indicating that in addition to STAT3, Il-6 requires the constitutive activation of further signaling pathways to induce endothelial hyper-permeability [150].

5.7. Reinforcing the endothelial barrier

S1P increases the junctional localization of N-Cadherin and VE-Cadherin in septic animals (Figure 18+19) and in vitro (Figure 23+24) thereby enhancing the vessel function and stability [104, 105]. Increased junctional deposition of adhesion proteins ameliorates edema and capillary leakage as observed in our work and others. Indeed, pre-treatment with S1P induces rearrangement of VE-Cadherin and occludins at the apical surface of endothelial tailored to decrease cellular gap in response to as bradykinin, a proinflammatory mediator [109]. The mechanism by which S1P elicits VE-Cadherin trafficking is suggested to be through S1PR1 since S1PR1 KO mice exhibit irregular localization of VE-Cadherin, a phenotype reminiscent to what we observed. Interstingly, Gaengel et al. hint to an interaction between S1PR1 and VE-Cadherin to overcome VEGF induced hyper permeability and angiogenic hyper sprouting [151]. Additionally, S1P induces the anchoring of the C-terminus of the N-Cadherin to the actin cytoskeleton that provides mechanical support to the Cadherin complex [152]. It has been shown that S1P induced the microtubule polymerization via the coupling to the Gi receptor and thereby activating the Rac GTPase pathway. The tubules serve as a pathway for transportation of N-Cadherin to the apical surface where it is deposited at the endothelial pericyte site of contact. Paik et al. reveal that S1PR1 receptor signalling activates the trafficking of N-Cadherin to the polarized apical surface of endothelial via S1PR1/Gi/Rac signalling pathway [153].

Beside its influence on adhesion protein trafficking, S1P signals to preserve the integrity of the endothelium by activating Ang1/Tie 2 signaling system. It known by now that Ang2 overexpression mediates vascular permeability and pericyte drop off, an observation that has been recapitulated in several lines of studies [44, 154]. In one of very few studies, McGuire et al. demonstrate that S1P reduced Ang2 expression [28] which abrogates pericyte investment across the capillary wall contributing to hemodynamic instability [44].

5.7.   RhoGTPase and regulation of actin cytoskeleton

The internalization of Cadherins involves internal cytoskeletal rearrangement mediated by the activation of RhoGTPase [65, 118, 141]. Also, their trafficking is a result of orchestrated cytoskeletal dynamics leading formation of F-actin and microtubule that facilitate the vesicular transport to cell junction site [65, 143].

RhoA exhibits differential role in endothelial cells since many studies address the role of Rho A in reducing endothelial barrier function [155] while several others suggest the function of RhoA as a positive regulator of the endothelial permeability [156]. For example, RhoA/ROCK activation mediates the phosphorylation of MLC kinases and formation of the contractile stress fibers [157, 158]. The isometric force mediate by F-actin is sufficient to promote the loss of VE-Cadherin and increase gaps between cells [159]. Inhibiting MLC kinase results in a decrease in the actomyosin related contraction and attenuates hyper-permeability [160]. In contrast to this, several studies show that RhoA enhances endothelial barrier via its downstream effector protein Dia which belongs to the formin family of actin binding proteins enhancing F-actin assembly [161, 162]. The distinct activation profiles of RhoA depend heavily on the external stimuli which elicit different cycles of internal phosphorylation events which result in different states of RhoA [163]. Here, we demonstrate that S1P increases RhoA activation and F-actin assembly in endothelial cells (Figure 26+27). Consistent with our finding, it has been shown that S1P elicits RhoA activation which results in the formation of F-actin along the endothelial cells border to enhance the barrier function [164]. On the other hand, the same stimulus, S1P, could elicit an opposite response mediate by RhoA leading to loss of barrier function. For example, Reinhard and colleagues reveal that S1PR2 couples to $G_{\alpha 13}$ leading to increased contraction [165]. These observations confirm the notion of 'dual function of RhoA' suggested by Van Nieuw Amerongen et al. where different activation profiles of RhoA are characterized in cultured endothelial cells [159].

5.8. The effects of Rho signaling

RhoA acts a cellular switch to regulate actin cytoskeleton, cell polarity, shape and even cell fate. A recent elegant study by Dorn et al. demonstrate that RhoA signaling mediates the formation of MRTF-A/SRF complex that is prominent to maintain cardiomyocyte identity. The study demonstrates that cell-cell contacts at the site of the intercalated disks signal via the RhoA-GTP to maintain a tight regulation of the G-actin pool to promote an active MRTF-A/SRF complex that contributes to myocyte gene expression. However, impaired contacts lead to cytoskeletal perturbations mediated by RhoA activation to increase the pool of G-actin thereby reducing MRTF-A/SRF nuclear event. The decrease in nuclear localization of MRTF-A prevents the activation of myocytic genes and by default switches on the PPARγ expression as an alternative adipocytic gene program. This results in a pathological myocyte to adipocyte switch

favoring adipogenesis [166]. The contribution of RhoA-GTPase in cell fate and decision has been additionally investigated by Soredella et al. who showed that RhoA-GTPase activity controls the insulin like growth factor 1, a potent regulator of the adipogenesis -myogenesis cell fate decision of mesenchymal precursors [167].

5.9.　G-actin regulation of MRTF-A

We present a novel observation by which S1P induces cytoskeletal rearrangements that lead to the dissociation of Actin/MRTF-A complex (Figure 28) enhancing nuclear localization of MRTF-A (Figure 29). Crystallography studies reveal the MRTF-A exhibit 3 actin binding domains at the N-terminus known as RPEL1,2 and 3 [168]. RPEL 3 has the weakest actin binding affinity however it contains B2 and B3 elements that constitute the nuclear localization signal (NLS) [169]. The actin mediated retention of MRTF-A is strictly accomplished by RPEL domains since studies have shown that mutant MRTF-A at RPEL domains are unable to bind to actin but could localize to the nucleus and activate SRF eliciting corresponding cellular response [170, 171]. That is because the binding of G-actin to REPL-domains competes with Importin alfa and Importin beta, a family of nuclear import factors that retain MTRF-A in the nucleus [169]. While G-actin seems to regulate nuclear localization of MRTF-A in the cytosol, nuclear actin exhibits the opposite effect promoting the nuclear exit of MRTF-A back to the cytosol. Therefore, cytosolic and nuclear actin are crucial regulators of the cellular localization. On the other hand, binding of nuclear actin to MRTF-A facilitates the interaction of the recombinant RPEL-Crm-1 domain with nucleoporin, an exportin, to promote for the nuclear export of MRTF-A [172]. In summary, actin modulates the sub-cellular localization of MRTF-A via regulating the import/export signal. Besides its direct interaction to actin, other mechanisms such as actin binding proteins or phosphorylation of MRTF-A are known regulate its the spatial localization. In addition, actin binding proteins are shown to mediate MRTF-A signaling upon regulating MRTF-A/SRF nuclear complex. For example, β-catenin inhibits the inhibitory effect of SMAD3 on MTRF-A. Briefly, SMAD3/MRTF-A complex induces the phosphorylation of MRTF-A leading to its ubiquitination and degradation [173]. Therefore, a decrease in the cytosolic β-catenin contributes negatively to the down regulation of MRTF-A in the cytosol.

5.10. Additional regulators of MRTF-A localization

S1P stimulates endothelial cell function and vascular stability upon enhancing the nuclear localization of MRTF-A as has been shown previously. Indeed, overexpression of MRTF-A using r.AAV.MRTF-A transduction in septic animals results in a significant increase in endothelial to pericyte density coupled with and decrease in the systemic hypotension at 12 and 24h during sepsis. Taken together, overexpression of MRTF-A in septic animals resulted in enhanced survival rate[114] (data not shown). Here we suggest two possible mechanisms to promote hemodynamic stability and pericyte investment. First, S1P induces RhoA activation and cytoskeletal rearrangement enhancing MRTF-A nuclear localization promoting the expression of CCN1 and CCN2 genes. CCN1 activation mediates angiogenesis and collateral vessel formation while CCN2 promotes pericyte retention and vessel maturation[74]. In light of this observation, S1P has been show to elicit MRTF-A nuclear localization in cardiac progenitor cells. There, the coupling of S1PR2 and S1PR3 to Gα12/13 elicits RhoA activation and nuclear localization of MRTF-A leading to a protective effect on cardiac progenitors [174]. The second mechanism is through overexpression of MRTF-A itself which enhanced survival in septic animals similar to the observations of the S1P septic model [114](Figure 30). Using genetic tools, our group elucidates a further mechanism to alter MRTF-A activity in sepsis mediated by overexpression of Thymosin β4. Tβ4, when abundantly expressed, captures globular actin resulting in increased nuclear translocation MRTF-A which interacts with Serum response factor to activate target genes such as CCN1 and CCN2. Most importantly, overexpression of Tβ4 in septic mice ameliorates pericyte loss and reduces perivascular leakage during LPS induced sepsis. These results are coupled with enhanced hemodynamic function suggesting the Tβ4 signalling axis as a potential therapeutic role in sepsis [68]. Taken together, Tβ4/MRTF-A signalling axis is crucial for pericyte investment which we have shown to be abolished by the Ang2 signaling cascade [44]. Therefore, the mechanism to enrich for MRTF-A can be achieved either by abolishing G-actin via Tβ4 overexpression and S1P treatment or by overexpressing MRTF-A itself.

5.11. Future directions

Further work could be performed make use of MRTF-A knockout cell lines and extrapolate our experimental setup with the LPS and S1P agonist treatment or generate and analyse MRTF-A knockout mice in sepsis and in response to S1P. It would be physiologically relevant to reproduce our in vivo septic model using cecal ligation and puncture procedure. CLP results in physiologically relevant kinetics of cytokines production that model the cytokine profile in sepsis better than the LPS model [175]. We hope future studies will build upon the presented work to de-convolute the molecular mechanism underlying S1P mediated barrier enhancement and pericyte retention.

Summary

In this work, we investigated the potential of Sphingosine-1-phosphate (S1P) to enhance barrier function and promote pericyte retention during LPS induced sepsis. LPS stimulation leads to a moderate loss of endothelial cells and pericyte coverage in the microcirculation which results in increased permeability and ultimately systemic hypotension. We revealed that S1P reduces capillary rarefaction and promotes pericyte investment in the microvascular unit. Improved capillary density led to reduced vascular edema, enhanced systemic blood pressure and survival. The observed microvascular disintegration is due to the dramatic loss in adhesion proteins mainly VE-Cadherin and N-Cadherin that mediate the endothelial cell-cell junction and endothelial pericyte contact respectively. The mechanism underlying enhanced barrier function was further investigated in vitro. There, we found that S1P reduces phosphorylation of Src kinase that phosphorylates VE-Cadherin at tyrosine 685 enhancing its internalization and degradation. The downregulation of VE-Cadherin in response to inflammation coincides with dramatic remodelling in the actin cytoskeleton orchestrated by RhoA activation. We observed that LPS stimulation alters the balanced G/F actin ratio favouring an increase in G-actin, while S1P induces RhoA activation and restores this balance by promoting F-actin assembly. The observed alterations in the G/F ratio correlate to changes in the cellular localization of MRTF-A since G-actin exhibits high binding affinity to MRTF-A. Therefore, in response to LPS, accumulating G-actin retains MRTF-A in the cytosol reducing its nuclear localization.

However, S1P overrides this effect and enhances MRTF-A nuclear localization due to the observed reduction in the cytoplasmic pool of G-actin. Upon translocating to the nucleus, MRTF-A regulates the transcription of target genes which are involved in vessel maturation and pericyte retention. This novel observation is mediated by RhoA activation which elicits severe changes in the actin network leading to the pronounced effects of S1P.
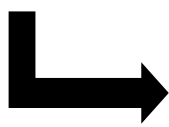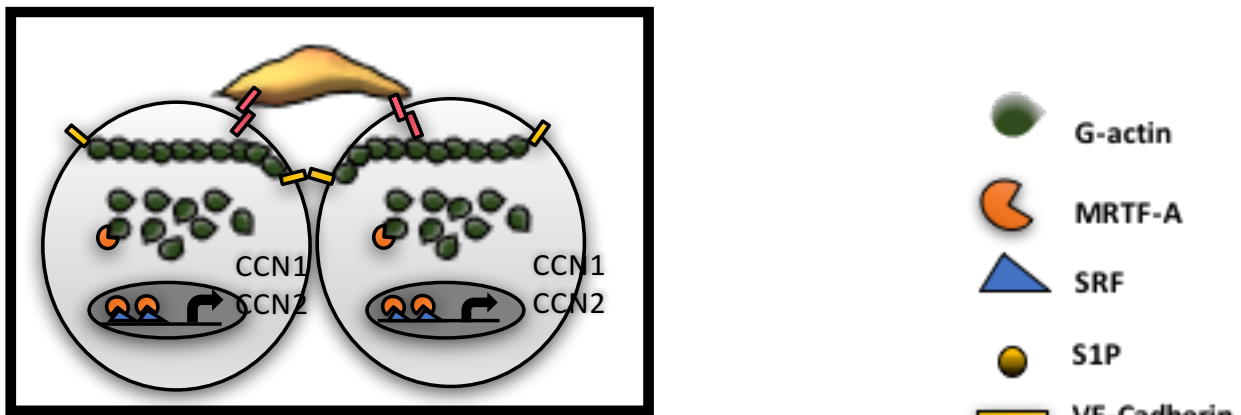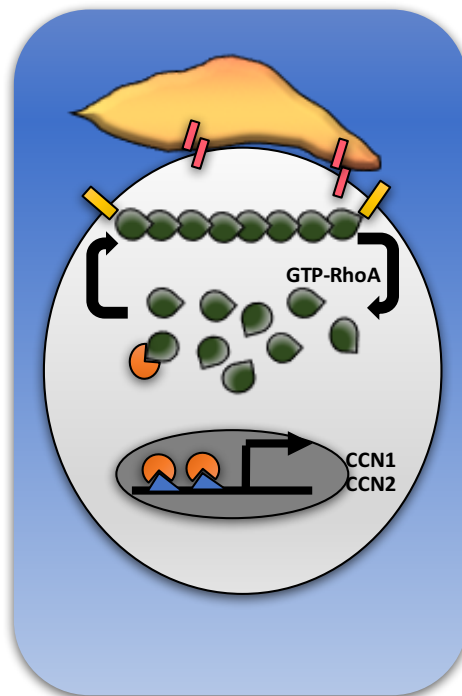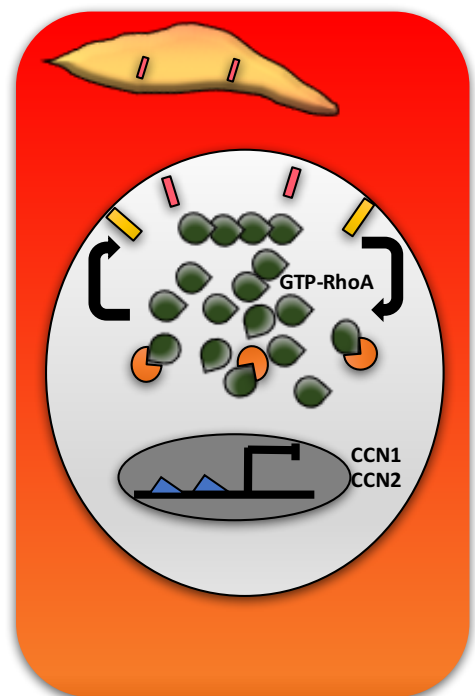
Figure30: (A) Under physiologic conditions, VE-Cadherin mediates the adhesion between endothelial cells while N-Cadherin mediates the adhesion between endothelial cells and pericytes. Both adhesion molecules are structurally supported by actin cytoskeleton that is dynamically regulated by GTP bound RhoA. LPS induces cytoskeletal rearrangements tailored to increase cytosolic G-actin and promote the loss of adhesion molecules leading to pericytes de-attachment. The binding of G-actin to MRTF-A ameliorates its nuclear translocation leading to downregulation of CCN1 and CCN2 genes which signal for vessel maturation and pericyte retention.

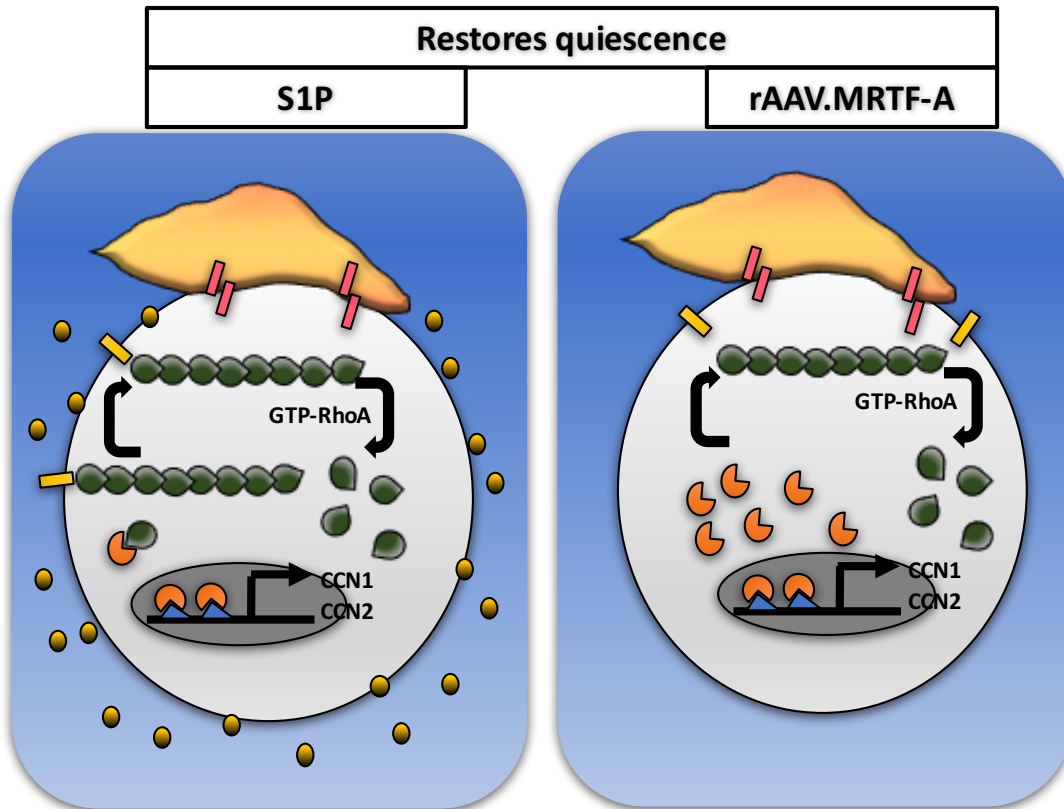**Figure 30: (B)** Administration of S1P restores adhesion molecule expression promotes F-actin assembly via RhoA activation. The decrease in cytosolic G-actin promotes MRTF-A nuclear localization and pericyte retention. Another possible mechanism to restore this phenotype is via overexpression of MRTF-A using rAAV.MRTF-A.

Abbreviations

AAV	Adeno-associated virus
Akt	Proteinkinase B
Ang	Angiopoietin
ATTC-CCL-226	Murine mesenchymal cell line
α-Catenin	Alpha catenin
BBB	Blood brain barrier
β-catenin	Beta catenin
bEnd3	mus musculus brain endothelial cells
bFGF	Basic fibroblast growth factor
BM	Basement membrane
CCN1	Cellular Communication Network Factor 1
CCN1	Cellular Communication Network Factor 2
cGMP	Cyclic guanosine monophosphate
CLP	Cecal ligation and puncture
CLR	C-type lectin receptors
C57BL/6J	'Black 6' strain of inbred laboratory mice.
DAPI	4′,6-diamidino-2-phenylindole
DLL4	Delta Like Canonical Notch Ligand 4
DMEM	Dulbecco's Modified Eagle Medium
DMSO	Dimethyl sulfoxide
DNA	Deoxyribonucleic acid
DSS	Disuccinimidyl suberate
DTT	Dithiothreitol
EC	Endothelial cells

ECM	Extra cellular matrix
EDTA	Ethylenediaminetetraacetic acid
EDG	Endothelial differentiation gene
ELISA	The enzyme-linked immunosorbent assay
ET	Endothelin
eNOS	Endothelial nitric oxide synthase
ER	Endoplasmic reticulum
E.coli	Escherichia coli
E-selectin	Endothelial-leukocyte adhesion molecule 1
f- actin	Polymeric filaments
FCS	Fetal calf serum
FDA	Food and Drug administration
FRAP	Fluorescence recovery after photobleaching
FTY720	Fingolimod
g-actin	Globular actin
GEF	Guanine nucleotide exchange factors
Gi/o	Heterotrimeric G protein alpha subunits
gp130	Glycoprotein 130
Gq	heterotrimeric G protein subunit
Gs	heterotrimeric G protein subunit
GTP	Guanosine-5'-triphosphate
GTPase	GTP hydrolase enzyme
HDL	High-density lipoprotein
HRP	Horseradish peroxidase
Hsp27	Heat shock protein 27
ICAM-1	Intercellular Adhesion Molecule 1

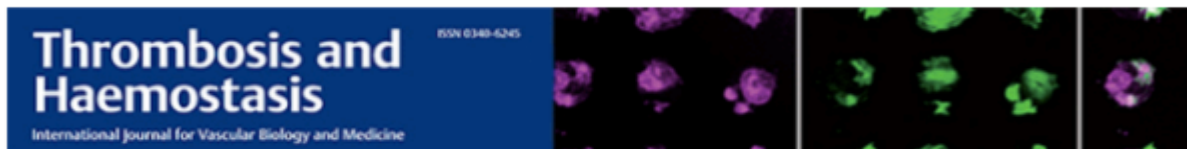|	
Il-1	Interleukin 1
Il-6	Interleukin 6
Il-6S	Interleukin 6 soluble receptor
IP_3	Inositol trisphosphate
IP	Immunoprecipitation
iv	Intravenous
JAK	Janus kinase
JAM	Junctional adhesion molecule
kDa	Kilodalton
KO	Knock out
LacZ	Lac operon
LPS	Lipopolysaccharides
MAP	Mean arterial pressure
MAPK	Mitogen-activated protein kinase
MEM	Minimum essential medium
MGV	Mean gray value
MLEC	Mouse lung endothelial cells
MLCK	Myosin light-chain kinase
MMF	Anesthetic mixture midazolam, medetomidine and Fentanyl
MT	Microtubule
MRTF-A	Myocardin Related Transcription Factor A
MYD88	Myeloid differentiation primary response 88
N-cadherin	Neural cadherin
NFκB	Nuclear factor kappa-light-chain-enhancer of activated B cells
NG2	Neural/glial antigen 2
NLR	Nucleotide-binding oligomerization domain-like receptors

NLS	Nuclear localization signal
NO	Nitric oxide
PAMP	Pathogen-associated molecular pattern
PRR	Pattern recognition receptors
PBS	Phosphate-buffered saline
PBST	Phosphate-buffered saline
PDGF-ß	Platelet-derived growth factor- ß
PECAM-1	Platelet endothelial cell adhesion molecule-1
PFA	Paraformaldehyde
PKC	Protein kinase C
PPO	Partian Pressure
PRR	Pattern recognition receptors
pSrc	Phospho Src
pSTAT3 (Tyr^{705})	Phospho Src
PVDF	Polyvinylidene difluoride
P120	Catenin delta-1
qSOFA	Quick sequential organ failure assessment
Rab7	Ras-related protein 7
RBC	Red blood cell
RHD	Rel homology domain
ROCK	Rho kinase
RhoGTPase	Family of signaling G proteins
RLR	Retinoic acid like receptor
RPEL	Repeats
SDS	Sodium dodecyl sulfate
SDS-PAGE	Sodium dodecyl sulfate–polyacrylamide gel electrophoresis

sGC	soluble guanylyl cyclase
SIRS	Systemic inflammatory response syndrome
SMAD3	Mothers against decapentaplegic homolog 3
Src	Proto-oncogene tyrosine-protein kinase
SRF	Serum response factor
STAT3	Signal transducer and activator of transcription 3
S1P	Sphingosine-1-phosphate
S1Pk	Sphingosine-1-phosphate kinase
S1PR	Sphingosine-1-phosphate receptor
pSTAT3 (Tyr^{705})	Phospho STAT3 at tyrosine 705
TBST	Tis buffered saline with tween
Tß4	Thymosin beta 4
TGF-β	Transforming growth factor beta
Tie	Tyrosine kinase with immunoglobulin-like and egf-like domains
TLR	Toll like receptor
TNF-α	Tumor necrosis factor alpha
TRITC	Tetramethylrhodamine
TRIF	TIR-domain-containing adapter-inducing interferon-β
Tyr	Tyrosine
TY52156	S1P receptor 3 antagonist
Ucn1	Urocortin 1
uPA	Urokinase plasminogen activator
VCAM-1	Vascular cell adhesion protein 1
VE-cadherin	Vascular endothelial cadherin
VEGF	Vascular endothelial growth factor

VEGFR	Vascular Endothelial growth factor receptors
VSMC	Vascular smooth muscle cells
VPR	Volume pressure recording
WT	Wild type
W146	S1P receptor 1 antagonist
ZO-1	Zonula occluden-1

Publication

The manuscript titled "Sphingosine 1-phosphate attenuates LPS-induced pericyte loss via activation of Rho-A and MRTF-A" was submitted to Thrombosis and Haemostasis.

Sphingosine 1-phosphate attenuates LPS-induced pericyte loss via activation of Rho-A and MRTF-A

Bibliography

1. Bone, R.C., et al., *Definitions for sepsis and organ failure and guidelines for the use of innovative therapies in sepsis. The ACCP/SCCM Consensus Conference Committee. American College of Chest Physicians/Society of Critical Care Medicine.* Chest, 1992. **101**(6): p. 1644-55.

2. Angus, D.C. and T. van der Poll, *Severe sepsis and septic shock.* N Engl J Med, 2013. **369**(9): p. 840-51.

3. Fleischmann, C., et al., *Assessment of Global Incidence and Mortality of Hospital-treated Sepsis. Current Estimates and Limitations.* Am J Respir Crit Care Med, 2016. **193**(3): p. 259-72.

4. Paoli, C.J., et al., *Epidemiology and Costs of Sepsis in the United States-An Analysis Based on Timing of Diagnosis and Severity Level.* Crit Care Med, 2018. **46**(12): p. 1889-1897.

5. *36th International Symposium on Intensive Care and Emergency Medicine : Brussels, Belgium. 15-18 March 2016.* Crit Care, 2016. **20**(Suppl 2): p. 94.

6. Kruttgen, A., et al., *Real-time PCR assay and a synthetic positive control for the rapid and sensitive detection of the emerging resistance gene New Delhi Metallo-beta-lactamase-1 (bla(NDM-1)).* Med Microbiol Immunol, 2011. **200**(2): p. 137-41.

7. Stearns-Kurosawa, D.J., et al., *The pathogenesis of sepsis.* Annu Rev Pathol, 2011. **6**: p. 19-48.

8. Bhatt, D. and S. Ghosh, *Regulation of the NF-kappaB-Mediated Transcription of Inflammatory Genes.* Front Immunol, 2014. **5**: p. 71.

9. Kruttgen, A. and S. Rose-John, *Interleukin-6 in sepsis and capillary leakage syndrome.* J Interferon Cytokine Res, 2012. **32**(2): p. 60-5.

10. Waage, A., et al., *The complex pattern of cytokines in serum from patients with meningococcal septic shock. Association between interleukin 6, interleukin 1, and fatal outcome.* J Exp Med, 1989. **169**(1): p. 333-8.

11. Tamura, T., et al., *Soluble interleukin-6 receptor triggers osteoclast formation by interleukin 6.* Proc Natl Acad Sci U S A, 1993. **90**(24): p. 11924-8.

12. Ellingsgaard, H., et al., *Interleukin-6 enhances insulin secretion by increasing glucagon-like peptide-1 secretion from L cells and alpha cells.* Nat Med, 2011. **17**(11): p. 1481-9.

13. Marz, P., et al., *Sympathetic neurons can produce and respond to interleukin 6.* Proc Natl Acad Sci U S A, 1998. **95**(6): p. 3251-6.

14. Aoki, Y., G.M. Feldman, and G. Tosato, *Inhibition of STAT3 signaling induces apoptosis and decreases survivin expression in primary effusion lymphoma.* Blood, 2003. **101**(4): p. 1535-42.

15. Gavard, J. and J.S. Gutkind, *VEGF controls endothelial-cell permeability by promoting the beta-arrestin-dependent endocytosis of VE-cadherin.* Nat Cell Biol, 2006. **8**(11): p. 1223-34.

16. Esteve, E., et al., *Serum interleukin-6 correlates with endothelial dysfunction in healthy men independently of insulin sensitivity.* Diabetes Care, 2007. **30**(4): p. 939-45.

17. De Backer, D., et al., *Microvascular blood flow is altered in patients with sepsis.* Am J Respir Crit Care Med, 2002. **166**(1): p. 98-104.

18.   Ho, K.L., *Ultrastructure of cerebellar capillary hemangioblastoma. IV. Pericytes and their relationship to endothelial cells.* Acta Neuropathol, 1985. **67**(3-4): p. 254-64.

19.   Guven, G., M.P. Hilty, and C. Ince, *Microcirculation: Physiology, Pathophysiology, and Clinical Application.* Blood Purif, 2019: p. 1-8.

20.   Diaz-Flores, L., et al., *Pericytes. Morphofunction, interactions and pathology in a quiescent and activated mesenchymal cell niche.* Histol Histopathol, 2009. **24**(7): p. 909-69.

21.   Armulik, A., A. Abramsson, and C. Betsholtz, *Endothelial/pericyte interactions.* Circ Res, 2005. **97**(6): p. 512-23.

22.   Joyce, N.C., M.F. Haire, and G.E. Palade, *Contractile proteins in pericytes. II. Immunocytochemical evidence for the presence of two isomyosins in graded concentrations.* J Cell Biol, 1985. **100**(5): p. 1387-95.

23.   Neuhaus, A.A., et al., *Novel method to study pericyte contractility and responses to ischaemia in vitro using electrical impedance.* J Cereb Blood Flow Metab, 2017. **37**(6): p. 2013-2024.

24.   Lee, S., et al., *Pericyte actomyosin-mediated contraction at the cell-material interface can modulate the microvascular niche.* J Phys Condens Matter, 2010. **22**(19): p. 194115.

25.   Sato, Y. and D.B. Rifkin, *Inhibition of endothelial cell movement by pericytes and smooth muscle cells: activation of a latent transforming growth factor-beta 1-like molecule by plasmin during co-culture.* J Cell Biol, 1989. **109**(1): p. 309-15.

26.   Watanabe, S., et al., *Cultured retinal pericytes stimulate in vitro angiogenesis of endothelial cells through secretion of a fibroblast growth factor-like molecule.* Atherosclerosis, 1997. **130**(1-2): p. 101-7.

27.   Montesano, R., et al., *Basic fibroblast growth factor induces angiogenesis in vitro.* Proc Natl Acad Sci U S A, 1986. **83**(19): p. 7297-301.

28.   McGuire, P.G., et al., *Pericyte-derived sphingosine 1-phosphate induces the expression of adhesion proteins and modulates the retinal endothelial cell barrier.* Arterioscler Thromb Vasc Biol, 2011. **31**(12): p. e107-15.

29.   Suri, C., et al., *Requisite role of angiopoietin-1, a ligand for the TIE2 receptor, during embryonic angiogenesis.* Cell, 1996. **87**(7): p. 1171-80.

30.   Sundberg, C., et al., *Stable expression of angiopoietin-1 and other markers by cultured pericytes: phenotypic similarities to a subpopulation of cells in maturing vessels during later stages of angiogenesis in vivo.* Lab Invest, 2002. **82**(4): p. 387-401.

31.   Mandarino, L.J., et al., *Regulation of fibronectin and laminin synthesis by retinal capillary endothelial cells and pericytes in vitro.* Exp Eye Res, 1993. **57**(5): p. 609-21.

32.   He, L., et al., *Analysis of the brain mural cell transcriptome.* Sci Rep, 2016. **6**: p. 35108.

33.   Liotta, L.A., et al., *Metastatic potential correlates with enzymatic degradation of basement membrane collagen.* Nature, 1980. **284**(5751): p. 67-8.

34.   Kubota, Y., et al., *Role of laminin and basement membrane in the morphological differentiation of human endothelial cells into capillary-like structures.* J Cell Biol, 1988. **107**(4): p. 1589-98.

35.   Birbrair, A., et al., *Role of pericytes in skeletal muscle regeneration and fat accumulation.* Stem Cells Dev, 2013. **22**(16): p. 2298-314.

36. Birbrair, A., et al., *Type-1 pericytes accumulate after tissue injury and produce collagen in an organ-dependent manner.* Stem Cell Res Ther, 2014. **5**(6): p. 122.

37. Walpole, J., et al., *Agent-based computational model of retinal angiogenesis simulates microvascular network morphology as a function of pericyte coverage.* Microcirculation, 2017. **24**(8).

38. London, N.R., K.J. Whitehead, and D.Y. Li, *Endogenous endothelial cell signaling systems maintain vascular stability.* Angiogenesis, 2009. **12**(2): p. 149-58.

39. Forstermann, U., et al., *Nitric oxide synthase isozymes. Characterization, purification, molecular cloning, and functions.* Hypertension, 1994. **23**(6 Pt 2): p. 1121-31.

40. Ignarro, L.J., et al., *Activation of purified soluble guanylate cyclase by endothelium-derived relaxing factor from intrapulmonary artery and vein: stimulation by acetylcholine, bradykinin and arachidonic acid.* J Pharmacol Exp Ther, 1986. **237**(3): p. 893-900.

41. Jones, K.A., et al., *cGMP modulation of Ca2+ sensitivity in airway smooth muscle.* Am J Physiol, 1999. **276**(1): p. L35-40.

42. Haynes, W.G. and D.J. Webb, *Contribution of endogenous generation of endothelin-1 to basal vascular tone.* Lancet, 1994. **344**(8926): p. 852-4.

43. Partanen, J., et al., *A novel endothelial cell surface receptor tyrosine kinase with extracellular epidermal growth factor homology domains.* Mol Cell Biol, 1992. **12**(4): p. 1698-707.

44. Ziegler, T., et al., *Angiopoietin 2 mediates microvascular and hemodynamic alterations in sepsis.* J Clin Invest, 2013.

45. Hippenstiel, S., et al., *VEGF induces hyperpermeability by a direct action on endothelial cells.* Am J Physiol, 1998. **274**(5): p. L678-84.

46. Domigan, C.K., et al., *Autocrine VEGF maintains endothelial survival through regulation of metabolism and autophagy.* J Cell Sci, 2015. **128**(12): p. 2236-48.

47. Jendreyko, N., et al., *Phenotypic knockout of VEGF-R2 and Tie-2 with an intradiabody reduces tumor growth and angiogenesis in vivo.* Proc Natl Acad Sci U S A, 2005. **102**(23): p. 8293-8.

48. Faure, E., et al., *Bacterial lipopolysaccharide activates NF-kappaB through toll-like receptor 4 (TLR-4) in cultured human dermal endothelial cells. Differential expression of TLR-4 and TLR-2 in endothelial cells.* J Biol Chem, 2000. **275**(15): p. 11058-63.

49. Jirik, F.R., et al., *Bacterial lipopolysaccharide and inflammatory mediators augment IL-6 secretion by human endothelial cells.* J Immunol, 1989. **142**(1): p. 144-7.

50. Mai, J., et al., *An evolving new paradigm: endothelial cells--conditional innate immune cells.* J Hematol Oncol, 2013. **6**: p. 61.

51. Abbassi, O., et al., *E-selectin supports neutrophil rolling in vitro under conditions of flow.* J Clin Invest, 1993. **92**(6): p. 2719-30.

52. Langer, H.F. and T. Chavakis, *Leukocyte-endothelial interactions in inflammation.* J Cell Mol Med, 2009. **13**(7): p. 1211-20.

53. Tauseef, M., et al., *TLR4 activation of TRPC6-dependent calcium signaling mediates endotoxin-induced lung vascular permeability and inflammation.* J Exp Med, 2012. **209**(11): p. 1953-68.

54. Goeckeler, Z.M. and R.B. Wysolmerski, *Myosin light chain kinase-regulated endothelial cell contraction: the relationship between isometric tension, actin polymerization, and myosin phosphorylation.* J Cell Biol, 1995. **130**(3): p. 613-27.

55. Sandoval, R., et al., *Ca(2+) signalling and PKCalpha activate increased endothelial permeability by disassembly of VE-cadherin junctions.* J Physiol, 2001. **533**(Pt 2): p. 433-45.

56. Navarro, P., et al., *Catenin-dependent and -independent functions of vascular endothelial cadherin.* J Biol Chem, 1995. **270**(52): p. 30965-72.

57. van Buul, J.D. and I. Timmerman, *Small Rho GTPase-mediated actin dynamics at endothelial adherens junctions.* Small GTPases, 2016. **7**(1): p. 21-31.

58. Gong, P., et al., *TLR4 signaling is coupled to SRC family kinase activation, tyrosine phosphorylation of zonula adherens proteins, and opening of the paracellular pathway in human lung microvascular endothelia.* J Biol Chem, 2008. **283**(19): p. 13437-49.

59. Wallez, Y., et al., *Src kinase phosphorylates vascular endothelial-cadherin in response to vascular endothelial growth factor: identification of tyrosine 685 as the unique target site.* Oncogene, 2007. **26**(7): p. 1067-77.

60. Turowski, P., et al., *Phosphorylation of vascular endothelial cadherin controls lymphocyte emigration.* J Cell Sci, 2008. **121**(Pt 1): p. 29-37.

61. Siehler, S., *Regulation of RhoGEF proteins by G12/13-coupled receptors.* Br J Pharmacol, 2009. **158**(1): p. 41-9.

62. Shasby, D.M., et al., *Role of endothelial cell cytoskeleton in control of endothelial permeability.* Circ Res, 1982. **51**(5): p. 657-61.

63. Birukova, A.A., et al., *Role of Rho GTPases in thrombin-induced lung vascular endothelial cells barrier dysfunction.* Microvasc Res, 2004. **67**(1): p. 64-77.

64. Amano, M., et al., *Phosphorylation and activation of myosin by Rho-associated kinase (Rho-kinase).* J Biol Chem, 1996. **271**(34): p. 20246-9.

65. Cao, J., et al., *Polarized actin and VE-cadherin dynamics regulate junctional remodelling and cell migration during sprouting angiogenesis.* Nat Commun, 2017. **8**(1): p. 2210.

66. Wan, R., et al., *Urocortin increased LPS-induced endothelial permeability by regulating the cadherin-catenin complex via corticotrophin-releasing hormone receptor 2.* J Cell Physiol, 2013. **228**(6): p. 1295-303.

67. McIlroy, M., et al., *Pericytes influence endothelial cell growth characteristics: role of plasminogen activator inhibitor type 1 (PAI-1).* Cardiovasc Res, 2006. **69**(1): p. 207-17.

68. Bongiovanni, D., et al., *Thymosin beta4 attenuates microcirculatory and hemodynamic destabilization in sepsis.* Expert Opin Biol Ther, 2015. **15 Suppl 1**: p. S203-10.

69. Kupatt, C., et al., *Cotransfection of vascular endothelial growth factor-A and platelet-derived growth factor-B via recombinant adeno-associated virus resolves chronic ischemic malperfusion role of vessel maturation.* J Am Coll Cardiol, 2010. **56**(5): p. 414-22.

70. Dor, Y., et al., *Conditional switching of VEGF provides new insights into adult neovascularization and pro-angiogenic therapy.* Embo j, 2002. **21**(8): p. 1939-47.

71. Badamchian, M., et al., *Thymosin beta(4) reduces lethality and down-regulates inflammatory mediators in endotoxin-induced septic shock.* Int Immunopharmacol, 2003. **3**(8): p. 1225-33.

72. Rossdeutsch, A., et al., *Essential role for thymosin beta4 in regulating vascular smooth muscle cell development and vessel wall stability.* Circ Res, 2012. **111**(4): p. e89-102.

73. Medjkane, S., et al., *Myocardin-related transcription factors and SRF are required for cytoskeletal dynamics and experimental metastasis.* Nat Cell Biol, 2009. **11**(3): p. 257-68.

74. Hinkel, R., et al., *MRTF-A controls vessel growth and maturation by increasing the expression of CCN1 and CCN2.* Nat Commun, 2014. **5**: p. 3970.

75. Lindblom, P., et al., *Endothelial PDGF-B retention is required for proper investment of pericytes in the microvessel wall.* Genes Dev, 2003. **17**(15): p. 1835-40.

76. Blow, O., et al., *The golden hour and the silver day: detection and correction of occult hypoperfusion within 24 hours improves outcome from major trauma.* J Trauma, 1999. **47**(5): p. 964-9.

77. Kumar, A., et al., *Duration of hypotension before initiation of effective antimicrobial therapy is the critical determinant of survival in human septic shock.* Crit Care Med, 2006. **34**(6): p. 1589-96.

78. Bochud, P.Y., et al., *Antimicrobial therapy for patients with severe sepsis and septic shock: an evidence-based review.* Crit Care Med, 2004. **32**(11 Suppl): p. S495-512.

79. Brown, R.M. and M.W. Semler, *Fluid Management in Sepsis.* J Intensive Care Med, 2019. **34**(5): p. 364-373.

80. Dellinger, R.P., et al., *Surviving sepsis campaign: international guidelines for management of severe sepsis and septic shock: 2012.* Crit Care Med, 2013. **41**(2): p. 580-637.

81. Jakob, S.M., E. Ruokonen, and J. Takala, *Effects of dopamine on systemic and regional blood flow and metabolism in septic and cardiac surgery patients.* Shock, 2002. **18**(1): p. 8-13.

82. Vincent, J.L., *Search for effective immunomodulating strategies against sepsis.* Lancet, 1998. **351**(9107): p. 922-3.

83. Chousterman, B.G., F.K. Swirski, and G.F. Weber, *Cytokine storm and sepsis disease pathogenesis.* Semin Immunopathol, 2017. **39**(5): p. 517-528.

84. Vincent, J.L., Q. Sun, and M.J. Dubois, *Clinical trials of immunomodulatory therapies in severe sepsis and septic shock.* Clin Infect Dis, 2002. **34**(8): p. 1084-93.

85. Winkler, M.S., et al., *Decreased serum concentrations of sphingosine-1-phosphate in sepsis.* Crit Care, 2015. **19**: p. 372.

86. Coldewey, S.M., et al., *Elevation of serum sphingosine-1-phosphate attenuates impaired cardiac function in experimental sepsis.* Sci Rep, 2016. **6**: p. 27594.

87. Le Stunff, H., S. Milstien, and S. Spiegel, *Generation and metabolism of bioactive sphingosine-1-phosphate.* J Cell Biochem, 2004. **92**(5): p. 882-99.

88. Hisano, Y., et al., *Mouse SPNS2 functions as a sphingosine-1-phosphate transporter in vascular endothelial cells.* PLoS One, 2012. **7**(6): p. e38941.

89. Olivera, A., M.L. Allende, and R.L. Proia, *Shaping the landscape: metabolic regulation of S1P gradients.* Biochim Biophys Acta, 2013. **1831**(1): p. 193-202.

90. Aoki, S., et al., *Sphingosine 1-phosphate-related metabolism in the blood vessel.* J Biochem, 2005. **138**(1): p. 47-55.

91. Venkataraman, K., et al., *Vascular endothelium as a contributor of plasma sphingosine 1-phosphate.* Circ Res, 2008. **102**(6): p. 669-76.

92. Ito, K., et al., *Lack of sphingosine 1-phosphate-degrading enzymes in erythrocytes.* Biochem Biophys Res Commun, 2007. **357**(1): p. 212-7.

93. Sassoli, C., et al., *Sphingosine 1-Phosphate (S1P)/ S1P Receptor Signaling and Mechanotransduction: Implications for Intrinsic Tissue Repair/Regeneration.* Int J Mol Sci, 2019. **20**(22).

94. Maceyka, M., et al., *Sphingosine-1-phosphate signaling and its role in disease.* Trends Cell Biol, 2012. **22**(1): p. 50-60.

95. Cantalupo, A., et al., *Nogo-B regulates endothelial sphingolipid homeostasis to control vascular function and blood pressure.* Nat Med, 2015. **21**(9): p. 1028-1037.

96. Lee, M.J., et al., *Akt-mediated phosphorylation of the G protein-coupled receptor EDG-1 is required for endothelial cell chemotaxis.* Mol Cell, 2001. **8**(3): p. 693-704.

97. Kono, M., et al., *The sphingosine-1-phosphate receptors S1P1, S1P2, and S1P3 function coordinately during embryonic angiogenesis.* J Biol Chem, 2004. **279**(28): p. 29367-73.

98. Okamoto, H., et al., *Inhibitory regulation of Rac activation, membrane ruffling, and cell migration by the G protein-coupled sphingosine-1-phosphate receptor EDG5 but not EDG1 or EDG3.* Mol Cell Biol, 2000. **20**(24): p. 9247-61.

99. Okazaki, H., et al., *Molecular cloning of a novel putative G protein-coupled receptor expressed in the cardiovascular system.* Biochem Biophys Res Commun, 1993. **190**(3): p. 1104-9.

100. Sanchez, T., et al., *Induction of vascular permeability by the sphingosine-1-phosphate receptor-2 (S1P2R) and its downstream effectors ROCK and PTEN.* Arterioscler Thromb Vasc Biol, 2007. **27**(6): p. 1312-8.

101. Nofer, J.R., et al., *HDL induces NO-dependent vasorelaxation via the lysophospholipid receptor S1P3.* J Clin Invest, 2004. **113**(4): p. 569-81.

102. Forrest, M., et al., *Immune cell regulation and cardiovascular effects of sphingosine 1-phosphate receptor agonists in rodents are mediated via distinct receptor subtypes.* J Pharmacol Exp Ther, 2004. **309**(2): p. 758-68.

103. Waeber, C., *Sphingosine 1-Phosphate (S1P) Signaling and the Vasculature*. 2013. p. 313-347.

104. Dantas, A.P., J. Igarashi, and T. Michel, *Sphingosine 1-phosphate and control of vascular tone.* Am J Physiol Heart Circ Physiol, 2003. **284**(6): p. H2045-52.

105. Peng, X., et al., *Protective effects of sphingosine 1-phosphate in murine endotoxin-induced inflammatory lung injury.* Am J Respir Crit Care Med, 2004. **169**(11): p. 1245-51.

106. Olivera, A., et al., *The sphingosine kinase-sphingosine-1-phosphate axis is a determinant of mast cell function and anaphylaxis.* Immunity, 2007. **26**(3): p. 287-97.

107. Lee, J.F., et al., *Dual roles of tight junction-associated protein, zonula occludens-1, in sphingosine 1-phosphate-mediated endothelial chemotaxis and barrier integrity.* J Biol Chem, 2006. **281**(39): p. 29190-200.

108. Mehta, D., et al., *Sphingosine 1-phosphate-induced mobilization of intracellular Ca2+ mediates rac activation and adherens junction assembly in endothelial cells.* J Biol Chem, 2005. **280**(17): p. 17320-8.

109. Adamson, R.H., et al., *Sphingosine-1-phosphate modulation of basal permeability and acute inflammatory responses in rat venular microvessels.* Cardiovasc Res, 2010. **88**(2): p. 344-51.

110. Peest, U., et al., *S1P-lyase independent clearance of extracellular sphingosine 1-phosphate after dephosphorylation and cellular uptake.* J Cell Biochem, 2008. **104**(3): p. 756-72.

111. Cohen, J.A., et al., *Oral fingolimod or intramuscular interferon for relapsing multiple sclerosis.* N Engl J Med, 2010. **362**(5): p. 402-15.

112. Sanchez, T., et al., *Phosphorylation and action of the immunomodulator FTY720 inhibits vascular endothelial cell growth factor-induced vascular permeability.* J Biol Chem, 2003. **278**(47): p. 47281-90.

113. Hou, T., et al., *Accuracy of serum interleukin (IL)-6 in sepsis diagnosis: a systematic review and meta-analysis.* Int J Clin Exp Med, 2015. **8**(9): p. 15238-45.

114. *<Abdel Rahman, F., et al., Sphingosine 1-phosphate attenuates LPS induced pericyte loss via activation of Rho-A and MRTF-A. J. Thromb. Haemost., 2020.pdf>.*

115. Zeng, H., et al., *LPS causes pericyte loss and microvascular dysfunction via disruption of Sirt3/angiopoietins/Tie-2 and HIF-2alpha/Notch3 pathways.* Sci Rep, 2016. **6**: p. 20931.

116. Tang, H.B., et al., *S1P/S1PR3 signaling mediated proliferation of pericytes via Ras/pERK pathway and CAY10444 had beneficial effects on spinal cord injury.* Biochem Biophys Res Commun, 2018. **498**(4): p. 830-836.

117. Dejana, E., F. Orsenigo, and M.G. Lampugnani, *The role of adherens junctions and VE-cadherin in the control of vascular permeability.* J Cell Sci, 2008. **121**(Pt 13): p. 2115-22.

118. Buchsbaum, R.J., *Rho activation at a glance.* J Cell Sci, 2007. **120**(Pt 7): p. 1149-52.

119. Patel, R.T., et al., *Interleukin 6 is a prognostic indicator of outcome in severe intra-abdominal sepsis.* Br J Surg, 1994. **81**(9): p. 1306-8.

120. Chalaris, A., et al., *The soluble Interleukin 6 receptor: generation and role in inflammation and cancer.* Eur J Cell Biol, 2011. **90**(6-7): p. 484-94.

121. Marechal, X., et al., *Endothelial glycocalyx damage during endotoxemia coincides with microcirculatory dysfunction and vascular oxidative stress.* Shock, 2008. **29**(5): p. 572-6.

122. Cabrales, P., et al., *Microvascular and capillary perfusion following glycocalyx degradation.* J Appl Physiol (1985), 2007. **102**(6): p. 2251-9.

123. Wang, L., et al., *Effects of FTY720 on Lung Injury Induced by Hindlimb Ischemia Reperfusion in Rats.* Mediators Inflamm, 2017. **2017**: p. 5301312.

124. Spiegel, S. and S. Milstien, *Sphingosine-1-phosphate: an enigmatic signalling lipid.* Nat Rev Mol Cell Biol, 2003. **4**(5): p. 397-407.

125. Gamble, J.R., et al., *Angiopoietin-1 is an antipermeability and anti-inflammatory agent in vitro and targets cell junctions.* Circ Res, 2000. **87**(7): p. 603-7.

126. Thurston, G., et al., *Leakage-resistant blood vessels in mice transgenically overexpressing angiopoietin-1.* Science, 1999. **286**(5449): p. 2511-4.

127. Geraldes, P., et al., *Activation of PKC-delta and SHP-1 by hyperglycemia causes vascular cell apoptosis and diabetic retinopathy.* Nat Med, 2009. **15**(11): p. 1298-306.

128. Pfister, F., et al., *Pericyte migration: a novel mechanism of pericyte loss in experimental diabetic retinopathy.* Diabetes, 2008. **57**(9): p. 2495-502.

129. Lee, S.Y., et al., *Sphingosine-1-phosphate reduces hepatic ischaemia/reperfusion-induced acute kidney injury through attenuation of endothelial injury in mice.* Nephrology (Carlton), 2011. **16**(2): p. 163-73.

130. Samarska, I.V., et al., *S1P1 receptor modulation preserves vascular function in mesenteric and coronary arteries after CPB in the rat independent of depletion of lymphocytes.* PLoS One, 2014. **9**(5): p. e97196.

131. Salomone, S., et al., *S1P3 receptors mediate the potent constriction of cerebral arteries by sphingosine-1-phosphate.* Eur J Pharmacol, 2003. **469**(1-3): p. 125-34.

132. Salomone, S., et al., *Analysis of sphingosine 1-phosphate receptors involved in constriction of isolated cerebral arteries with receptor null mice and pharmacological tools.* Br J Pharmacol, 2008. **153**(1): p. 140-7.

133. Lorenz, J.N., et al., *Vascular dysfunction in S1P2 sphingosine 1-phosphate receptor knockout mice.* Am J Physiol Regul Integr Comp Physiol, 2007. **292**(1): p. R440-6.

134. Cantalupo, A. and A. Di Lorenzo, *S1P Signaling and De Novo Biosynthesis in Blood Pressure Homeostasis.* J Pharmacol Exp Ther, 2016. **358**(2): p. 359-70.

135. Bolz, S.S., et al., *Sphingosine kinase modulates microvascular tone and myogenic responses through activation of RhoA/Rho kinase.* Circulation, 2003. **108**(3): p. 342-7.

136. Orsenigo, F., et al., *Phosphorylation of VE-cadherin is modulated by haemodynamic forces and contributes to the regulation of vascular permeability in vivo.* Nat Commun, 2012. **3**: p. 1208.

137. Chichger, H., et al., *p18, a novel adaptor protein, regulates pulmonary endothelial barrier function via enhanced endocytic recycling of VE-cadherin.* Faseb j, 2015. **29**(3): p. 868-81.

138. Chichger, H., et al., *Select Rab GTPases Regulate the Pulmonary Endothelium via Endosomal Trafficking of Vascular Endothelial-Cadherin.* Am J Respir Cell Mol Biol, 2016. **54**(6): p. 769-81.

139. Gavard, J., *Breaking the VE-cadherin bonds.* FEBS Lett, 2009. **583**(1): p. 1-6.

140. Lampugnani, M.G., et al., *The molecular organization of endothelial cell to cell junctions: differential association of plakoglobin, beta-catenin, and alpha-catenin with vascular endothelial cadherin (VE-cadherin).* J Cell Biol, 1995. **129**(1): p. 203-17.

141. Nanes, B.A., et al., *p120-catenin binding masks an endocytic signal conserved in classical cadherins.* J Cell Biol, 2012. **199**(2): p. 365-80.

142. Garrett, J.P., et al., *Regulation of endothelial barrier function by p120-cateninVE-cadherin interaction.* Mol Biol Cell, 2017. **28**(1): p. 85-97.

143. Chen, X., et al., *p120 catenin associates with kinesin and facilitates the transport of cadherin-catenin complexes to intercellular junctions.* J Cell Biol, 2003. **163**(3): p. 547-57.

144. Chi, L., et al., *Interleukin-6 production by endothelial cells via stimulation of protease-activated receptors is amplified by endotoxin and tumor necrosis factor-alpha.* J Interferon Cytokine Res, 2001. **21**(4): p. 231-40.

145. Duzagac, F., et al., *JAK/STAT pathway interacts with intercellular cell adhesion molecule (ICAM) and vascular cell adhesion molecule (VCAM) while prostate cancer stem cells form tumor spheroids.* J buon, 2015. **20**(5): p. 1250-7.

146. Hou, T., et al., *Roles of IL-6-gp130 Signaling in Vascular Inflammation.* Curr Cardiol Rev, 2008. **4**(3): p. 179-92.

147. Han, X., et al., *Enhancement of ICAM-1 via the JAK2/STAT3 signaling pathway in a rat model of severe acute pancreatitis-associated lung injury.* Exp Ther Med, 2016. **11**(3): p. 788-796.

148. Alsaffar, H., et al., *Interleukin-6 promotes a sustained loss of endothelial barrier function via Janus kinase-mediated STAT3 phosphorylation and de novo protein synthesis.* Am J Physiol Cell Physiol, 2018. **314**(5): p. C589-c602.

149. Hox, V., et al., *Diminution of signal transducer and activator of transcription 3 signaling inhibits vascular permeability and anaphylaxis.* J Allergy Clin Immunol, 2016. **138**(1): p. 187-199.

150. Alsaffar, H., N. Martino, and A.J.T.F.J. Adam, *STAT3 and MEK Mediate IL6-Induced Increase in Endothelial Permeability.* 2017. **31**(1_supplement): p. 55.6-55.6.

151. Gaengel, K., et al., *The sphingosine-1-phosphate receptor S1PR1 restricts sprouting angiogenesis by regulating the interplay between VE-cadherin and VEGFR2.* Dev Cell, 2012. **23**(3): p. 587-99.

152. Daub, H., et al., *Rac/Cdc42 and p65PAK regulate the microtubule-destabilizing protein stathmin through phosphorylation at serine 16.* J Biol Chem, 2001. **276**(3): p. 1677-80.

153. Paik, J.H., et al., *Sphingosine 1-phosphate receptor regulation of N-cadherin mediates vascular stabilization.* Genes Dev, 2004. **18**(19): p. 2392-403.

154. Hammes, H.P., et al., *Angiopoietin-2 causes pericyte dropout in the normal retina: evidence for involvement in diabetic retinopathy.* Diabetes, 2004. **53**(4): p. 1104-10.

155. Segain, J.P., et al., *Rho kinase blockade prevents inflammation via nuclear factor kappa B inhibition: evidence in Crohn's disease and experimental colitis.* Gastroenterology, 2003. **124**(5): p. 1180-7.

156. Pronk, M.C.A., et al., *RhoA, RhoB and RhoC differentially regulate endothelial barrier function.* Small GTPases, 2019. **10**(6): p. 466-484.

157. Carbajal, J.M. and R.C. Schaeffer, Jr., *RhoA inactivation enhances endothelial barrier function.* Am J Physiol, 1999. **277**(5 Pt 1): p. C955-64.

158. van Nieuw Amerongen, G.P., et al., *Involvement of RhoA/Rho kinase signaling in VEGF-induced endothelial cell migration and angiogenesis in vitro.* Arterioscler Thromb Vasc Biol, 2003. **23**(2): p. 211-7.

159. van Nieuw Amerongen, G.P., et al., *Involvement of Rho kinase in endothelial barrier maintenance.* Arterioscler Thromb Vasc Biol, 2007. **27**(11): p. 2332-9.

160. Shen, Q., et al., *Myosin light chain kinase in microvascular endothelial barrier function.* Cardiovasc Res, 2010. **87**(2): p. 272-80.

161. Birukova, A.A., et al., *Microtubule disassembly induces cytoskeletal remodeling and lung vascular barrier dysfunction: role of Rho-dependent mechanisms.* J Cell Physiol, 2004. **201**(1): p. 55-70.

162. Watanabe, N., et al., *p140mDia, a mammalian homolog of Drosophila diaphanous, is a target protein for Rho small GTPase and is a ligand for profilin.* Embo j, 1997. **16**(11): p. 3044-56.

163. Kholodenko, B.N., *Cell-signalling dynamics in time and space.* Nat Rev Mol Cell Biol, 2006. **7**(3): p. 165-76.

164. Zhang, X.E., S.P. Adderley, and J.W. Breslin, *Activation of RhoA, but Not Rac1, Mediates Early Stages of S1P-Induced Endothelial Barrier Enhancement.* PLoS One, 2016. **11**(5): p. e0155490.

165. Reinhard, N.R., et al., *The balance between Galphai-Cdc42/Rac and Galpha12/13-RhoA pathways determines endothelial barrier regulation by sphingosine-1-phosphate.* Mol Biol Cell, 2017. **28**(23): p. 3371-3382.

166.   Dorn, T., et al., *Interplay of cell-cell contacts and RhoA/MRTF-A signaling regulates cardiomyocyte identity.* Embo j, 2018. **37**(12).

167.   Sordella, R., et al., *Modulation of Rho GTPase signaling regulates a switch between adipogenesis and myogenesis.* Cell, 2003. **113**(2): p. 147-58.

168.   Mouilleron, S., et al., *Molecular basis for G-actin binding to RPEL motifs from the serum response factor coactivator MAL.* Embo j, 2008. **27**(23): p. 3198-208.

169.   Pawlowski, R., et al., *An actin-regulated importin alpha/beta-dependent extended bipartite NLS directs nuclear import of MRTF-A.* Embo j, 2010. **29**(20): p. 3448-58.

170.   Vartiainen, M.K., et al., *Nuclear actin regulates dynamic subcellular localization and activity of the SRF cofactor MAL.* Science, 2007. **316**(5832): p. 1749-52.

171.   Miralles, F., et al., *Actin dynamics control SRF activity by regulation of its coactivator MAL.* Cell, 2003. **113**(3): p. 329-42.

172.   Engelsma, D., et al., *Supraphysiological nuclear export signals bind CRM1 independently of RanGTP and arrest at Nup358.* Embo j, 2004. **23**(18): p. 3643-52.

173.   Charbonney, E., et al., *beta-catenin and Smad3 regulate the activity and stability of myocardin-related transcription factor during epithelial-myofibroblast transition.* Mol Biol Cell, 2011. **22**(23): p. 4472-85.

174.   Castaldi, A., et al., *Sphingosine 1-phosphate elicits RhoA-dependent proliferation and MRTF-A mediated gene induction in CPCs.* Cell Signal, 2016. **28**(8): p. 871-9.

175.   Remick, D.G., et al., *Comparison of the mortality and inflammatory response of two models of sepsis: lipopolysaccharide vs. cecal ligation and puncture.* Shock, 2000. **13**(2): p. 110-6.

Acknowledgment

This work became reality with the support of many people whom I would like to thank.

My deep gratitude goes first to my supervisor Prof. Dr. Christian Kupatt for his incredible contribution in shaping my dissertation. His support, constructive criticism, and wisdom enriched my growth as a graduate student. He gave me the freedom to explore on my own and guided me to recover when my steps faltered. I'm thankful I was part of his working group.

My further gratitude goes to the distinguished members of my doctoral thesis committee, Professor Roland Rad and Professor Alessandra Moretti for generously offering their precious time to hold enlightening discussions and read my thesis.

I'm in debt for Dr. Tilman Ziegler for his unflinching support and encouragement throughout my journey. His motivation, competence, and scientific intuition is unmatched. I'm grateful we crossed paths and I thank you for training me to be a better scientist in every sense of word.

My appreciation also goes to the members of Prof. Kupatt working group who accompanied me over the past years and supported me in the completion of this work. Special thanks should be made to Dr. Tarik Bozoglu for guiding me to implement novel research methods and to Anja wolf for her excellent technical guidance.

I would also like to extend my gratitude to Dr. Tatjana Dorn who was always available to help and advise me on scientific protocols and in some cases designing new protocols.

Finally, I dedicate this thesis to my parents, Moussa and Soultaneh and my siblings Ali and Ghinwa for their unconditional support. Thank you for always being gracious.

Curriculum vitae

PERSONAL INFORMATION

Farah Abdel Rahman
Date of birth: 18. March 1991
Pace of birth: Beirut, Lebanon
Nationality: Lebanese
Marital status: Single, no children

ACADEMIC EXPERIENCE

09.16 - 04.20	Scientific researcher at Klinik & Poliklinik Für Innere Medizin I, at klinikum rechts der Isar
09.12 - 10.15	Graduate research assistant at Department of Anatomy, Cell Biology and Physiological Sciences, American University of Beirut
09.11 - 05.12	Teaching internship, International College Lebanon.

EDUCATION

09.16 - 04.20	PhD in Medical Life Science and Technology at Technical University of Munich
09.12 - 10.15	Masters in Physiology at American University of Beirut
09.09 - 05.12	Bachelor of Science, biology at American University of Beirut
09.11 - 05.12	Diploma for secondary education at American University of Beirut

PUBLICATION

Abdel Rahman, F., et al., Sphingosine 1-phosphate attenuates LPS induced pericyte loss via activation of Rho-A and MRTF-A. J. Thromb. Haemost., 2020.

Moretti, A., et al., *Somatic gene editing ameliorates skeletal and cardiac muscle failure in pig and human models of Duchenne muscular dystrophy.* Nat Med, 2020.

Ziegler, T., et al., *Atherosclerosis and the Capillary Network; Pathophysiology and Potential Therapeutic Strategies.* Cells, 2019. 9(1).

Ghantous, C.M., et al., *Assessment of Basilar Artery Reactivity in Stroke and Subarachnoid Hemorrhage Using Wire Myograph.* Methods Mol Biol, 2016. 1462: p. 625-43.Ghantous,

C.M., et al., *Mechanical stretch-induced vascular hypertrophy occurs through modulation of leptin synthesis-mediated ROS formation and GATA-4 nuclear translocation.* Front Pharmacol, 2015. 6: p. 240.